U.PORTO
FEUP FACULDADE DE ENGENHARIA
UNIVERSIDADE DO PORTO

U.PORTO
INSTITUTO DE CIÊNCIAS BIOMÉDICAS ABEL SALAZAR
UNIVERSIDADE DO PORTO

M 2016

Molecularly Imprinted Intelligent Scaffolds for Tissue Engineering Applications

Mariana Isabel Fonseca Neves

DISSERTATION FOR THE
DEGREE OF MASTER OF SCIENCE IN BIOENGINEERING
AT THE FACULDADE DE ENGENHARIA DA UNIVERSIDADE DO PORTO
AND INSITUTO DE CIÊNCIAS BIOMÉDICAS ABEL SALAZAR

Molecularly Imprinted Intelligent Scaffolds for Tissue Engineering Applications

Mariana Isabel Fonseca Neves

Dissertation
for the Degree of Master of Science in Bioengineering,
at the Faculdade de Engenharia da Universidade do Porto
And Instituto de Ciências Biomédicas Abel Salazar

Supervisor: Dr. Pedro Granja
Co-supervisor: Dr. Manuela Gomes

September 2016

This work was financed by Portuguese funds through FCT - Fundação para a Ciência e a Tecnologia/Ministério da Ciência, Tecnologia e Inovação in the framework of the project “RECOGNIZE – Intelligent scaffolds by molecular recognition for advanced applications in regenerative medicine” - UTAP-ICDT/CTM-BIO/0023/2014.

“I am among those who think that science has great beauty. A scientist in his laboratory is not only a technician: he is also a child confronting natural phenomena that impress him as though they were fairy tales.

[…] Neither do I believe that the spirit of adventure runs any risk of disappearing in our world. If I see anything vital around me, it is precisely that spirit of adventure, which seems indestructible and is akin to curiosity.”

Marie Skłodowska Curie

Acknowledgments

First of all, I would like to thank my supervisor, Professor Pedro Granja, for all the opportunities he provided to me; for believing in me and my capabilities and for always motivating me to go further; for his unconditional availability, and finally, for his inspiring professionalism and optimism. I would also like to thank my co-supervisor, Professor Manuela Gomes, for all her support and motivation throughout this work.

An honest thank you goes to all my colleagues from Biocarrier for the way they welcomed me into the group, for their friendship and good moments, their help and motivation, both at professional and personal levels, and for all that I have learned with every one of you throughout these last six months.

To all my classmates, with whom I spent my best moments of these last five years and with whom I grew up and learnt so much. In particular, to all my ladies Rita Ribeiro, Bárbara Mesquita, Andreia Granja, Eva Carvalho, Rita Castro, Sofia Assis, Lúcia Rebelo, Rita Pinto and Ana Nascimento: for all the dramas and joys we spent together, a special thank you!

To my aunt and uncle, Luísa and João, who supported me in my first years of this course like I was a daughter of your own, an everlasting thank you.

I would also like to thank my brother João for all the pranking and teasing, that only an older brother like you knows how to do… and also for being an example that resilience and willpower are the way to reach our dreams.

To my boyfriend Pedro, for being with me throughout these last ten years of my short life, in particular throughout this long five-year journey of mine trying to be an engineer and ending

up being a biotechnologist; for always having shown me what I am capable of and all that I have learnt with you. For that, and all the rest, a huge thank you.

Finally, to my parents, Fátima and Licínio, for the example you have always been to me; for having stimulated me to feel curious about everything and always wanting to learn more; for having showed me, through your own effort, that perseverance and work are fundamental for professional success and that nothing comes to our hands if we are simply waiting without looking; for all the values you taught me that made me who I am today; for all the opportunities you gave me, a lot of times with sacrifice, so I could go further. And most of all, for teaching me that if I fell, I could always get up, and that I could walk ahead without having to look back. Thank you.

Agradecimentos

Em primeiro lugar, queria agradecer ao meu orientador, Professor Pedro Granja, por todas as oportunidades que me providenciou; por acreditar em mim e nas minhas capacidades e por me ter sempre motivado a tentar chegar mais longe; pela disponibilidade incansável sempre que precisei e finalmente pelo seu inspirador profissionalismo e optimismo.

Queria também agradecer à minha co-orientadora, Professora Manuela Gomes, por todo o seu apoio e motivação ao longo do trabalho.

Um sincero agradecimento a todos os meus colegas do Biocarrier pelo modo como me receberam, pela amizade e momentos bem passados, pela ajuda e motivação a nível profissional e pessoal, e por tudo o que pude aprender com vocês ao longo destes seis meses.

A todos os meus colegas de turma, com os quais passei os meus melhores momentos destes últimos cinco anos e com os quais cresci e aprendi tanto. Em especial a todas as minhas meninas: Rita Ribeiro, Bárbara Mesquita, Andreia Granja, Eva Carvalho, Rita Castro, Sofia Assis, Lúcia Rebelo, Rita Pinto e Ana Nascimento. Por todos os dramas e alegrias que passamos juntas, um obrigado!

Aos meus tios, Luísa e João, que me apoioaram e me receberam durante os primeiros anos deste curso como se fosse vossa filha, um eterno obrigado.

Tenho também de agradecer ao meu irmão João, por todas as traquinices e arrelias que só um irmão mais velho como tu sabe fazer… E também por seres um exemplo para mim de como a resiliencia e a vontade são o caminho para atingirmos aquilo que queremos e sonhamos.

Ao meu namorado Pedro, por me ter acompanhado nos últimos dez anos desta minha curta vida, e em especial nesta minha longa travessia de cinco anos a tentar ser engenheira, mas a

acabar a ser uma biotecnóloga; por sempre me teres mostrado do que sou capaz e por tudo o que aprendi contigo. Por isso, e por tudo o resto, um enorme obrigado.

Finalmente, aos meus pais, Fátima e Licínio, por todo o exemplo que sempre foram para mim; por me terem estimulado a sentir curiosidade por tudo e a querer sempre aprender mais e mais; por me terem mostrado, através do vosso próprio esforço, que a preserverança e o trabalho são fundamentais para o sucesso profissional e que nada vem ter connosco se simplesmente estivermos à espera sem procurar; por todos os valores que me transmitiram e me fazem ser a pessoa que sou hoje; por todas as oportunidades que me deram, muitas vezes com sacrifício vosso, para que pudesse chegar mais longe. E sobretudo por me ensinarem que se caísse me podia levantar, e que podia andar para a frente sem olhar para trás. Obrigada.

Abstract

It is widely accepted that material-cell interactions are mediated and affected by the type of molecules adsorbed to the material. Such key concept has driven the tissue engineering field to pursuit different ways of modifying or functionalizing materials, achieving a better control over molecular adsorption and triggering of favorable cellular response.

Molecular imprinting is a technology inspired by highly selective interactions, such as antibody/antigen bonding, which aims to induce molecular recognition into polymeric materials. In order to do so, polymerization occurs in the presence of a template molecule, *i.e.*, the molecule of interest. Once polymerization is accomplished and the template molecule is removed, specific cavities either in shape or position of binding sites are formed and available to selectively recognize any molecule such as the template used. This feature can be an interesting approach for scaffolds used for tissue engineering applications by enabling specific molecular adsorption.

Even though this technology is widely described for low molecular weight molecules, the same does not occur for molecular imprinting of high molecular weight molecules (macromolecules), such as proteins, which are the ones that bear greater interest for Tissue Engineering. The high molecular weight and size of these molecules, together with their complex structure, lead to obstacles in the molecular imprinting process which are not addressed for small molecules. Besides, most of the existent literature is intended for applications which do not require mild or biocompatible conditions (*e.g.* biosensing).

The main aim of the project presented herein was to develop and study a biocompatible molecular imprinting system based on a photosensitive polymer, methacrylated alginate. The premature profile of the system required the study of basic features inherent either to the

material or the molecular imprinting process itself. In order to optimize the system and compare the obtained results with the literature, the chosen template molecule was bovine serum albumin, a model protein.

On the first stage of development, methacrylation of alginate was optimized and achieved, with polymeric solutions forming gel discs under UV light exposure. In this stage, two different methacrylated alginate materials were produced which differed in their pH value (5 or 7).

An evaluation of swelling behavior of these materials was then performed under different pH and salt conditions in order to further optimized production steps related to the molecular imprinting process. Results showed that both pH and presence of salts affected the swelling behavior. While increasing the pH to 7.4 allowed the swelling of the discs, lower pH values lead to deswelling events. The effect of salts on swelling behavior and template removal was also evaluated by comparing the effects of Tris solutions, with or without the presence of divalent cations salts, with the effects provoked by deionized water.

Once an optimized molecular imprinting protocol was set, template removal and rebinding capacity were studied and characterized for molecularly imprinted polymer discs using different protein quantification approaches. Results revealed for template removal were promising as they ranged from 70-98%, depending on the type of material used. Results concerning the capacity of the molecularly imprinted material to recognize the template molecule showed no significant differences when comparing to a non-imprinted material. These lack of recognition was most likely caused by the high swelling and deswelling rates observed during the whole processing.

Overall, this study enabled the understanding of the effect of different external stimuli in the developed material and how these potentially affected the molecular imprinting process. The preliminary studies developed herein are crucial to further define the right directions to follow in order to successfully achieve molecular recognition and ultimately transpose this system to biomolecules with more specific interest for tissue engineering applications.

Table of Contents

- *This page was intentionally left in blank* -

Abbreviation List

AcOH – Acetic acid

AL - Alginate

ALMA 5 – Methacrylated alginate, pH 5

ALMA 7 – Methacrylated alginate, pH 7

AU – Arbitrary Units

BMP – Bone morphogenetic proteins

BSA – Bovine serum albumin

Cyt – Cytochrome

Cryo-SEM – Cryo Scanning electron microscopy

DAP – Diammonium phosphate

DI water – Deionized water

ECM – Extracellular matrix

EMIPM – Embedded molecularly imprinted polymer microspheres/microcapsules

EtOH – Ethanol

FGF – Fibroblast growth factor

Fn – Fibronectin

GTA – Glutaraldehyde

Hb – Hemoglobin

H NMR – Proton nuclear magnetic resonance

HSA – Human serum albumin

IF – Imprinting factor

IGF – Insulin-like growth factor

IntDen – Integrated Density

Lyz – Lysozyme

MA – Methacrylate/methacrylic anhydride

MI – Molecular imprinting

MIP – Molecularly imprinted polymer

MPC – Methacryloyloxyethyl phosphorylcholine

NIP – Non-imprinted polymer

PAAm - Polyacrylamide

PDGF – Platelet derived growth factor

PDMS – Polydimethylsiloxane

PGA – Polyglycolic acid

pI – Isoelectric point

PIM – Post-imprinting modifications

PLGA – Poly(lactic-co-glycolic) acid

PLLA - Poly-L-lactic acid

Q – Rebinding capacity

RGD – Arginine-Glycine-Aspartic acid tripeptide

RT – Room Temperature

SDS – Sodium dodecyl sulfate

SEM – Scanning Electron Microscopy

SMIPM – Surface molecularly imprinted polymer microspheres/microcapsules

SR – Swelling Ratio

TE – Tissue Engineering

UV – Ultraviolet

VEGF – Vascular endothelial growth factor

List of Figures

- *This page was intentionally left in blank* -

List of Tables

- *This page was intentionally left in blank* -

Outline

This work is divided into four main chapters. A general overview of the currently available literature on molecular imprinting and its potential applications in tissue engineering is explored in Chapter 1 – Introduction. In Chapter 2 – Aim of the Project, both general particular aims of this thesis are enounced and specified. In Chapter 3 – Materials and Methods, all methodologies performed during this project are described. Chapter 4 – Results and Discussion presents and explores all relevant results obtained throughout this project. In Chapter 5 – Conclusions and Perspectives, the main results of this project are highlighted and future lines of work are proposed.

- *This page was intentionally left in blank* -

The following Chapter corresponds to a review article already accepted for publication in the journal Tissue Engineering.

Molecularly Imprinted Intelligent Scaffolds for Tissue Engineering Applications

Mariana I. Neves[1,2,3], Marissa E. Wechsler[4,5], Manuela E. Gomes[6], Rui L. Reis[6], Pedro L. Granja[1,2,3,7], Nicholas A. Peppas[4,5,8,9,10]

[1] Instituto de Investigação e Inovação em Saúde (i3S), Universidade do Porto, Porto, Portugal
[2] Instituto de Ciências Biomédicas Abel Salazar (ICBAS), Universidade do Porto, Porto, Portugal
[3] Faculdade de Engenharia da Universidade do Porto (FEUP), Porto, Portugal
[4] Department of Biomedical Engineering, The University of Texas at Austin, Austin, TX, USA
[5] Institute of Biomaterials, Drug Delivery and Regenerative Medicine, The University of Texas at Austin, Austin, TX, USA
[6] 3B's Research Group, Universidade do Minho, Guimarães, Portugal
[7] Instituto de Engenharia Biomédica (INEB), Universidade do Porto, Porto, Portugal
[8] McKetta Department of Chemical Engineering, The University of Texas at Austin, Austin, TX, USA
[9] Department of Surgery and Perioperative Care, Dell Medical School, The University of Texas at Austin, Austin, TX, USA
[10] Division of Pharmaceutics, College of Pharmacy, The University of Texas at Austin, Austin, TX, USA

- *This page was intentionally left in blank* -

Chapter 1
Introduction

Molecular imprinting is a widely investigated technology with applications in the fields of chemical sensing, chromatography, immunoassays, antibody mimicking, artificial enzymes and catalysis processes [1, 2]. Molecular imprinting is a technology based on natural molecular events (*e.g.,* antibody/antigen interactions and enzyme catalysis) which aims to incorporate molecular memory into a material using intelligent polymers [3, 4].

Intelligent polymers are macromolecular systems that exhibit strong thermodynamic interaction with the surrounding environment and with associated components. Therefore, an intelligent polymer material has strong interactions with the environment based on pH-, or temperature sensitivity, but most importantly based on thermodynamic interactions with a recognitive compound. This "intelligence" is rendered to the polymer either by external decoration with required functional groups, or (better) by internal molecular imprinting of micro- and nanocavities that provide recognitive characteristics.

Therefore, the fundamental idea for these new technology platforms is to combine a template molecule with a functional monomer giving rise to a polymer network (after crosslinking and removal of the template) with template-specific cavities in size, shape and chemical functionality [5] (**Fig. 1**). The ability of these molecular imprinted polymers to then recognize template molecules through thermodynamic interacts present the intelligent capabilities of these polymers.

Molecular imprinting is well characterized for low-molecular weight molecules although, despite the promising results, products based on this technology are currently not available on

the market [2]. In contrast, molecular imprinting of high-molecular weight molecules exhibit several obstacles, such as, size, structure, functionality and solubility which are not relevant when imprinting small molecules [6]. The large size of these molecules restricts their transfer within highly crosslinked polymer networks during both template removal and rebinding studies. The complex structure of biomacromolecules (*e.g.,* proteins) plays an important role in their functionality, leading to high sensitivity to pH, ionic strength, temperature and organic solvents [6, 7]. Despite these challenges, studies have reported results of the molecular imprinting of proteins supporting its application, namely in the fields of biosensing and chromatography [8-15].

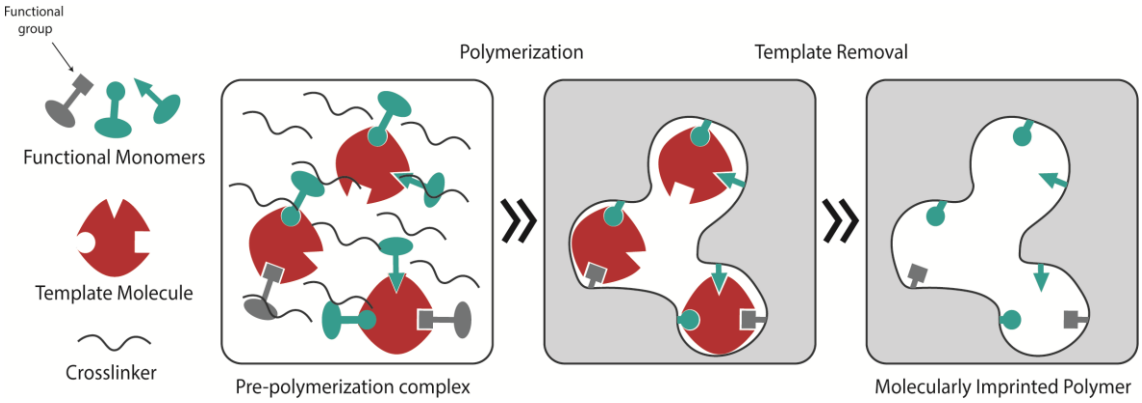

Figure 1. Molecular imprinting process. Once the appropriate template molecule, functional monomer(s) and crosslinker(s) are selected, all components are mixed together in a proper solvent (e.g. deionized water, phosphate buffer) forming the pre-polymerization complex (template-functional monomer). Polymerization is then allowed to take place and specific cavities and binding sites are stabilized. Finally, removal of the template and other washing steps eliminate unreacted monomer and crosslinker molecules, resulting in a molecularly imprinted polymer (MIP). The use of heteropolymeric systems (or a functional monomer with more than one functional groups) may improve imprinting features as the different polymer functional groups can interact with various protein domains. In addition, these functional groups can modify the chemical and/or mechanical properties of the final MIP.

Due to the specificity and recognition capabilities of molecular imprinting, this has the potential to become a tool utilized for the production of scaffolds with high bioactivity and recognition capacity towards specific molecules or cells for tissue engineering (TE) applications. TE is an alternative clinical approach to conventional therapies which resort to the use of organ

grafts and transplantation (xeno, allo or auto). Organs and tissues are difficult to obtain and have short storage time. The methods used for organ and tissue transplantation are highly invasive, usually comprising tremendous burden to the patient, and are associated with high risk of rejection and permanent need for immunosuppressive therapy [16]. TE aims to restore, replace and/or regenerate tissues or organs to their normal function by combining acquired knowledge on the wound healing process with cell- and/or scaffold-based approaches.

The design of biomimetic structures can be accomplished by either *top-down* or *bottom-up* strategies. In *top-down* TE strategies, scaffolds are seeded with cells so that they can populate the structure to eventually form a tissue. *Bottom-up* approaches create small modular parts which are then assembled to form the final tissue structure [17]. The latter approach in particular has been of recent interest due to its potential to better mimic the microarchitectural features of native tissues, therefore, providing additional guidance at the cellular- and molecular- levels [17].

Despite the potential of using molecular imprinting as a tool for tissue regeneration applications, this topic is currently far from being fully explored. Biomacromolecules (*i.e.*, high molecular weight molecules present in living organisms) are ones that bear great importance for TE applications due to their involvement in the wound healing processes. However, biomacromolecules present major challenges when used for molecular imprinting. Nonetheless, molecular imprinting could specifically be used in *bottom-up* techniques to create complex cues at a microstructural level to improve cell- and scaffold-based approaches. This review aims to provide an overview of utilizing molecular imprinting as a tool for various TE applications by exploring the fundamentals and challenges, specifically, regarding the use of imprinting macromolecules. Additionally, potential strategies of molecular imprinting in TE based on recent approaches in the field of protein molecular recognition will be surveyed.

1.1. Natural body response to injury

The design of effective TE approaches requires the understanding of the body's natural recovery from an injury. Upon tissue injury, the wound healing process is divided in three stages: inflammation, tissue formation and tissue remodeling [18]. This is a highly regulated and complex process of paracrine, autocrine and juxtacrine signaling events [19]. In summary,

immediately after injury, platelets and polymorphonuclear leukocytes (neutrophils) aggregate and become entrapped within a fibrin mesh forming a thrombus [18]. Initial release of growth factors [*e.g.* platelet-derived growth factor (PDGF) or vascular endothelial growth factor (VEGF)] by these cells give rise to the inflammatory process, where monocytes-macrophages, lymphocytes, fibroblasts and endothelial cells are chemo-attracted to the site, and activated to scavenge the damaged tissue [18, 19]. These cells then produce various growth factors and cytokines which promote the formation of granulation tissue. Angiogenesis (*i.e.*, the formation of new blood vessels) then promotes and accelerates the wound healing process [20].

Two major outcomes can result from this body response to injury: scarring or regeneration of tissue. In mammals, the most frequent body response is to quickly produce a fibrous tissue, usually referred to as scar, to immediately stop the bleeding and avoid microbial infection at the injury site. In this typical response, the overall function of the tissue or organ is maintained, even though not fully recovered since composition, aesthetic and structure is not preserved. Harty *et al.* [21] proposed this lack of regenerative capacity as a possible result of the evolution of the mammalian immune system, which rather promoted wound microenvironments to improve tissue defense and facilitate tissue repair. The second, and less frequent response to injury, is regeneration. Upon injury, the tissue or organ is able to fully recover structure, composition and function at a functional-unity level. In mammals, this process occurs namely at embryonic stages [22], and below a critical size injury. Duration and intensity of each wound healing stage, namely inflammation, dictate the final outcome of tissue repair. In fact, inflammation has been proposed to play an important role in the success of the wound healing process. Unbalanced inflammatory reactions and/or cytokine profiles frequently result in differences in scarring [19]. Such an example is observed in spinal cord injuries, where the occurrence of inflammatory events with subsequent formation of a glial scar are the primary barriers to achieving neuroregeneration [23]. Successful tissue repair after injury requires resolution of the inflammatory response, with inflammation being a prerequisite to scarring [19]. The topics of wound healing and repair processes have been extensively reviewed and revised over the past few decades [18, 19, 24].

The wound healing process is characterized by the existence of direct cell-cell and cell-matrix interactions, along with indirect crosstalk between different cell populations through soluble mediators [18]. These interactions are highly complex and tissue-specific, comprising of a series of biochemical and mechanical signals. These signals then modulate subsequent cell

behavior, such as, migration, proliferation and differentiation. The extracellular matrix (ECM) plays a pivotal role in this process. The natural ECM not only provides mechanical support to cells, but is also a reservoir of growth factors (matrix-embedded). In addition, the ECM serves as platform for cell-cell interaction by allowing dispersion of secreted factors and mechano-transduction signals [25]. Therefore, the ECM is largely capable of modulating cell migration, cytoskeletal organization, proliferation and differentiation [26]. Tissue vascularization is also affected by the ECM structure, namely by its microporosity, which will promote or incapacitate angiogenesis [19]. Thus, effective design of biomimetic structures for TE applications should involve a complex combination of topographical, architectural and biochemical features mimicking the natural ECM.

1.2. Tissue engineering and the relevance of cell-instructing scaffolds

An important goal of TE is to replace tissues or organs by mimicking and/or modulating the natural events of wound healing to produce a fully regenerated and functional tissue. Significant understanding of the wound healing process has led to the development of several TE strategies which can be divided into either cell- or scaffold-based approaches. Cell-based approaches use both adult and embryonic stem or progenitor cells to induce the formation new tissue. These approaches are centered on stimulating tissue progenitor cells *in situ*, or promoting their expansion and differentiation *in vitro*, for further implantation to the site where regeneration is desired [27]. Limitations using cell-based approaches include difficulties regarding cell obtainment from scarce sources, and *in vitro* cell expansion and differentiation.

Scaffold-based approaches rely on the understanding of the ECM function, maintaining homeostasis (a dynamic process achieved through a balance between degradation of the old and formation of the new ECM) and providing signals (*viz.,* chemical, physical and mechanical) to cells. TE uses this understanding to create 2D or 3D matrices, which can provide mechanical support and physical-chemical cues to promote cell seeding. This can be accomplished by either using man-made scaffolds, or natural-based scaffolds, such as decellularized ECM from allogenic or xenogenic tissues [25].

Developing scaffolds with degradable biomaterials is pivotal in TE research. It has been established that mimicking the natural cell environment produces favorable outcomes with

successful cases reported in a wide variety of tissues (*e.g.,* heart valves or skin) when decellularized extracellular matrices were used [25]. However, these matrices do present drawbacks including the methods in which they are processed, and possibilities of contamination and immunogenicity. A significant portion of these efforts is followed in order to create a bridge between man-made and natural structures. This requires development of new, intelligent biomaterials and production technologies which better resemble the native structural, mechanical and biological cues. TE scaffolds can be made from many types of biomaterials, although polymeric scaffolds are widely investigated due to their chemical and mechanical versatility associated with biodegradability. Natural polymer biomaterials present high biocompatibility and biodegradability, but low mechanical properties, limiting their applications. Commonly studied natural polymer biomaterials used for TE applications include collagen [28], alginate [29, 30], chitosan [31] and silk [32]. Extensively explored scaffolds based on synthetic polymeric biomaterials produced with poly-L-lactic acid (PLLA), polyglycolic acid (PGA) or poly(lactic-co-glycolic) acid (PLGA) are easily tailored in their architecture, mechanical properties and degradation characteristics. However, these materials have been associated with risks of rejection due to reduced bioactivity, and may cause cell and tissue necrosis upon degradation [33]. Bioceramic-based TE scaffolds, primarily made of calcium phosphates, such as hydroxyapatite [34] and tricalcium-phosphate, [35] are biocompatible and characterized by high mechanical stiffness and low elasticity, limiting their use to hard tissues (*e.g.*, for orthopedic applications).

Several characteristics should be considered when developing a biomaterial/scaffold for TE applications. Ideally, a scaffold for such applications should be designed considering the following: i) biocompatibility, (*i.e.*, promote cell adhesion, support native cell activity, such as proliferation or migration, without causing an immune reaction which could lead to severe inflammation or rejection); ii) biodegradability (*i.e.*, scaffolds should be replaced by cells and their ECM, in addition to having degradation byproducts be non-toxic and be excreted by the body without harming other tissues or organs); iii) bioactivity, which can be provided by including biochemical, biophysical and mechanical cues into the scaffold (*e.g.* biological relevant molecular features, such as proteins, or functionalizing with chemical functional groups able to interact with these molecules); iv) architecture, by designing scaffolds with adequate porosity and preferentially interconnected pore allowing cell migration and diffusion of oxygen, nutrients and waste products, while promoting vascularization; v) mechanical profile, by designing

scaffolds as a temporary mechanical stabilizers with mechanical properties similar that of the tissue/organ of interest; vi) manufacturing technology, as cost-effective and scalable as possible [33].

1.3. Molecularly imprinted polymers

1.3.1. Molecular imprinting characteristics

Molecular imprinting is a technology based on naturally occurring molecular events which aim to insert molecular memory into a material, usually polymeric [3], increasing specificity, loading capacity and release control of biomaterials [5]. A molecularly imprinted polymer (MIP) is produced by combining a functional monomer (or mix of monomers) with a template molecule. These monomers interact with the template molecule either by reversible covalent interactions, or non-covalent interactions, forming a pre-polymerization complex [36]. Macromolecular MIPs usually rely on non-covalent interactions (*e.g.* H-bonding, electrostatic and hydrophobic interactions) for recognition [3]. Polymerization is allowed to take place, and the addition of a cross-linker promotes the fixation of polymer positions to help memorize the geometry of the cavities once the template is removed. Template removal is achieved by performing a series of washing steps using organic or inorganic solvents, or by enzymatic digestion [37]. Once the imprinting process is completed, imprinting success can be evaluated by two main parameters: adsorption capacity (Q, μg mg^{-1}) (1), which determines the amount of adsorbed molecules per weight of polymer; and imprinting efficiency, or imprinting factor (IF) (2), which corresponds to the ratio between both MIP and correspondent non-imprinted polymer (NIP) adsorption capacities.

$$Q = \frac{(C_i - C_f)V}{W} \quad (1)$$

Ci and Cf – initial and final concentration of template solution, respectively (μg mL^{-1})

V – volume of template solution (mL)

W – weight of MIP or non-imprinted polymer (mg)

$$IF = Q_{MIP}/Q_{NIP} \quad (2)$$

1.3.2. Molecular imprinting considerations

In order to create a material for TE applications, one should carefully mind several aspects of MIP production. After choosing an appropriate template molecule, the choice of the functional monomer(s) (and their ratios) bears great importance. The selected monomer(s) should be biocompatible, nontoxic and have high affinity to the template so that template-monomer complexes are thermodynamically favorable and stable under reaction conditions [3]. Since proteins contain many different binding sites and heterogeneous regions, the choice of the polymer matrix will influence MIP selectivity by enabling or preventing cross-reactivity with proteins similar to the template molecule [38]. For instance, it is not desirable for the polymer to reactively polymerize with the template, a phenomenon frequently observed while imprinting biomolecules into polyurethanes, where one of the monomeric units is an isothiocyanate, capable of reacting with alcohol or amine groups present in most biomolecules [2]. On the other hand, heteropolymer systems seem to favor macromolecular memory [5, 12, 39]. This can be explained by the conjugation of their different functional groups, thereby increasing the number of available interaction sites with the different regions of the template and improving their physico-chemical properties [12, 13]. Another possibility is the use of natural ligand derivatives as functional monomers for the polymer matrix. Chou *et al.* [40] produced a C-reactive protein imprinted polymer using a phosphorylcholine derivative (4NPPC) as the functional monomer and the micro-contact approach. This approach uses a monolayer of a minimal protein mass to which the recognition substrate will form an imprint [40]. The resulting MIP showed rebinding capacity and selectivity towards the C-reactive protein, leading the authors to conclude that the proposed micro-contact approach is a suitable method to produce protein MIPs [40]. The MIP should be biodegradable to promote its replacement by the natural ECM, but stable to withstand the harsh environmental body conditions. Biodegradability is also important to allow exposure of new binding sites, especially in bulk imprinted materials. MIP biodegradability, as well as flexibility, can be controlled by the degree and type of crosslinking used. Higher degrees of crosslinking can promote higher selectivity by reducing movement (*e.g.* swelling) and fixating binding sites [1]. However, an excessive degree of crosslinking interactions can result in difficulties during template removal, and reduce rebinding capacity due to impaired diffusion [41]. Despite existing covalent and non-covalent crosslinking techniques used for MIP production, biological applications of MIPs prefer non-covalent techniques due to more mild template removal methods [1].

Molecular imprinting conditions should be mild in order to avoid protein denaturation or polymer distortion. Biomacromolecules have complex structures that are highly sensitive to pH, ionic strength, temperature and solvents [6]. If imprinting conditions are non-physiological, changes in the natural conformation of the protein may result in imprinting cavities specific for this altered form [3]. Kryscio *et al.* [42] performed an elaborate study on how different functional monomers (acrylamide, methacrylic acid, acrylic acid, 3-aminophenylboronic acid and N-isopropyl acrylamide) and crosslinkers (N,N'-methylenebisacrylamide and ethylene glycol dimethacrylate) widely used in MI influence protein template conformational stability. The authors used circular dichroism studies to analyze conformational changes in bovine serum albumin (BSA), and concluded that these reactants induced significant changes in the secondary structure of the template protein. This is a severe matter of concern as it can explain the low rate of success of macromolecular imprinting [42].

The choice of the polymerization solvent brings challenges when it comes to protein solubility [2]. While proteins are usually more soluble and stable in aqueous solutions, these types of solvents are far from ideal as they affect the pre-polymerization complex by interfering with hydrogen bonding (an extremely important type of interaction for many template-monomer complexes) [3]. The solvent is responsible for mixing all of the components (*i.e.,* template, functional monomer(s), crosslinkers and polymerization initiators) into one phase, in addition to, creating pores in macroporous polymers [43]. Some studies on protein molecular imprinting use organic solvents, such as chloroform [44], as they better stabilize the polymerization process. However, for biomedical applications involving cell contact (*i.e.*, drug delivery and TE applications), these solvents must be avoided or replaced during MIP production processes due to their high toxicity [45, 46].

During the imprinting of macromolecules, template removal is one of the critical phases and consists on several washing steps using solvents, acids, bases, or detergents [2]. Other possibilities include template removal by enzymatic digestion [37, 47]. Template removal is a particularly delicate step during the imprinting process due to the large sizes of macromolecules. Efficient template removal is often hard to obtain and still presents a major challenge when imprinting large molecules. For each developed system, it is important to work on the optimization of the template removal phase since it influences the final rebinding capacity and success of the MIP. Hawkins *et al.* [47] optimized a template removal strategy for a bovine hemoglobin (Hb) molecularly imprinted polyacrylamide gel using sodium dodecylsulphate (SDS)

and acetic acid (AcOH). Even though a SDS:AcOH ratio of 10%(w/v):10%(v/v) did not present the highest template removal percentage (only 47.6%), the highest imprinting efficiency (>90%) was obtained. Higher template removal percentages can result in lower imprinting efficiencies if the agents begin to promote conformational changes on the imprinting matrix [47]. The authors also tested an enzymatic digestion-based template removal system with trypsin. This showed an even higher template removal capacity (87.4%), compared to the SDS:AcOH maximum (71.5%), but a significantly lower imprinting efficiency (20.4%). This can be a result of remaining protein fragments inside the polymer matrix which may block potential binding sites [47]. On the other hand, SDS can damage the cell membrane and lead to cell death. In BSA-imprinted hydrogel films, even after several washing steps with deionized water, Zhao *et al.* [9] reported that SDS remains a possible cause for total cell death of L929 cells after 5 days of culture. Optimization of molecular imprinting systems should also focus on improving the wash steps needed for template removal as the reagents can be toxic to cells.

Finally, depending on the final application of a MIP system, various polymerization methods can also be applied. These methods include bulk suspension, two-step swelling, precipitation, emulsion core-shell polymerization, film synthesis, aerosol polymerization and polymerization on silica-beads [48]. Bulk polymerization is the most widely used method by molecular imprinting groups, however it is used exclusively with organic solvents, and has the disadvantage of wasting a significant percentage of polymer produced in the process of grinding to obtain smaller irregular particles [48]. On the other hand, two-step polymerization requires an aqueous polymerization medium and produces monodispersed particles with control of the final size and number of particles [48]. Ideal molecular imprinting production methods should be controllable and reproducible. For instance, Ying *et al.* [49] developed a gas jetting-dropping method to produce beads of a controllable diameter in aqueous medium at a constant rate of production (600 mL/h). This possibility is very important when it comes to industrial applications for MIP materials.

1.3.3. Molecularly imprinted intelligent scaffolds

Molecular Imprinting can be a powerful tool used to create scaffolds with high bioactivity and recognition capacity to specific molecules. Recognition, neutralization and clearance of target peptides, such as toxin melittin, in the bloodstream has been achieved *in vivo* using

molecularly imprinted polymeric nanoparticles with binding affinity and selectivity comparable to that of natural antibodies [50]. Similarly, molecular imprinting can be applied during the construction of TE scaffolds with the ability to recognize and adsorb a biomolecule transported through the bloodstream, or present *in situ*, for ultimately promoting cell recruitment to the site of injury or to trigger specific cell behaviors.

For TE applications, biomacromolecules bear great relevance due to their involvement in the healing process. Increasing interest on the imprinting of macromolecules to exploit its potential for clinical and pharmaceutical applications has driven many research groups to develop protein MIP systems. The majority of protein MIP studies are usually developed for model macromolecules like lysozyme (Lyz), BSA and Hb. However, few studies use biomolecules of interest for TE technologies such as fibronectin (Fn). Fn, a high molecular weight protein (composed of two polypeptides of molecular ~220 kDa each) with adhesive activity, is present in the ECM and involved in several biological events, including wound healing and tissue repair [51]. Recent advancements in the protein molecular imprinting field can strongly impact regenerative medicine technologies through the use of molecular imprinted intelligent scaffolds [52].

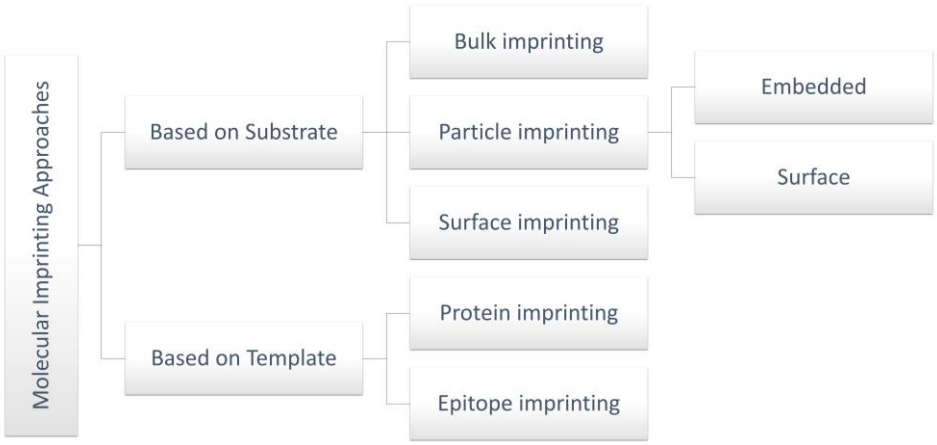

Figure 2. Molecular imprinting strategies for macromolecules. Molecular imprinting approaches can be divided according to the imprinted substrate they produce: bulk imprinting involves creating imprinting cavities in a material, namely in its inner layers (bulk); particle imprinting is based on the direct production of embedded- or surface-imprinted nano/microparticles; surface imprinting creates scaffolds which are only imprinted at the surface, or at the layers near it. Additionally, molecular imprinting approaches can be divided according to the type of template used, namely, in protein imprinting when the whole protein is used as a template, or in epitope imprinting when only relevant portions or domains of the molecule of interest are used.

Many imprinting strategies exist, although majority are successful when imprinting small molecules, but present several challenges for use with larger molecules such as proteins. **Fig. 2** represents the main molecular imprinting strategies for macromolecules divided into two categories: namely, according to either the substrate, or template type used.

1.3.3.4. Molecular imprinting mechanisms

Molecular Imprinting approaches can be classified according to the substrate imprinted and further sub-divided into bulk, particle or surface imprinting. Bulk imprinting is a rather successful strategy used for small molecules which involves imprinting cavities in the inner layers of a polymeric material. However, this strategy presents some challenges when addressing mass transfer, associated with the size of macromolecules. Usually, macromolecularly imprinted materials produced by this approach strongly retain their templates and require extensive grinding and sieving. This process to produces irregularly shaped polydisperse particles and shorter lengths of diffusional pathways [6, 53]. For protein MIP strategies, particle-based imprinting and surface imprinting are more commonly used. These are some of the most successful because they reduce the diffusion pathway length, promoting protein movement inside-out and outside-in. Not only does this lead to successful removal of the template and increasing the number of available binding sites, but also promotes protein rebinding by facilitating diffusion of proteins through the imprinted material. Particle-based strategies use polymerization methods, such as emulsion or suspension, to directly synthetize micro-/nanoparticles with the advantage of using lower quantities of monomers and template molecules [3]. However, this presents the drawback of using stabilizers and surfactants (which may cause the disruption of monomer-template complexes), since residual levels of stabilizers remain even after an extensive washing process [3]. Surface imprinting is the most common approach for protein MIPs, and consists of imprinting binding sites only at the surface or on the superficial layers. This approach is similar to bulk imprinting, with the difference being that surface imprinting is applied on thin films, or by attaching the protein on the surface of a substrate [3]. In addition to alleviating macromolecule transfer, surface imprinting enables the imprinting performance to be improved through the introduction of surface functional ligands. These ligands allow for interaction with the template protein by reversible covalent binding or affinity interactions, and by physical adsorption on the surface [54].

An alternative way to address the classification of molecular Imprinting of macromolecules is based on whether the whole protein is used during the imprinting process, or if only relevant domains (epitopes) are used (**Tab. 1**). Epitopes are small domains or sequences exposed in macromolecules that can be recognized by their receptors. Epitope imprinting uses small protein domains or sequences, as opposed to the whole protein, to create materials with molecular recognition towards proteins. This approach aims to overcome obstacles inherent to protein imprinting caused by size complexity, and conformational characteristics of proteins [3]. In the same way, a MIP can recognize a whole protein if previously imprinted with its epitope. Since these sequences can be synthetically produced, this approach also overcomes difficulties associated with obtaining pure template proteins [53]. Additionally, epitope imprinting can create highly selective scaffolds as reported by Zhao *et al.* [55] who developed Fe_3O_4 silica coated nanoparticles with high adsorption rates and high selectivity towards BSA by using a BSA-specific nonapeptide C-terminal amino-acid sequence as a template. The authors reported these MIPs to have low tolerance for single amino acid mismatch since a significant reduction of imprinting factor values were observed in MIPs imprinted with mismatched sequences of BSA, compared to MIPs imprinted with the original sequence [55]. The authors also reported better recognition features on epitope imprinted particles when compared to BSA imprinted particles [55]. This supports the idea that molecular imprinting can be used to create highly specific and selective systems at a sequence level.

Papaioannou *et al.* [56] reported promising results regarding epitope imprinting by producing a MIP for RGD (Arg-Gly-Asp tripeptide) recognition, based on non-covalent interactions. The RGD domain is known to be responsible for Fn adhesive activity [51]. RGD and Fn are frequently used to functionalize different types of substrates (*e.g.* alginate) to promote desirable cellular responses, either alone, or in combination with other bioactive molecules or sequences [57, 58]. This approach could be applied to several other biologically relevant domains or sequences. For instance, different domains of neural cell adhesion molecules (*e.g.* fibronectin type III motifs FGL and BCL) have been proven to interact with fibroblast growth factor (FGF) receptors, inducing neurite outgrowth in primary cerebellar granule neurons, promoting synaptogenesis and enhancing presynaptic function [63]. Wang *et al.* [64] produced a self-assembling $RADA_{16}$ peptide nanofiber hydrogel functionalized with FGL enabling it to promote spinal cord-derived neural stem cell proliferation and migration into the three-dimensional scaffold. These and other biologically relevant motifs, could be imprinted in a

Table 1. Recently developed systems on epitope imprinting of biomolecules.

Template	Functional Monomer(s)	Crosslinker	Solvents / Template removal agents	Competitors	Observations	Ref.
RGD	MAA AAm	TRIM MBAm EGDMA	Methanol / Methanol, AcOH	KGD, CCK-3 and CCK5 peptides, gramicidin	Production of polymers with different combinations of functional monomer and crosslinker. Higher IF and % net rebinding with MAA and TRIM. Selectivity achieved.	[56]
ANP	MAA NIPAm	MBAm	SDS / AcOH	BSA, scrambled ANP	MIPs presented higher adsorption capacity than NIPs nanoparticles. Selectivity achieved. MIP recognition capacity tested and verified in cell cultured media spiked with ANP.	[59]
IgG F_{ab} fragment	MAH	MBAm	DW	BSA, F_c fragment, IgG	Production of monolithic cryogels with direct and Cu(II) assisted MAH. Effect of pH, template concentration, temperature and flow rate on adsorption capacity was analyzed. MAH[Cu(II)]-assisted MIP with higher adsorption capacity. Selectivity achieved.	[60]
PPA	EGMPA	PEGDA, MBAm	DW / MeCN, NaOH, methanol	BA, DPP	Ti^{4+}-immobilized EGMPA. Higher adsorption capacity of MIPs than NIPs. Selectivity and regeneration achieved.	[61]
BSA C-terminal nonapeptide	APTES	TEOS	Methanol-MeCN-highly purified water, PBS / Methanol, AcOH	BHb, Cyt, HRP, Lyz	Fe_3O_4-silica coated nanoparticles. Better performance of epitope-imprinted than BSA-imprinted. Selectivity achieved at an amino acid sequence level. Good reusability performance.	[55]
L-Lysine	MAsp HEMA	PVA	DW, SDS, $NaHCO_3$ / DW, EtOH	HSA, Hb	Production of poly(HEMA-MASp) monodisperse imprinted nanoparticles. Recognition of IgG through F_c fragment obtained. IgG orientation preserved upon recognition. Selectivity achieved. Effect of pH on IgG adsorption analyzed. Good reusability performance.	[62]

AAm – acrylamide; AcOH – acetic acid; ANP – atrial natriuretic peptide; APTES – 3-aminopropyl triethoxysilicane; BA – benzoic acid; BHb – bovine hemoglobin; BSA – bovine serum albumin; Cyt – cytochrome c; DPP – diphenyl phosphate; DW – deionized water; EGDMA –ethylene glycol dimethacrylate; EGMPA – ethylene glycol methacrylate phosphate; HEMA – hydroxyethyl methacrylate; HRP – horseradish peroxidase; HSA – human serum albumin; IF – imprinting factor; Lyz – lysozyme; MAA – methacrylic acid; MAsp –N-methacryolyl-(L)-aspartic acid; MBAm – N,N'-methylenebisacrylamide; MAH – N-methacryoyl-L-histidine; MeCN – acetonitrile; NIPAm – N-isopropylacrylamide; PBS – phosphate buffered saline; PPA – phenylphosphonic acid; PEGDA – poly(ethylene glycol) diacrylate; PVA – poly(vinyl alcohol); RGD – Arg-Gly-Asp tripeptide; SDS – sodium dodecyl sulfate; TEOS – tetraethoxysilicane; TRIM – trimethylpropane trimethacrylate.

biocompatible polymer scaffold to promote molecular recognition and desired cell functions. High protein adsorption rates can occur in a biomaterial without any significant outcomes if proteins undergo conformational changes, or hide relevant functional groups upon adsorption, preventing cell adhesion to the scaffold. Using anti-BMP-2, a monoclonal antibody against bone morphogenetic protein 2 (a protein known to promote the osteodifferentiation of progenitor cells), Ansari *et al.* [65] reported the influence of orientation during protein immobilization (without imprinting) in scaffolds for bone repair. While using Protein G as a linker to immobilize the antibody through its Fc fragment on a collagen scaffold, the authors were able to achieve higher antibody binding to cells concomitant with increased bone formation *in vivo*, compared to passively adsorbing anti-BMP-2 antibodies to the same scaffolds [65]. This enhanced performance can be explained by the increase in the number of available binding sites for the anti-BMP-2 antibody to interact with its ligand. Protein orientation control has been achieved by epitope imprinting of L-lysine residues, typical of C-terminus of immunoglobulin G F_c fragment in poly(hydroxyethyl methacrylate-N-methacryolyl-(L)-aspartic acid) nanoparticles [62]. Corman *et al.* [62] reported higher human serum albumin (HSA) adsorption in particles previously imprinted with L-lysine residues and exposed to anti-HSA antibodies, when compared to non-imprinted nanoparticles, to which the antibodies randomly adsorbed. Molecular imprinting can therefore be a suitable strategy for the production of scaffolds with enhanced bioactivity consequent of an effective protein orientation upon adsorption, which will ultimately promote cell adhesion and behavior at the site of injury due to the existence of increased binding domains available.

One methodology which could further amplify potential applications of molecular imprinting are post-imprinting modifications (PIMs), by allowing the modulation of on/off switching of the molecular recognition, or the introduction of other desirable functions (such as transduction of binding events into fluorescence events) [66, 67]. PIMs can be used to improve imprinting features by the transformation of binding sites as reported by Taguchi *et al.* [37], who produced thin films with the ability to molecularly recognize cytochrome-c (Cyt) by generating peptide-fragment binding sites inside imprinted cavities. This was possible by using enzymatic digestion as the template removal strategy, where pepsin would digest Cyt at specific sites, leaving behind lysine residues grafted to the polymer backbone [37]. The authors reported high selectivity of these scaffolds towards Cyt as only enzyme-accessible regions of MIPs can be

transformed into protein-binding cavities, reducing the possibility of non-specific binding sites commonly left behind by other conventional removal processes [37].

1.4. Hydrogels for macromolecular imprinting

The use of hydrogels constitutes another promising approach to overcome molecular imprinting problems related to mass transfer of high molecular weight templates, and provide the additional possibility of creating sensitive systems which respond to external stimuli [5, 6]. Hydrogels have been widely explored for biomedical applications, including TE, due to their natural similarity to the ECM. Hydrogels are commonly used as drug carriers in pharmaceutical applications, and are useful tools to create controlled release systems.

Hydrogels are polymeric networks with high hydrophilicity, *i.e.*, they can absorb considerably high amounts of water, expanding their volume and promoting diffusion within their bulk [68]. They can be produced from natural or synthetic polymers, are chemically stable, have biodegradable capabilities, and perform interactions which are reversible, depending on the external stimuli applied (*e.g.* pH or temperature) [68]. Additionally, they can be processed to acquire different forms (*e.g.* coatings, capsules, microspheres, tubes or sheets) and functionalizations [58, 68], in order to improve their bioactivity.

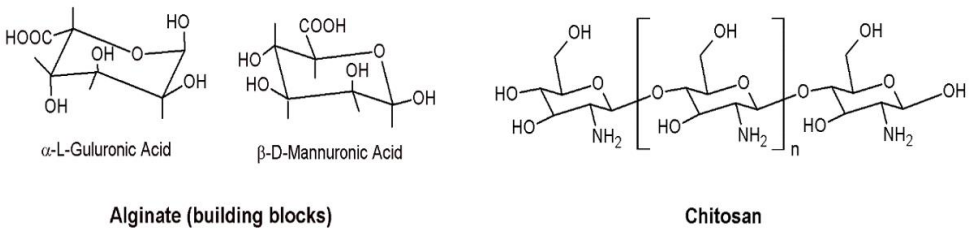

Figure 3. Molecular structure of alginate and chitosan building blocks.

Molecular imprinting within hydrogels may be more challenging than in rigid structures, owing to their inherent movement capacity [5]. Hydrogels can either expand or collapse easily,

deeply affecting the imprinting efficiency by distortion of binding sites. So far, most studies using molecular imprinting in hydrogels are intended to develop drug delivery systems with high loading capacity and to improve controlled release [1, 5]. Nevertheless, several considerations are taken into account for these systems and can be applied for TE applications. This section will be focused on molecular imprinting using natural functional monomers, namely alginate and chitosan (**Fig. 3**), due to their common use and great potential in TE applications.

1.4.1. Alginates and alginate composite polymeric hydrogels

Molecular imprinting studies in alginate hydrogels have been performed using Fn and the model protein BSA (**Tab. 2**). Alginates are water soluble linear polysaccharides derived from brown seaweed, composed of alternating blocks of 1-4 linked α-L-guluronic and β-D-mannuronic acid residues [69]. Along with their great biocompatibility and biodegradability, alginates have the ability to form gels with good mechanical properties by reacting with divalent cations [69]. Alginates enable the production of various platforms for biomedical applications [70], including the development of alginate microspheres for growth factor delivery, such as bioactive VEGF to promote osteogenic differentiation [71].

Significant work using sodium alginate as a functional monomer to create BSA-MIP has been performed by Zhao and co-workers [9, 44, 72-75]. This group uses an inverse suspension-method and ionic gelation to develop MIPs under mild conditions to avoid protein denaturation. Furthermore, Zhao and co-workers frequently conjugate alginate with phosphate groups by adding diammonium phosphate [$(NH_4)_2HPO_4$, DAP], creating composite hydrogels with improved imprinting features [44, 72, 74, 75]. The addition of phosphates into alginate matrices combines the functionality of organic compounds with the stability of inorganic compounds [72].

In addition to developing heteropolymeric systems based on both natural and synthetic polymers (where alginate is combined with acrylamide (AAm) and sodium polyacrylate [9, 73-75]) to improve mechanical and imprinting properties of the final MIP, the group has developed MIPs fully based on synthetic polymers [76]. Throughout some of these studies [44, 72, 74, 75], the authors compared imprinting parameters (adsorption capacity and imprinting effect) of

Table 2. Molecularly imprinted polymers (MIPs) developed with natural polymers, namely alginate, chitosan, and other synthetic polymers.

Template	Functional Monomer(s)	Crosslinker	Solvents / Template Removal Agents	Competitor (s)	Observations	Ref.
Hb	CS, AAm	MBAm	Sodium phosphate buffer / SDS, AcOH	BSA	Macroporous CS beads used as a matrix to improve mechanical and chemical properties of polyacrylamide as this latter polymer would fill the macroporous of the beads, forming a two-phase structure. Adsorption dynamic curve shows an initial rapid adsorption of Hb to MIPs, followed by a plateau where adsorption is slowed down, indicating rapid protein adsorption onto the surface at the beginning that difficults further Hb penetration into the bead. Selectivity tests performed with BSA showed high selectivity of the MIPs towards Hb. Good stability and reproducibility of the MIP were achieved.	[12]
Hb	CS, Am	MBAm	Sodium phosphate buffer / SDS, AcOH	BSA	Phase-inversion method. Chitosan beads primarily produced as in [12]. A graft-MIPs was produced by graft copolymerization of CS beads and AAm. Adsorption patterns of Hb similar to the ones obtained in [12]. Selectivity tests performed with BSA showed high selectivity of the MIPs towards Hb. Good stability and reproducibility of the MIPs achieved.	[13]
Hb	CS, Am	MBAm	Sodium phosphate buffer / SDS, AcOH	BSA	Comparison between MIPs produced similarly to [12] and [13]. graft-MIPs showed better adsorption capacity but lower selectivity than MIPs alone towards the template Hb. The authors justified this by the fact that in graft-MIPs, PAAm chains grow vertically out of the surface of the CS beads (faster adsorption due to easier access to binding sites) but do not to stabilize their spatial shape, losing molecular memory.	[14]
Hb	CS, Am	MBAm	Sodium phosphate buffer / SDS, AcOH	BSA	Hydrogels based on semi-interpenetrating polymer networks (MIH-s-IPNs) were produced with CS and PAAm to improve mechanical properties. MIH-s-IPNs contained high water content (~94%). MIH-s-IPNs adsorption capacity was significantly higher than MIPs composed of PAAm alone. Selectivity analysis showed that MIH-s-IPNs had high selectivity towards the template. Analysis of the effects of temperature on water retaining of the hydrogel carried.	[39]
Hb	CS, AAm	MBAm	Phosphate buffer / SDS, AcOH	BSA, My, α-C, Lyz	CS-coated silica particles were used to covalently immobilize the template molecule while PAAm was used to perform the imprinting. Adsorption capacity of MIPs was lower than NIP but MIP presented higher selectivity both with single-compound and mixed solutions.	[77]
Ova	SA, CS	GTA	Phosphate buffer / NaCl	BSA, Hb, Lyz	SA coated Fe_3O_4 magnetic nanoparticles were produced with a CS imprinted shell. SA to CS mass ratio influenced the imprinting effect, with 1:2 exhibiting higher adsorption capacity and imprinting efficiency. MIPs presented high selectivity towards Ova and good reusability profile. Different MIPs were also produced using BSA, Hb and Lyz as template molecules and selectivity achieved.	[15]
BSA	SA	$CaCl_2$	Chloroform, hexane, Span85 and Tween80 / DW		Production of SMIPMs and EMIPMs. DAP was introduced to add phosphate groups to the polymer matrix (composite microspheres). Qe and IE tested for different concentrations of DAP, $CaCl_2$ and SA and optimum Qe results were obtained at 0.15% DAP, 5% $CaCl_2$ and 2.5% SA for SMIPMs. Qe(SMIPMs)> Qe(EMIPMs) and IESMIPMs> IEEMIPMs.	[44]

BSA	SA, SPA	CaCl2	Castor oil, butyl acetate / CaCl2, Tris-HCl buffer	———	Production of SMIPMs and EMIPMs. DAP was introduced to add phosphate groups to the polymer matrix (composite microspheres). Qe(SMIPMs)> Qe(EMIPMs) and IE(SMIPMs)> IE(EMIPMs) until 180 mins of rebinding time.	[74]
BSA	SA	CaCl2	Chloroform, hexane, Span85 and Tween80 / CaCl2,Tris-HCl buffer	Hb, Lyz, Glo, EAB	Production of SMIPMs and EMIPMs. DAP was introduced to add phosphate groups to the polymer matrix (composite microspheres). Qe(SMIPMs)> Qe(EMIPMs) and IESMIPMs> IEEMIPMs. Effect of CaCl2 and BSA concentrations and pH values on Qe and EI tested. MIP presented high selectivity towards BSA even though Lyz was also highly adsorbed due to smaller size which facilitated diffusion through the MIPs.	[72]
BSA	SA, SPA	CaCl2	Castor oil, butyl acetate ethylic cellulose / CaCl2,Tris-HCl buffer	Lyz, Hb, Glo, EAB	Production of multi-hybrid polymer microspheres. Qe and IE tested for different concentrations of CaCl2. MIPs presented higher adsorption capacity than NIP and selectivity towards BSA. Lyz was also highly adsorbed due to smaller size which facilitated diffusion through the MIPs.	[73]
BSA	SA, SPA	CaCl2	Castor oil, butyl acetate / CaCl2,Tris-HCl buffer	Hb, Lyz, EAB	Production of SMIPMs and EMIPMs. DAP was introduced to add phosphate groups to the polymer matrix (composite microspheres). Qe(EMIPMs)> Qe(SMIPMs) and IEEMIPMs> IESMIPMs IEEMIPMs. Qe and IE tested for different concentrations of CaCl2 and BSA and pH values.	[75]
BSA	SA, AAm	MBAm CaCl2	DW / HAc containing SDS	Hb, Ova, Glo	Hydrogel film. Ionic crosslinking and covalent crosslinking. Different AAm/SA ratios (6:1, 8:1, 10:1 and 12:1) tested. Better Qe and IE at 6:1 ratio. Different MBAm and CaCl2 concentrations tested. Effect of thickness on imprinting performance tested. High adsorption capacity of MIPs was reduced with increasing thickness. Adhesion tests with mouse fibroblast cells (L929). MIPs promoted cell adhesion but residual SDS was believed to be the reason for cell death after 5 days of culture. Selectivity was achieved.	[9]
BSA	SA	CaCl2	DW / CaCl2, Tris-HCl buffer	Ova	Description of gas jetting-dropping (GJD) method for production, with controlled dropping speed and droplet dimension as diameter and volume of alginate microspheres is indirectly proportional do nitrogen pressure. Smaller diameters can be achieved with GJD method that gravitational method but morphology can be affected at higher pressure levels. MIPs presented higher adsorption capacity than NIPs. Differences in diameters lead to differences in rebinding properties: smaller microspheres show better Qe and IE and selectivity increased with diameter of MIPs.	[49]
BSA	SA, PU	CaCl2	DW / CaCl2, Tris-HCl buffer	Ova	2-step process where PU-grafted calcium alginate (PU-g-CA) hydrogel microspheres were initially produced, followed by an imprinting process which occurred under ionic gelation with CaCl2 to avoid protein denaturation. Grafting process improved mechanical strength of matrix and leads to rougher surface (comparing to calcium alginate beads). MIP presented higher adsorption capacity than NIPs. Rebinding capacity was seriously affected by pH of polymer assembly solutions and by external pH of template solution. Both BSA-MIPs Ova-MIPs were produced and selectivity was achieved.	[78]
BSA	SA	CaCl2	DW / CaCl2, Tris-HCl buffer	Ova, HSA, Hb	Production of hydrogel film by biocompatible gelation method in aqueous media, intended for biomedical applications. Higher adsorption capacity of MIPs achieved but no selectivity.	[79]
BSA	SA	CaCl2	DW / CaCl2, Tris-HCl buffer	———	Production of hydrogel microcapsules by biocompatible gelation method in aqueous media, intended for biomedical applications. Analysis of different template removal protocols on the percentage of recovered template and recognition capacity of the MIPs.	[80]
BSA	SA	CaCl2 GTA	DW / Tris-HCl buffer	———	Production of semi-interpenetrating polymer networks containing SA and HEC to improve mechanical stability. Dual crosslinked microspheres presented lower water uptake over time. Adsorption capacity higher in SA/HEC microspheres than SA alone.	[81]

Fn	SA, AAm	MBAm	DW / Tris-HCl buffer	———	Non-woven PP fiber used as support for MIP. Lamellar macroporous structure at the surface which facilitated diffusion of template. Fn adsorption 2.6 times higher on MIP than NIP. Cell adhesion tests were performed with L929 cells. Higher cell adhesion rates and higher number of living cells on MIP than NIP. Cell morphology analysis showed cell spreading on MIP surface.	[82]
BSA	NIPA, [VAFMIM]Cl	MBAm	Tris-HCl buffer / NaCl solution	Ova, Lyz, Hb	Thermosensitive hydrogel system capable of reversible volume transition between shrinking and swelling according external stimuli. Effects of two different drying methods in morphology and mechanical properties analysed. Analysis of the effect of functional monomer on BSA stability. Analysis of the influence of BSA, [VAFMIM]Cl and MBA in recognition capacity. Higher adsorption capacity of MIPs than NIPs. Selectivity achieved.	[83]
BSA	AAm	MBAm	DW / SDS, AcOH	Hb, Ova, Glo, Lyz	Production of hydrogel membrane using non-woven PP fiber. UV radiation-reduced graft polymerization. Effect of monomer concentration, cross-linker concentration, amount of template molecule and pH in BSA solution on Qe and IE tested. Higher adsorption capacity of PP-grafted-PAAm-MIPs than NIPs and improved regeneration properties than PAAm-MIP beads. Selectivity achieved.	[76]
Hb	AAm	MBAm	Phosphate buffer / SDS, AcOH	Lyz, EAB, Pep, Pap, Try	Silica coated magnetic (Fe3O4) nanospheres functionalized with MAPS to add vinyl groups served as substrate for the imprinting process. Higher adsorption capacity of MIPs than NIPs. Selectivity achieved. Good regeneration and reproducibility features.	[84]
BSA	AAm	MBAm	Phosphate buffer / SDS, AcOH	Lyz, Lac, Glo	Higher adsorption capacity of MIPs than NIPs. Analysis of the influence of crosslinking density, polymerizing temperature, protein type and BSA amount on imprinting efficiency. Selectivity analyzed and achieved for BSA-MIPs. Regeneration was not achieved.	[85]
Hb	AAm	MBAm	RO water / SDS, AcOH or Trypsin solution	Cyt, Myo	Higher adsorption capacity of MIPs than NIPs. Different template removal strategies analyzed, including varying ratios of SDS:AcOH and enzymatic digestion with trypsin. Optimum ratio SDS:AcOH at 10%(w/v):10%(v/v) with 48% template removal and more than 90% imprinting efficiency. Trypsin treatment achieved high template removal (up to 84%) but low imprinting efficiency (20%). Selectivity achieved.	[47]
Lyz	AAm MAA	MBAm	Tris buffer / DW, NaCl solution	Cyt, BSA	Different ratios of crosslinker, PAAm and MAA analyzed. Effect of NaCl on binding activity towards the template.	[41]

AA – acrylic acid; AAm – acrylamide; AcOH – acetic acid; AMPS – 2-acrylamido-2-methyl-propanosulfonic acid; APTES – 3-aminopropyl triethoxysilane; BSA – bovine serum albumin; CaCl2 – calcium chloride; CS – chitosan; Cyt – cytochrome c; DAP – Diammonium phosphate (NH4)2HPO4; DW – deionized water; EAB – egg albumin; ECH – ephichlorohydrin; EMIPMs – embedded molecularly imprinted polymer microspheres; Fn – fibronectin; Glo – γ-globulin; HAc – anhydrous acetic acid; Hb – hemoglobin; HSA – human serum albumin; g-MIP – grafted-molecularly imprinted polymer; HEC – hydroxyethyl cellulose; HSA – human serum albumin; Lac – α-lactalbumin; Lyz – lysozyme; MAA – methacrylic acid; MAH – maleic anhydride; MAPS – 3-methacryloxypropyl trimethoxysilane; MBAm – N,N'-methylenebisacrylamide; MIP – molecularly imprinted polymer; Myo – myoglobulin; NIP – non-molecularly imprinted polymer; NIPA – N-isopropylacrylamide; Ova - ovalbumin; PAAm – poly(acrylamide); Pap – papain; Pep – pepsin; PP – polypropylene; PU – polyurethane; SA – sodium algiante; SDS – sodium dodecyl sulfate; SMIPMs – surface molecularly imprinted polymer microspheres; SPA – sodium polyacrylate; TEOS – tetraethoxysilicane; Try – trypsin; [VAF- MIM]Cl – 1-vinyl-3-aminoformylmethyl imidazolium chloride.

alginate embedded MIP microspheres (EMIPMs) and surface MIP microspheres (SMIPMs) using BSA as the template molecule. Preparation methods for these approaches differ on the timing and the amount of template added. Despite SMIPMs requiring lower template concentrations during the molecular imprinting process, the microspheres usually present increased imprinting performance compared to EMIPMs [44, 72, 74, 75]. This is easily explained since EMIPMs face mass transfer problems inherent to bulk imprinted approaches. A practical application of these natural polymer-based microspheres is as building blocks for TE scaffolds, specifically in bottom-up approaches, to improve protein loading within the scaffold [86]. As the majority of template molecules of interest for TE applications are expensive and difficult to obtain in high rates of purification, it is important to mind cost/efficiency ratio, which will dictate production viability and market diffusion of any biomedical product.

A problem encountered by many of the previously cited works is the use of cytotoxic compounds as solvents or template removal agents (*e.g.* SDS) which may impair the application of these systems for TE. However, the development of more biocompatible systems for biomedical and food industry applications is the subject of continuing research. Peppas and co-workers [79, 80] have developed molecular imprinting methodologies for biomedical purposes using alginate and calcium chloride. Herrero *et al.* [80] developed a biocompatible system with the ability to achieve 3.0 mg of BSA per gram of capsules, compared to 0.7 mg achieved via inverse suspension by Zhao *et al.* [72], without using any chemicals besides sodium alginate and calcium chloride. These results are promising and are the first steps towards optimization of protein molecular imprinting systems for delivery and implantation in the human body.

The potential of alginate imprinted systems for generating platforms for cell culture studies has been previously investigated. Zhu *et al.* [82] recently created a Fn-imprinted alginate/polyacrylamide (PAAm) hydrogel, supported by a polypropylene non-woven scaffold, which promoted Fn adsorption in addition to adhesion and spreading of mouse fibroblast cells (L929). The combination of more than one functional monomer is a widely used methodology to improve imprinting efficiency. This increases the number of potential binding sites available for the template, and improves physical and chemical characteristics (*e.g.* swelling behavior or mechanical stability) of molecularly imprinted hydrogels. In this particular case of alginate/PAAm, an improvement in mechanical and elastic properties of the combined polymer systems was reported [87]. Alginate/PAAm scaffolds have also proven to be suitable platforms to support human stem cell proliferation and chondrogenesis [87]. An additional study, also

based on the imprinting of Fn, was developed by Fukazawa *et al.* [88] who created a Fn-MIP system based on a water soluble biocompatible phospholipid polymer constituted by 2-methacryloyloxyethyl phosphorylcholine (MPC). MPC is a biocompatible polymer unfavorable for protein adsorption, thus frequently used as a coating to achieve antithrombogenicity for medical devices [88]. Using silica beads with adsorbed Fn to create protein stamps, cavities with high selectivity to Fn were imprinted on the polymer, creating a cell capturing system with low rates of nonspecific adsorption [88]. Cell adhesion tests performed with L929 cells, the authors proved that cells only adhered in the bead cavities where Fn had been imprinted, and not on the surface of the non-imprinted polymer (NIP). This approach has the potential to be applied as a cell patterning technique by designing scaffolds with precise control of local cell adhesion [89].

1.4.2. Chitosan and chitosan composite hydrogels

Another widely used polymer is chitosan, a natural polysaccharide obtained from the deacetylation of chitin from the exoskeleton of crustaceans. It has been widely explored for biomedical applications due to its abundant source, biocompatibility and biodegradability [90]. Chitosan amino and hydroxyl groups make it possible to interact with different protein regions through van der Waals interactions, hydrogen bonding and hydrophobic interactions [90]. Chitosan has already been used as a functional monomer for molecular imprinting of low molecular weight molecules such as dye adsorption, enantioselective separation of amino acids, metal ions removal in decontamination activities, and some chemical/pharmaceutical applications [91-96]. A MIP sensitive system was reported by Singh *et al.* [92] who created a hydrogel system sensitive to pH, temperature and ionic strength with molecular recognition to carnosine, a dipeptide highly concentrated in muscle and brain tissues with reported antioxidant properties [92]. However, for macromolecular imprinting, most studies performed with chitosan combine this polymer with synthetic monomers (*e.g.* PAAm or 2-hydroxyethyl methacrylate) or use modified chitosan (**Tab. 2**).

Chitosan is commonly used to improve mechanical properties of other polymeric materials during the molecular imprinting processes. Guo and co-workers [12-14, 39, 77] developed several studies focusing on chitosan-based matrices for Hb recognition for biosensing applications. In most of these studies, chitosan is combined with epichlorhydrin, a water soluble

crosslinker that preserves the cationic amine function of chitosan and improves its wet strength, to produce beads which are used as a matrix for acrylamide monomers during the molecular imprinting process [12-14]. Guo *et al.* [13] reported a chemical modification of porous chitosan beads by adding maleic anhydride groups to improve chitosan bonding to AAm. This modification increased vertical growth of PAAm chains from the surface of the beads, leading to higher protein adsorption rates, but lower selectivity towards the template molecule since the geometry of cavities could not be successfully preserved [13]. Later, Xia *et al.* [39] developed a Hb-imprinted semi-interpenetrating polymer network in an aqueous medium by combining chitosan and AAm. The MIP produced revealed high capacity to retain water, and higher adsorption and selectivity when compared to molecular imprinting hydrogels made only of PAAm [39]. Nevertheless, there is evidence of significant non-specific binding of imprinted chitosan/PAAm polymers [97]. Fu *et al.* [97] analyzed different conditions where BSA and Hb-imprinted polymers showed increased recognition when compared to non-imprinted polymers, but in much higher quantities than those used as a template during MIP synthesis. This behavior was hardly explained, since the yield in binding sites relative to the amount of imprinting molecule should be low [97]. When washing non-imprinted polymers the same way as MIPs (*i.e.*, including template removal solutions), the authors found that NIPs presented an increase in protein binding which was comparable to MIPs [97]. Therefore, all procedures, with the exception of template addition, should be equally performed on the controls as they are for imprinted polymers in order to assure chemical changes promoted by solvents are taken into account when both materials are compared. Very few studies are performed solely on AAm as a functional monomer [47, 85] despite its great biocompatibility. Combining AAm with other functional monomers has been shown to improve mechanical properties and imprinting features of the matrix when comparing separate functional monomers [9, 12-14, 39].

Dan *et al.* [90] studied different copolymerization systems for chitosan and other synthetic polymers at different pH values and temperatures for the recognition of ovalbumin. Copolymers composed of chitosan and methacrylic acid showed increased imprinting features and selectivity at different pH and temperature levels [90]. Gao *et al.* [15] recently reported a MIP system conjugated with alginate and chitosan to improve imprinting features of a magnetite (Fe_3O_4) nanoparticles-based system for molecular recognition of ovalbumin. With a two-step method, the authors modified Fe_3O_4 nanoparticles with sodium alginate to attract chitosan onto the surface (since these polysaccharides are oppositely charged) and promoted polymerization to

create a molecularly imprinted shell around the particles. The imprinting effect was reported to be dependent on the alginate to chitosan mass ratio, with 1:2 exhibiting the best adsorption capacity and imprinting efficiency values towards ovalbumin [15]. The authors also showed that this system was highly selective towards different template molecules, including ovalbumin, BSA, Hb and Lyz [15]. The existence of oppositely charged functional groups, carboxyl and hydroxyl groups from alginates, and amine groups from chitosan, may have promoted the imprinting effect as they support interactions between the polymer matrix and the differently charged domains of these proteins.

1.5. Cell imprinting

Molecular imprinting principles for macromolecules can be applied for the imprinting of larger templates such as cells. Cell imprinting has been vaguely explored, but is based on the imprinting of morphological and topographic features of cells to improve cell adhesion in/on a substrate. To program mammalian cell adhesion and growth, DePorter *et al.* [98] proposed a cell-imprinting approach to produce a culture system as an alternative to the conventional high cost, multi-step fabrication processes. The authors successfully imprinted substrates by casting a PAAm gel on pre-fixed (4% formaldehyde/PBS) monolayers of HeLa, HEK-293T (epithelial-like cells) and MRC-9 (fibroblast-like cells) cells. Although cell viability was maintained, there is room for improvement. Adhesion experiments revealed that HEK-293T and MRC-9 cells adhered preferentially to epithelial-like imprinted surfaces, with MRC-9 cells losing their fibroblast-like morphology features, and HeLa cells adhering to all imprinted-substrates [98]. Jeon *et al.* [99] developed a PDMS imprinted surface using MG63 osteoblast-like cells (as a template) fixed with glutaraldehyde at the proliferation stage. The group used an electric field assisted casting method during different culturing times and showed that rough surfaces promoted cell viability and increased alkaline phosphatase activity and mineralization [99].

Currently, cell imprinting is at its early stages, and more studies need to be performed to further explore its applications and influences on various cell functions. Further investigation of this topic would lead to an understanding if this technology is feasible and reproducible compared to existing technologies for cell patterning and culturing.

1.6. Future prospects for molecular imprinting

Molecular imprinting is a technology with the potential to be applied for biomedical applications, such as tissue engineering. Even though little work has been developed on biologically relevant macromolecules for TE applications, studies performed on model proteins are a helpful platform to optimize molecular imprinting systems. One can expect molecular imprinting technologies to evolve for more biocompatible production approaches, which will enable cell growth and survival. Mild conditions to avoid protein denaturation are required during molecular imprinting, and all cytotoxic components should be avoided without compromising imprinting features, something already achieved. Additionally, more systematic and reproducible technologies with greater control of imprinting parameters and molecularly imprinted polymer (MIP) structure (*e.g.*, beads diameter or porosity) will present greater industrial viability. Once solved, these key aspects will undoubtedly catapult the use of molecular imprinting with living organisms and biomedical applications. Some additional aspects of biopolymer polymeric design have been recently discussed by Peppas and Clegg [100].

Molecular imprinting will especially be relevant for scaffold-based strategies (**Fig. 4**) as they depend on scaffold bioactivity to modulate cell activity in situ. As previously mentioned, scaffold-based approaches rely on the knowledge of the extracellular matrix as an important source of signals to cells and the maintenance of ECM homeostasis. Developing a scaffold with molecular recognition capabilities, enables MIP technologies to not only promote loading capacity of MIPs, but to promote recognition of a specific molecule in a complex mixture of biological compounds (a real scenario all implants face when introduced in the organism) (**Fig.4A**). The latter option brings a new set of possibilities for scaffold-based strategies, since the majority of conventional methods rely on the delivery of previously immobilized factors. Besides poor loading capacity, these methods have therapeutic efficacy impaired as protein conformation changes due to immobilization methods. Molecular imprinting systems can be optimized to overcome these problems as research performed in the protein template area proceeds. As adsorption capacity and selectivity are essential to dictate the success of a MIP-based based technology, if any major conformational changes were to occur during the production process, basic imprinting features would be compromised, and the MIP would

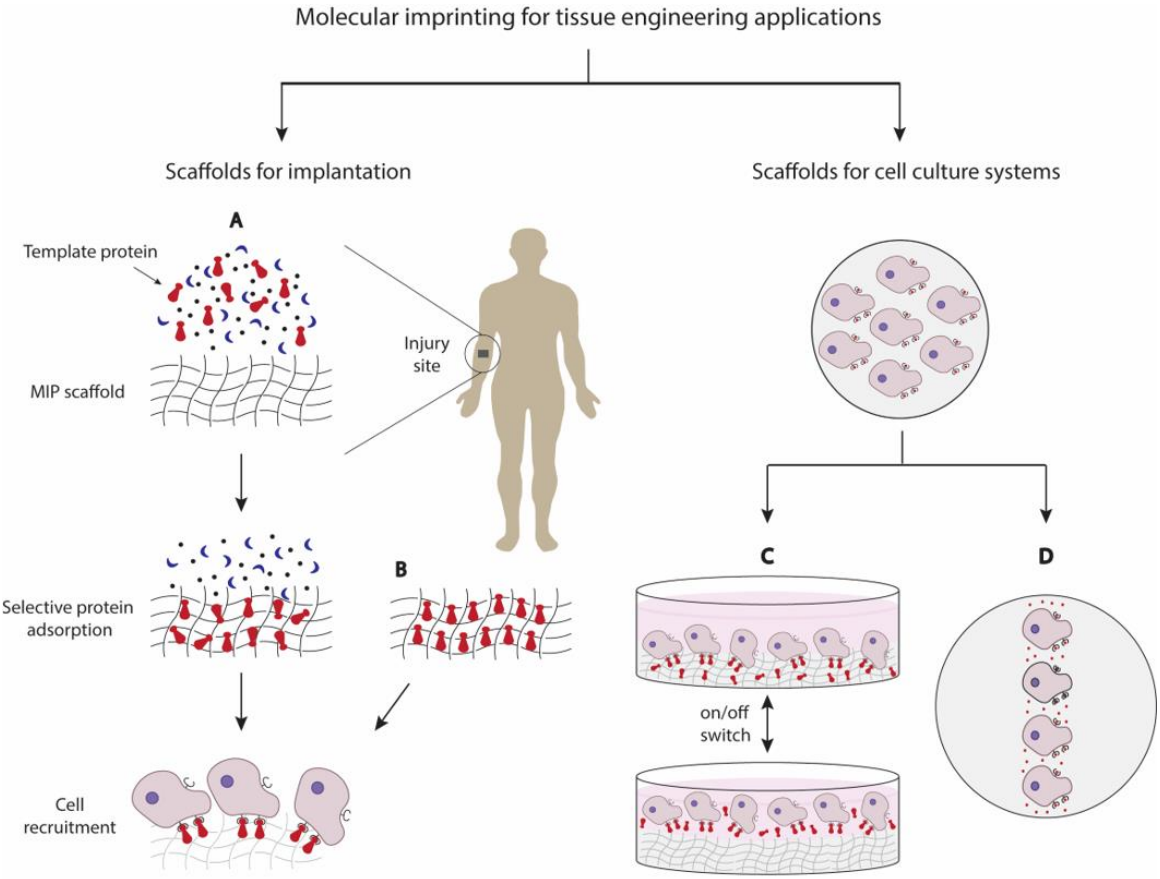

Figure 4. Applications of molecular imprinting in tissue engineering (TE). Molecular imprinting of proteins can support TE approaches, especially scaffold-based bottom-up strategies on the development of cell instructive scaffolds for implantation, or for cell culture systems. Regarding scaffolds for implantation, scaffolds produced by molecular imprinting are capable of selectively recognizing and adsorbing a macromolecule within a complex mixture of biological compounds present at the injury site. As a result of the molecular memory imprinting process (**A**), cell recruitment can be promoted as a final outcome. Molecular imprinting technologies enable the production of scaffolds with high loading capacity of the template molecule and/or control of protein orientation upon adsorption. In addition, the number of active binding sites for protein-ligand interactions can be increased and may favor cell recruitment upon implantation (**B**). Scaffolds produced by molecular imprinting can also be used for cell culture systems. Post-imprinting modifications give rise to a wide variety of functions which may be used to study cell behavior. Such modifications can be explored for cell sheet technologies where the performance of post-modifications may promote an increase (on) or decrease (off) of the recognition capacity (**C**). Another possibility is to use molecular imprinting as a cell patterning technique (**D**), where cell adhesion only occurs on molecularly imprinted regions of a scaffold. Nevertheless, these scaffolds can also be of great value for some cell-based TE approaches as they may require cell or tissue expansion *in vitro*.

present no major differences from a non-imprinted polymer. Epitope imprinting approaches can also be an alternative to minimize these effects, as they are less prone to conformational changes by their significantly lower complexity and size, with the additional advantage of promoting correct protein orientation, thereby increasing scaffold bioactivity as more protein binding sites are available for interaction with cell receptors (**Fig. 4B**).Several biomolecules can be used as a template for developing scaffolds for regenerative medicine applications. Growth inducing cytokines, peptides and proteins, including bone morphogenetic proteins (BMPs), transforming growth factor beta (TGF-β), vascular growth factor (VEGF), fibroblast growth factor (FGF), platelet derived growth factor (PDGF), insulin-like growth factor (IGF) and stromal derived growth factor (SDF1) have generated interest by their roles in the wound healing processes. Additionally, ECM molecules such as Fn can be successfully imprinted to promote cell adhesion on/in scaffolds. Once molecularly imprinted with these molecules, scaffolds can be implanted at the site of injury and adsorb the template molecule at higher rates than other compounds, promoting cell binding to the adsorbed proteins, which will consequently lead to a specific cellular response. MIPs have been shown to selectively adsorb template molecules when in a complex solution and promote cell adhesion, prospecting the potential application for scaffolds capable to attract the template molecule *in situ* and trigger a specific cell behavior. An application of molecular imprinting for the near future will definitely go through cell culture systems *in vitro*. Post-imprinting modifications allow further versatility of MIP scaffolds enabling an on/off switch of the binding recognition, a feature which can be suitable for cell sheet technologies (**Fig. 4C**). MIPs can also be considered for cell patterning techniques, as cell adhesion can be controlled by the imprinted and non-imprinted regions (**Fig. 4D**).

Hydrogels present themselves as suitable solutions to overcome current drawbacks in molecular imprinting of bio-macromolecules due to the inherent characteristics and tunable mechanical and chemical properties of these biomaterials. Similarly to other functionalization techniques, several natural and synthetic biomaterials, or their combinations, have been characterized in the literature for the production of MIPs with promising results. The possibility of utilizing different polymerization and production methods in mild and biocompatible conditions (without compromising imprinting features) gives rise to the potential of developing molecularly imprinted hydrogels on the design of highly precise bottom-up strategies for the production of scaffolds with improved bioactivity.

Another imprinting strategy is cell imprinting, a technology currently at its early stages, but presents itself as a dauntless new perspective. Nevertheless, the imprinting of cells is an untapped molecular imprinting approach which is the topic of continuing research.

Chapter 2
Aim of the Project

The overall aim of the project presented herein was to develop and characterize an alginate-based molecularly imprinted system for potential biomedical applications.

More precisely, this project intended to create a system based on photocrosslinkable alginate discs for the recognition of the model protein bovine serum albumin. The choice of this protein as the template is justified by the primary need to characterize and understand the effect of particular parameters in this new system. For that purpose, the first specific objective of this project was to develop and optimize a protocol to create a photocrosslinkable polymer based on the modification of alginate, replacing its functional groups by photosensitive methacrylate groups. Secondly, this project aimed at evaluating how this new material was affected by different production parameters (UV exposure time and disc thickness) and external stimuli (pH and presence or absence of salts) which could influence the molecular imprinting process. To do so, molecularly imprinted polymers were produced and a template removal protocol was optimized by adapting the effect of different variables of the system. Also, different protein quantification methodologies were tested to evaluate the system.

Finally, the capacity of these discs to specifically recognize the template molecule was evaluated by rebinding assays as a proof of concept.

- *This page was intentionally left in blank* -

Chapter 3
Materials and Methods

The principal objective of this project was the development of a molecular imprinting protocol in a photosensitive alginate-based system. To accomplish this, different stages of the production process had to be optimized according to different parameters (**Fig. 5**).

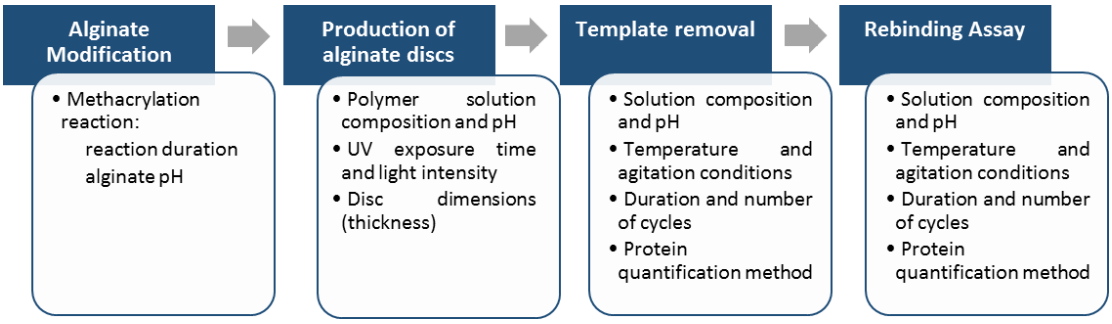

Figure 5. The four main stages of development of this project.

3.1. Alginate Methacrylation

Methacrylation of alginate was performed by replacement of hydroxyl groups by methacrylate groups. A 1% w/v alginate (AL, PRONOVA UP MVG, 248.13 kDA, Novamatrix) solution was produced by dissolving alginate in a Tris Buffered Saline (TBS, pH 8) solution.

Alginate methacrylation was performed for 5, 10 or 24h by adding methacrylic anhydride (MA, 154.16 g/mol, Sigma-Aldrich, **Fig. 6**) to the alginate solution in a total proportion of 1 g AL/15 mL MA (0.07 g/mL). MA additions were performed at three different timepoints (0, 1 and 3h or 0, 3 and 6h). The solution was maintained in ice and 5M NaOH (VWR) was added dropwise during methacrylation to keep pH=8. The reaction between MA and the alginate solution is exothermic and MA hydrolyzes at pH levels lower than 8 and high temperature. To stop the reaction 100% EtOH (4^{o}C) was added in excess to promote polymer precipitation and the pellet was left to dry overnight. Rehydration of the pellet was performed by adding deionized (DI) water under magnetic agitation. Dialysis was performed against DI water for 3 days using dialysis membranes (Spectra/Por 3 Dialysis, MWCO 3.5 kDa). After dialysis, the pH of methacrylated alginate (ALMA) solutions was adjusted to 5 (ALMA 5) or 7 (ALMA 7) using HCl or NaOH solutions, respectively. The final solutions were frozen at -20^{o}C and lyophilized (Virtris BenchTop Pro 9 L -85^{o}C, SP-Scientific). All the procedure was performed protecting samples from light using aluminum foil.

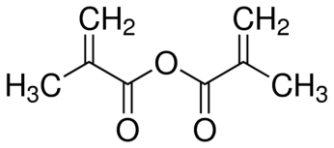

Figure 6. Molecular structure of methacrylic anhydride [101].

3.2. ^{1}H NMR analysis

Unmodified and methacrylated alginates ALMA 5 and ALMA 7 were dissolved in deuterium oxide (D2O, Sigma-Aldrich) to produce a 1% w/v solution at 4^{o}C overnight. 5 µl of 3-(trimethylsilyl)propionic-2,2,3,3-d4 acid sodium salt (TSP-d4, Euriso-top) were added to the solution as internal standard. The ^{1}H NMR spectra were recorded on a BRUKER AVANCE III (400 MHz, 9.4 Tesla) NMR spectrometer (CEMUP, University of Porto, Portugal). The degree of methacrylation (DM) was calculated from ^{1}H NMR spectra based on the ratio of the integrals from the protons of alginate backbone to the protons of methacrylate compound. The final DM

was determined as an average of ALMA 5 DM and ALMA 7 DM values determined by the following equation (3)

$$DM\ (\%) = \frac{Average\ (\frac{H_a}{3} + \frac{H_b + H_c}{2})}{\frac{HAA}{6}} \quad (3)$$

3.3. Production of methacrylated alginate non-imprinted and molecularly imprinted discs

Alginate discs were produced from methacrylated alginate ALMA 5 and ALMA 7 using photo-polymerization with UV light. A 0.05% w/v photoinitiator solution was prepared by dissolving 2-hydroxy-1-[4-(hydroxyethoxy)phenyl]-2-methyl-1-propanone (Irgacure 2959, Sigma-Aldrich) in 0.9% NaCl at pH 4.2. Irgacure 2959 (**Fig. 7**) is a moderately water-soluble photoinitiator and was selected for this protocol since it has been reported to cause minimal cellular toxicity in a wide range of mammalian cell types and species [102], therefore being suitable for biomedical applications.

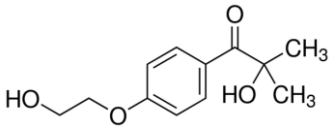

Figure 7. Molecular structure of Irgacure 2959 [103].

To produce molecularly imprinted polymers (MIP), the template molecule, bovine serum albumin (BSA, ~66 kDa, Sigma-Aldrich), was dissolved in 0.05% Irgacure solution to make a 1% w/v BSA solution. To that solution enough alginate was added to make a 1.5% w/v polymer solution and left mixing at room temperature for approximately 30mins. To produce discs without the template, *i.e.*, non-imprinted polymer (NIP) alginate discs, the same protocol was

performed but no BSA was added to the initial Irgacure solution. 20µL of MIP or NIP solutions were dispensed with a gel pipette to a TEFLON platform, covered with glass and exposed to UV light adjusted to a light intensity of 7 mW/cm^2 (320-395nm, BlueWave 200 Light-Curing Spot Lamp, Dymax, adjusted using ACCU-CAL-30 Smart UV intensity Meter, Dymax) for 60 or 70s and using 250, 500 or 750µm spacers (**Fig. 8**). This spacer-based methodology enables an easy control of disc dimensions such as thickness and diameter, by varying the size of spacer used or the volume of solution used.

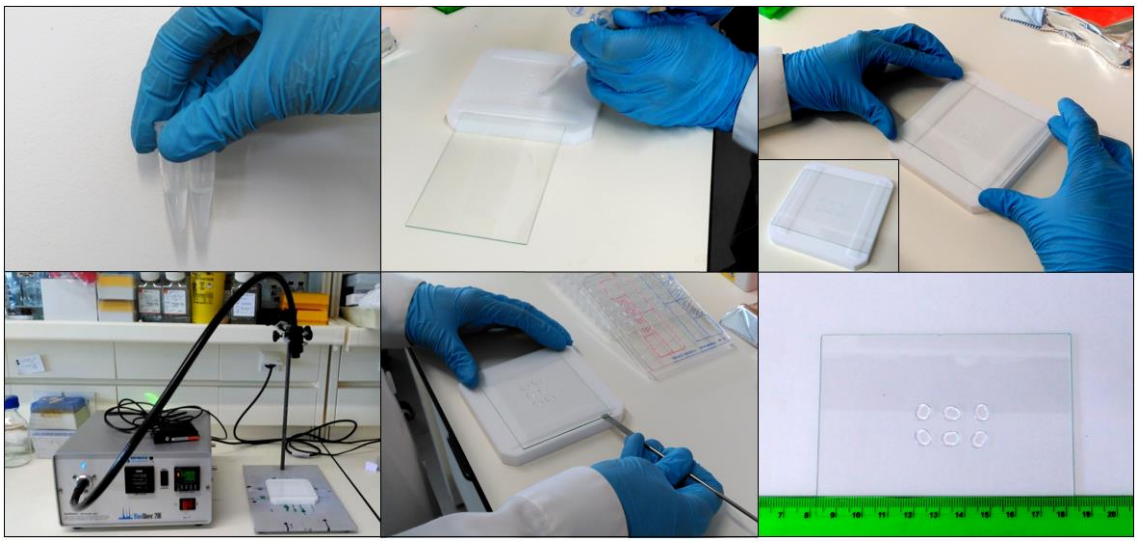

Figure 8. Spacer-based approach used to produce methacrylated alginate discs.

3.4. Swelling behavior of alginate discs

In this project, the swelling capacity of methacrlyated alginate discs was evaluated at two different stages using two different approaches.

3.4.1. Variation of disc diameter: in this approach, the swelling behavior was evaluated by the diameter variation of discs incubated in solutions of varying composition and throughout

certain timepoints. Briefly, ALMA 5 and ALMA 7 discs produced with 750μm spacers and exposed to 60 or 70s of UV light were incubated in a 24-well plate for 3 cycles of 1h (RT) in 1mL of a particular incubation solution: DI water (pH 5.6), 0.05M Tris HCl (pH 7.4), 0.05M Tris HCl with 1% $CaCl_2$ (pH 7.4) or 0.05M Tris HCl with 1% $MgCl_2$ (pH 7.4). At the end 3h, the solution was removed and changed to DI water and kept at 4°C throughout the rest of the experiment (15 days). At each timepoint (3, 24 and 48h and 7d and 15d), the incubation solution was removed from the wells and discs were observed under a Stereomicroscope (SZX10, Olympus) coupled to a digital camera (DP21, Olympus) and measured using ImageJ (ImageJ, version 1.50b; Rasband, W.S., ImageJ, U. S. National Institutes of Health, Bethesda, Maryland, USA, http://imagej.nih.gov/ij/, 1997-2016). In this case, the swelling ratio (SR) was calculated according to equation (4):

$$SR_{\emptyset} = \frac{\emptyset_t}{\emptyset_0} \tag{4}$$

Where $\emptyset_t(cm)$ corresponds to the diameter of the alginate disc at a specific timepoint t, and $\emptyset_0\ (cm)$ corresponds to the diameter of the alginate disc immediately after production.

3.4.2. Variation of disc weight: in this approach, the swelling behavior was evaluated by measuring the weight of alginate discs at different timepoints in an analytical balance (Mettler AG285 Analytical Balance). The swelling ratio (SR) was calculated according to equation (5):

$$SR = \frac{m_t}{m_0} \tag{5}$$

Where $m_t\ (mg)$ corresponds to the wet weight of the alginate disc at a specific timepoint t, and $m_0\ (mg)$ corresponds to the weight of the alginate disc immediately after production.

3.5. Photoinitiator influence in absorbance reading at 280nm

In this work, spectrophotometry was used to obtain an absorbance spectrum from wavelengths between 200-400nm. Samples tested corresponded to incubation solutions described in section 3.4.1. (Lambda 35 UV/Vis Spectrometer).

3.6. Morphological analysis by Cryo-SEM

To perform a morphological analysis, Cryo-Scanning Electron Microscopy (Cryo-SEM) was performed. Briefly, ALMA 5 and ALMA 7 NIP and MIP discs were hydrated in DI water for approximately 6h (swelling equilibrium is reached around 3h). For the Cryo-SEM assay, samples were cut in small parallelepiped shapes and placed in the support, rapidly cooled (plunging it into sub-cooled nitrogen – slush nitrogen) and transferred under vacuum to the cold stage of the preparation chamber. Samples were fractured, sublimated ('etched') for 100s at -90°C, and coated with Au/Pd by sputtering for 60s. Samples were then transferred into the SEM chamber and studied at a temperature of -150°C. The SEM / EDS exam was performed using a High resolution Scanning Electron Microscope with X-Ray Microanalysis and CryoSEM experimental facilities: JEOL JSM 6301F/ Oxford INCA Energy 350/ Gatan Alto 2500 (CEMUP, University of Porto, Portugal).

3.7. Mechanical characterization

To characterize the mechanical properties of the alginate discs, preliminary rheology studies were performed (n=1) using a Kinexus Pro rheometer (Malvern Instruments, Malvern) at RT using parallel plate geometry (Ø 4mm) and compressing discs by approximately 10% of their height. Samples from ALMA 5 and ALMA 7 NIP and MIP discs were prepared and tested right after production by frequency sweep measurements (start frequency 0.01 Hz, ending frequency 10Hz, constant strain 1%, points per decade 10).

3.8. Template removal

A template removal protocol was optimized in this project. During this stage of development, several variables were tested (**Tab. 3**). Right after production of discs (250, 500 or 750μm thickness) they were incubated in different volumes (0.25, 0.40, 0.60, 0.80 or 1mL) in DI Water (pH 5.6), 0.05M Tris HCl solution (pH 7.4) or both, for a certain number of cycles (1 up to 4) of different durations (1 up to 96h); these protocols were developed in temperatures ranging from 4°C or RT, with or without agitation (150rpm). Template removal was determined by protein quantification using different approaches (item 3.10.).

Table 3. Studies performed to optimize the template removal protocol.

Protocol	Initial solution	Cycles no.	T (°C)	Agitation	Volume/well (mL)	Disc thickness (μm)
A	DI water	3 cycles 1h 1 cycle 24h	RT 4	No	1	750
B	DI water or Tris HCl (pH 7.4)	1 cycle total 96h	RT 4	Yes (3h) No (up to 96h)	0.25, 0.40, 0.60 and 0.80	750
C	Tris HCl (pH 7.4) and DI Water	1 cycle 3h 1 cycle 24h	RT 4	Yes (3h) No (up to 24h)	0.25	250 and 500
D	Tris HCl (pH 7.4) and DI Water	2 cycles 1.5h 2 cycles 24h	RT	Yes	0.25	500

3.9. Rebinding Assay

Rebinding assays were performed in order to analyze the imprinting features of MIPs when comparing to NIP discs. NIP and MIP discs (n=3) were produced accordingly to item 3.3. using 500μm spacers. Both NIP and MIP discs underwent the template removal protocol D (**Tab. 3**) described in item 3.8.. Briefly, NIP and MIP discs were incubated in a 0.05M Tris HCl (pH 7.4) solution for 2 cycles of 1h 30min each and posteriorly in DI water for 2 cycles of 24h each. At the end of each cycle, the incubation solution was removed and changed. After template removal, discs were incubated in 0.1% or 1% w/v BSA solution in 0.9% NaCl solution (pH 4.2), similarly to the initial imprinting solution, with agitation (150rpm) at RT for 72h. Afterwards, samples were tested for protein quantification (item 3.10.).

3.10. Protein Quantification

In this project, analysis of protein content was performed using three different methods: 1) protein quantification by analysis of supernatant (*i.e.*, incubation solution), 2) protein quantification by analysis of digested discs and 3) protein quantification by analysis of glutaraldehyde (GTA) induced BSA-autofluorescence.

3.10.1. Protein quantification by analysis of supernatant

This is an indirect method where samples from supernatant were tested using DC Protein Assay (detection range 0.2-1.5mg/mL, Bio-Rad) by reading absorbance at 750nm using a Synergy Mx HM550 microplate instrument (Biotek Instruments). The amount of protein present in the supernatant was calculated by correlation of absorbance values with a calibration curve obtained from standard samples (3 readings per sample, standard curve performed for each plate reading). The protein present in the supernatant (m_{BSA}, µg) was obtained by the following equation (6)

$$m_{BSA} = \frac{[Abs_{sample} - b]}{a} \times V * 1000 \qquad (6)$$

Where Abs_{sample} ($A.U.$) corresponds to the relative absorbance value (i.*e.,* $Abs_{sample\_measured} - Abs_{blank}$) of a sample, a and b correspond to constants obtained for the calibration curve,$y = ax + b$, where y is in $A.U.$ and x in mg/mL. V corresponds to the volume of supernatant (mL) and 1000 is the conversion factor from mg to μg.

The amount of removed protein (%) was obtained by comparison of m_{BSA} values obtained for each sample with initial theoretical values of 200µg per MIP disc (n=4).

3.10.2. Protein quantification in digested discs

For this direct quantification method, discs were digested in 200µL of 0.25M NaOH and tested using DC Protein Assay by reading absorbance at 750nm using a Synergy Mx HM550 microplate instrument (Biotek Instruments). The amount of protein present in the disc was calculated by correlation of absorbance values with a calibration curve obtained from standard

samples (3 readings per sample, standard curve performed for each plate reading). The protein present in the disc (m_{BSA}, µg) was obtained by the following equation (7)

$$m_{BSA} = \frac{[Abs_{sample} - b]}{a} \times V' * 1000 \quad (7)$$

Where Abs_{sample} $(A.U.)$ corresponds to the relative absorbance value of a sample (i.*e.*, $Abs_{sample\_measured} - Abs_{blank}$), a and b correspond to constants obtained for the calibration curve, $y = ax + b$, where y is in $A.U.$ and x in mg/mL. V' corresponds to the volume of 0.25M NaOH solution (0.2mL) and 1000 is the conversion factor from mg to µg.

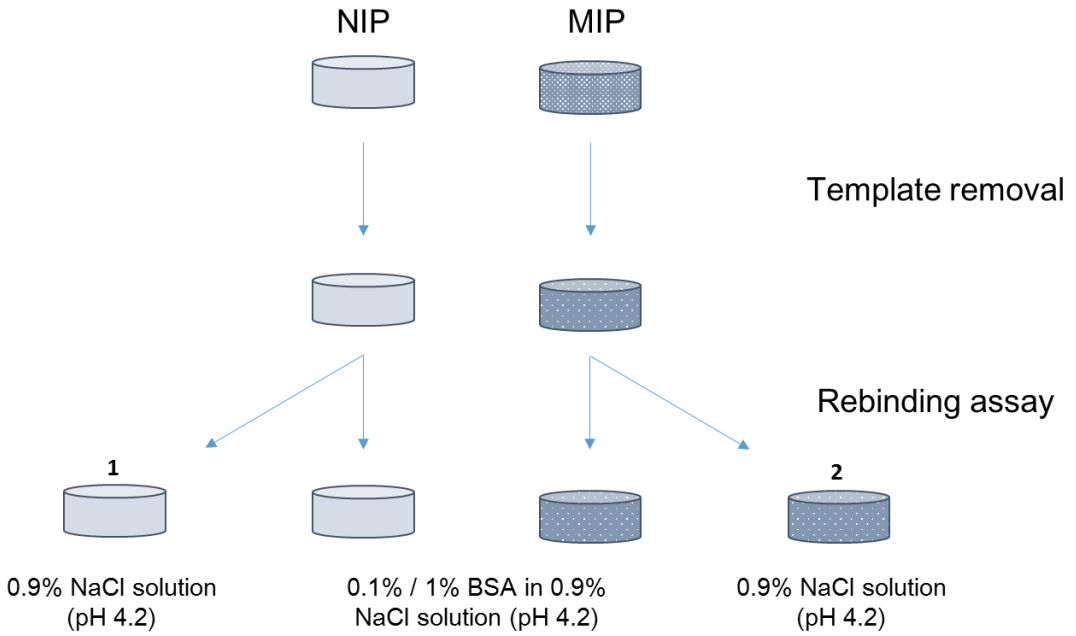

Figure 9. Schematic representation of samples used throughout the molecular imprinting process and for rebinding assay. While disc 1 works as a general control of the molecular imprinting process and an internal control for rebinding assay for NIP discs, disc 2 works as an internal control for MIP discs during rebinding assay. Performing quantifications in relation to disc no. 1 gives the amount of protein effectively present in discs after the rebinding incubation protocol. In the case of NIP discs, this value corresponds also to Q, while for MIP discs Q can only be determined while performing quantifications in relation to disc no. 2.

To determine the amount of protein per weight of disc, m_{BSA}/m_{disc} $(\mu g/mg)$, the following calculation was performed as in (8)

$$m_{BSA}/m_{disc} = \frac{m_{BSA}}{m_{disc_{wet}}} \times SR \quad (8)$$

Where SR is the swelling ratio (non-dimensional) and was used to normalize quantifications as a dilution factor.

The amount of removed protein (%) was obtained by comparison of m_{BSA} values obtained for each sample with m_{BSA} measured for MIP discs as produced (n=4).

For rebinding analysis (n=3), m_{BSA}/m_{disc} always corresponded to the rebinding capacity (Q) for NIP discs. For MIP discs, m_{BSA}/m_{disc} corresponded to the amount of protein effectively present in the discs, while Q was obtained following the same equation but determining Abs_{sample} using a different internal control (**Fig. 9**).

3.10.3. Protein quantification by GTA method

This method is based on BSA-autfluorescence induced by GTA [104] and was developed during this project as a way to overcome obstacles faced regarding protein detection. As such, this method was used as a supportive method, offering both qualitative and quantitative data even though optimization is still required. This technique was applied for ALMA 5 samples.

In preliminary studies, qualitative analysis of protein amount present in discs was performed by incubating discs from different processing timepoints (upon production, t=0h, or during the template removal protocol, t=3, 24 or 48h) in 250µL of 25% GTA solution (Sigma-Aldrich) for 30mins at RT using a wide-field microscope Zoe Fluorescent Cell Imager (Bio-Rad). For acquiring images the following settings for gain, exposure time, LED intensity, and contrast were selected and kept for each channel: green (36, 460, 35, 0), red (40, 460, 35, 0) and blue (20, 460, 25, 0). Excitation and emission wavelengths (λex and λem) are the following for each channel: green (λex=480/17nm and λem=517/23nm), red (λe=556/20nm and λem=615/61nm) and blue (λex=355/40nm and λem=433/36nm). Images of brightfield were also acquired.[105]

In order to obtain a quantitative analysis of protein content another protocol was followed using Inverted Confocal Microscopy. Briefly, discs and standard samples (discs containing 0, 0.25, 0.5 and 1% BSA) were incubated overnight in 250µL of 25% GTA solution at 4ºC. Prior to observation, samples were immersed in Vectashield mounting medium (VECTOR Laboratories) to avoid discs to dry and shrink during exposure to the laser beams. Discs were visualized using a Confocal Laser Scanning Microscope (CLSM, Leica TCS-SP5 AOBS; Leica Microsystems, Wetzlar, Germany) under the 10x objective and with parameters kept constant. Images were acquired at λex=488nm and λem=500-599nm.

For each sample, four different stacks were obtained and a Z-projection of all stacks was performed using ImageJ software. For quantification purposes, in each projected image, 3 measurements of Mean Gray Value (A.U.) of disc region and 3 of the background region were obtained (**Fig. 10**). The amount of protein in disc was calculated by a correlation of the Mean Gray Value (Mean) using calibration curves produced from standard samples. Standard samples were prepared each time that samples were observed under the microscope (previously prepared on the day before and incubated overnight simultaneously to the samples to be tested). This was performed to avoid any possible differences caused by laser beam fluctuations.

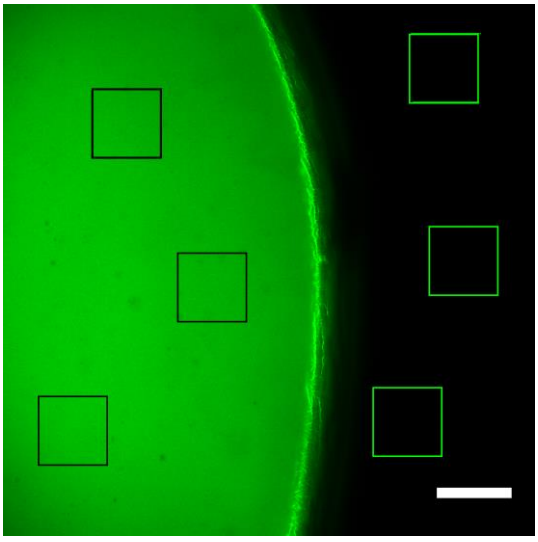

Figure 10. Example of measurements performed in projected images obtained by inverted confocal microscopy (excitation at 488 nm). ImageJ ROI Manager tool was used to assure a fixed dimension for all measurements. For each sample, 3 measurements were performed in the disc region (left) and 3 in the background region. Scale bar represents 200µm.

3.11. Statistical analysis

Statistical analysis was performed using GraphPad Prism 5 software for Windows, (GraphPad Software, San Diego California USA, www.graphpad.com). Mean and standard deviation were determined for each sample. Statistical differences between groups was performed using t test with Welsh correction. Samples were considered significantly different if $P<0.05$.

Chapter 4
Results and Discussion

In this section, the main results obtained regarding the main stages of development of this project will be presented and discussed.

4.1. Alginate modification

As referred in Chapter 1 (Introduction), alginates are water soluble polysaccharides frequently used in biomedical applications due to their great biocompatibility and biodegradability.

Alginates have the ability to form gels by reacting with divalent cations, such as calcium ions (Ca^{2+}) [69], occurring an ionic crosslinking between the divalent cations and the polymer chains. This type of crosslinking is believed to occur between the G blocks of alginate (**Fig. 3**, Chapter 1) and the divalent ions. Since G and M contents can vary between different sources of alginates and with the length of each block, this ionic crosslinking is widely dependent on the type of alginate used [70]. Consequently, this will interfere with the final properties of the alginate hydrogels formed [70]. Also, when in physiological conditions, ionically crosslinked hydrogels can lose these divalent cations into the surrounding media leading to lower long-term physical stability [70]. In fact, this exit of Ca^{2+} from the bulk of the material can affect recognition features of molecularly imprinted polymers (MIP) as they lead to a slow degradation of the mesh [79].

Photocrosslinking was the alternative method of crosslinking chosen for this project, where covalent bonding between modified alginate polymer chains is induced upon light exposure

[106-110]. In the particular case of alginate, this type of crosslinking can be performed by previously modifying alginate to contain photosensitive functional groups. Methacrylate functional groups can replace hydroxyl or carboxyl groups of alginate (methacrylation) and undergo free radical polymerization if exposed to UV light in the presence of a photoinitiator [106]. This type of crosslinking enables the control of mechanical properties and swelling of alginate hydrogels while still allowing ionic crosslinking to occur, a feature which can be advantageous to create dual-crosslinked systems.

4.1.2. Alginate methacrylation

Following the main objectives of this project, an alginate methacrylation protocol was optimized. Several factors can affect the methacrylation process (*e.g.* temperature, pH and time), namely the extent at which alginate functional groups are replaced and, consequently, affect the capacity of methacrylated materials to form gels. Therefore, studies evaluating different parameters were carried out in order to optimize an alginate methacrylation protocol.

Firstly, three different protocols of alginate methacrylation were tested (**Tab. 4**). In all three protocols, the methacrylate compound used (methacrylic anhydride) was intended to replace hydroxyl groups, since no carboxyl activators were added during the reaction in order to allow for dual crosslinking, as previously mentioned (**Fig. 11**).

Table 4. Methacrylation protocols tested and gel formation capacity of produced materials.

Protocol	T (°C)	Duration (h)	MA addition timepoints (h)	AL/MA ratio (g/mL)	pH	Gel formation
1	Ice cold	24	0, 3 and 6	~0.07	5 or 7	Yes
2		10				Yes
3		5	0, 1 and 3			No

Protocols no. 1 and 2 consisted of a preliminary test to set basic parameters of the system such as temperature, pH and the minimum reaction time required for the methacrylated alginate to form gels upon UV exposure. To accomplish this, the methacrylation reaction was either performed during 10h or 24h. Additionally, at the end of methacrylation and dialysis the pH of polymer solution was adjusted either to pH 5 (ALMA 5) or 7 (ALMA 7) prior to

lyophilization. This adjustment was performed for two main reasons: firstly, the knowledge that pH conditions influence the molecular imprinting process and thus the final molecular recognition features of the material - this is especially true in the case of macromolecules such as proteins [111]; and secondly to evaluate potential differences in mechanical and physical behavior or crosslinking yield of these materials [112].

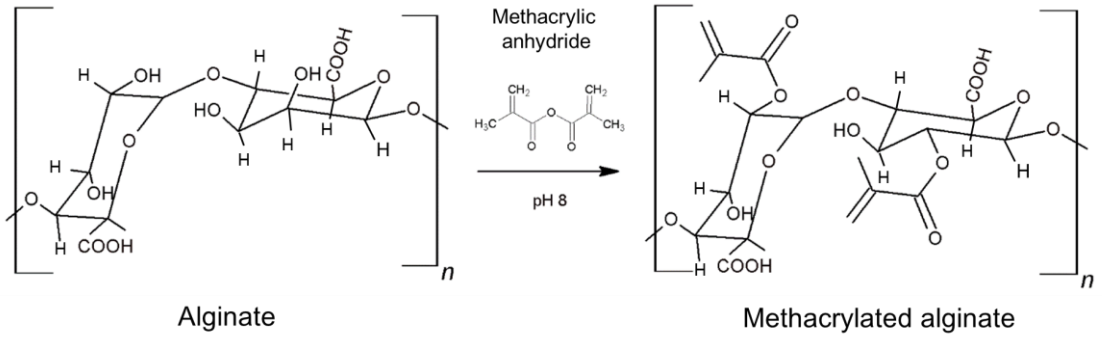

Figure 11. Alginate methacrylation reaction with methacrylic anhydride. During this methacrylation reaction, methacrylic anhydride molecules will react with hydroxyl groups present in alginate backbone. The extent at which this replacement occurs, either in G, M or both blocks, is tightly dependent on the protocol design.

Polymer solutions with modified alginate produced with different protocols presented the same appearance (**Fig. 12**). When exposed to UV light for 60s and in the presence of a photoinitiator (Irgacure 2959) polymer solutions produced in both protocols were able to form gels (**Tab. 4**). In fact, methacrylated alginate solutions adjusted to the same pH value but with different reaction times produced discs with no apparent differences. However, for the same reaction time, discs derived from methacrylated alginate with different pH values presented perceptible differences in apparent stiffness. While discs produced from ALMA 5 presented a stiffer appearance, ALMA 7 alginate discs were softer and presented remains of what seemed to be non-polymerized solution surrounding the disc. This perception was later confirmed by preliminary rheological studies performed in ALMA 5 and ALMA 7 discs right after production (**S 2**).

Following these results, protocol no. 3 was performed to see if the reaction time could be further diminished. The reduction of the reaction time to 5h led to polymer solutions unable to successfully polymerize under the same conditions, being liquid after 60s of UV exposure.

Figure 12. ALMA 5 and ALMA 7 polymer solutions.

Overall, these results were indicative of a significant dependence between the extent of alginate hydroxyl groups replaced by methacrylate groups (methacrylation degree, DM) and the time of reaction up to 10h. To confirm this assumption, methacrylated alginate from protocols 2 and 3 was analyzed by ^{1}H NMR. The resultant NMR spectra are presented in **Fig. 13** and were consistent with the differences previously observed in gel formation capacity: whereas methacrylated alginate produced in protocol no. 2 (**Fig. 13A**) presented large peaks, alginate produced in protocol no. 3 (**Fig. 13B**) presented smaller peaks for the same ppm values. This indicates higher DM values for ALMA when reaction was carried out for 10h comparing to 5h, since higher peak areas indicate a higher proportion between newly existent protons and the protons in the non-modified alginate backbone. Therefore, reaction time was not only a limiting factor in the methacrylation reaction, but was in fact the reason why such differences in polymerization were observed.

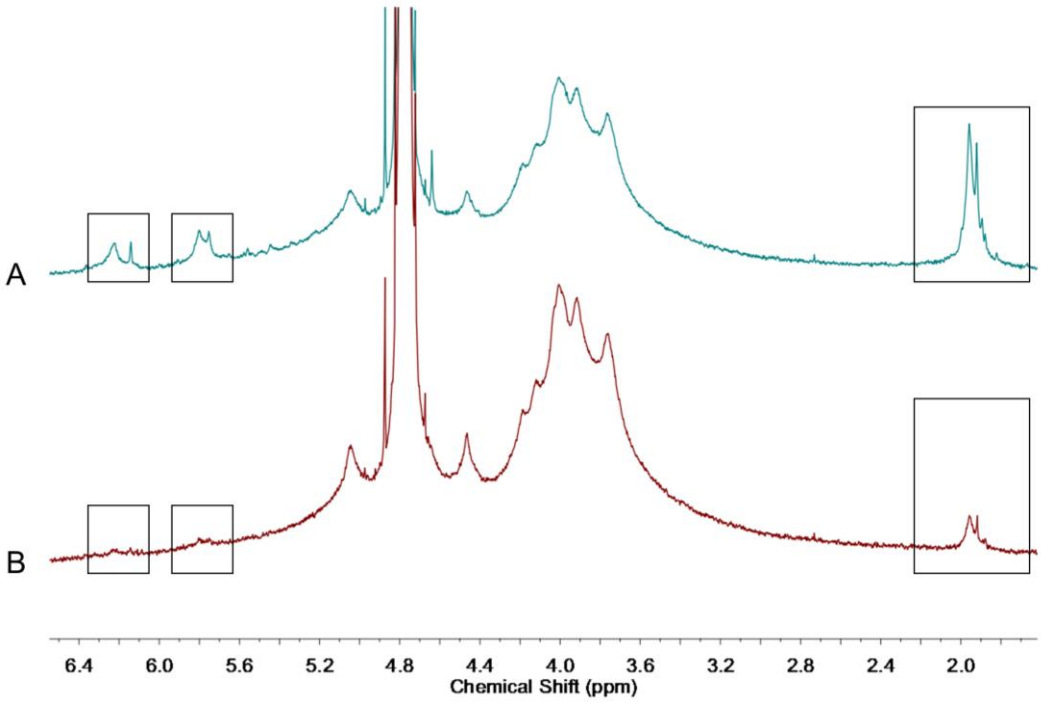

Figure 13. ^{1}H NMR spectra of alginates produced in 10h (A) and 5h methacrylation reactions (B).

Considering these results, protocol no. 2 was selected as the methacrylation procedure to produce the photosensitive alginate to be used throughout this project, since it reduced mehtacrylation reaction time to 10h while still being able to produce gels upon UV exposure.

Fig. 14 represents the resultant ^{1}H NMR spectra of non-modified alginate (**Fig. 14A**) and ALMA 5 (**Fig. 14B**) and ALMA 7 (**Fig. 14C**) alginates. It is possible to observe the appearance of three distinguishable peaks corresponding to protons a, b and c (**Fig. 14D**) both in ALMA 5 and ALMA 7 spectra when comparing to non-modified alginate. This indicates a successful replacement of –OH groups of alginate by new MA groups. For both materials, the chemical shift of these peaks is approximately 1.9, 5.7 and 6.1 ppm, respectively (**S 2**). Using these data, it was possible to determine a degree of methacrylation of approximately 18.25 % [110].

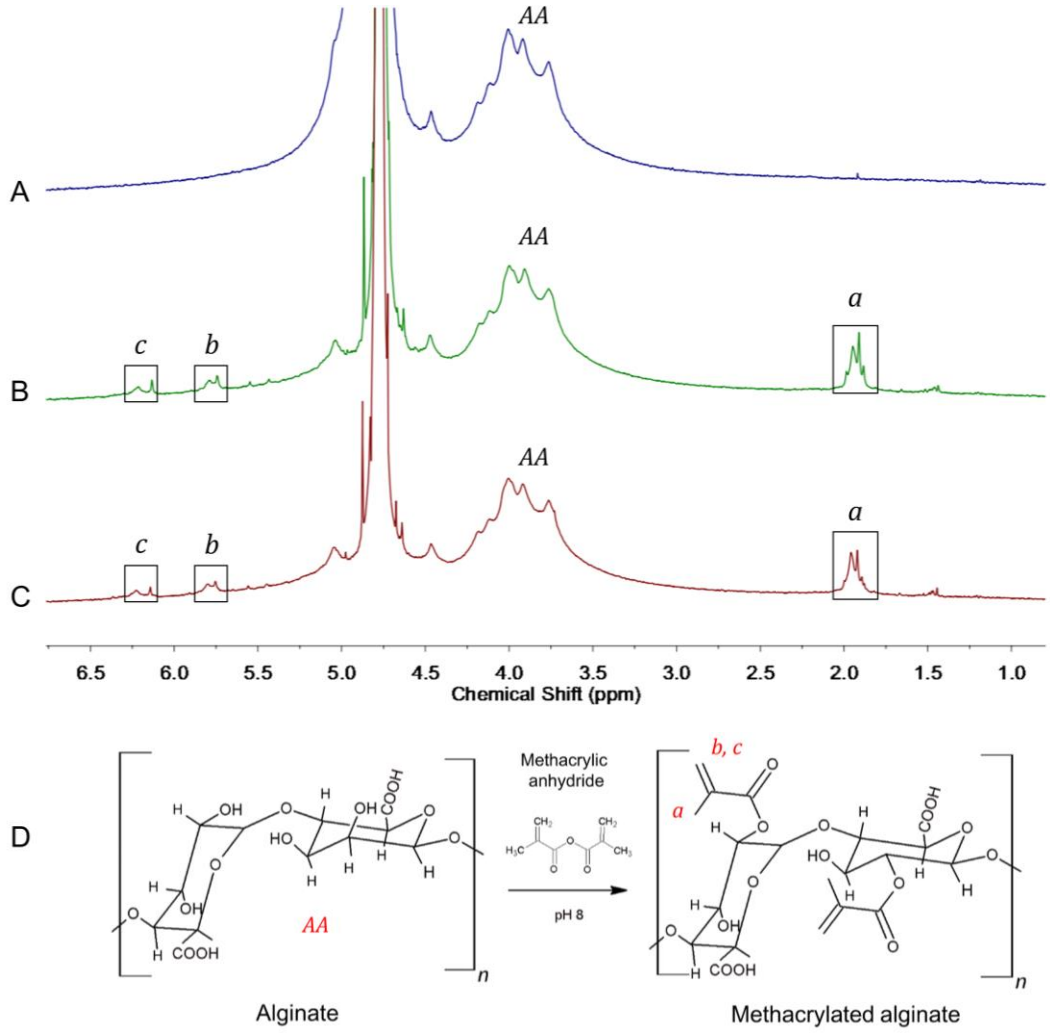

Figure 14. Comparison between ^{1}H NMR spectra of non-modified alginate (A) and modified alginates ALMA 5 (B) and ALMA 7 (C). It is possible to observe the appearance of three distinguishable peaks (a, b and c) corresponding to the new protons added to non-modified alginate during the methacrylation reaction (D). AA peak corresponds to protons present in the backbone of non-modified alginate.

Alginate methacrylation protocols are reported in the literature for biomedical applications using methacrylate compounds such as 2-aminoethyl methacrylate and methacrylic anhydride [106-110, 113]. The time dependence of methacrylation reactions is evident, with reported protocols comprising methacrylation reaction times of 24 up to 72h [106-110, 113]. In comparison, the 10h protocol developed in this project considerably shortens the reaction time while providing consistent gel formation. Besides, the reported literature performs these

protocols with low viscosity alginates which usually present higher DM values [106-110, 113, 114] since DM is inversely affected by polymeric molecular weight [115].

In this project a medium viscosity alginate (248.13kDa, apparent viscosity 343mPas) was used, instead of low viscosity alginates, to improve mechanical properties. For the same polymer concentration, alginates with higher molecular weights give rise to polymer solutions with higher viscosity. Consequently, gels formed by alginates with higher molecular weight usually have their mechanical properties improved, *i.e.*, they originate gels with increased elastic modulus [70]. Since molecular imprinting success is affected by the extent of polymer distortion, as imprinting cavities can lose their specificity due to this event, higher elastic modulus are preferred up to a certain extent. Using a high viscosity alginate could further increase elastic modulus of formed gels but these would be concomitant with considerably viscous polymer solutions which could risk to damage proteins by shear forces during ejection from the narrow gel tips [70]. Besides, even though it is desirable to minimize distortion, it is important to allow some relaxation of the mesh during template removal in order to potentiate protein exit from the less superficial layers of the material [111].

Despite using a medium viscosity alginate in this project, the achieved DM of 18.25 % is an encouraging result when comparing to values reported in the literature (3.5-25 %), which correspond to modifications in low viscosity alginates. Most of the literature only refers an excessive addition of MA in the preparation of methacryalated alginates and does not refer the way this addition is performed (*e.g.*, at once or successively) [106-110, 113, 114]. In the protocols developed herein, the total amount of methacrylate required was divided in three independent additions to be performed at specific timepoints (**Tab. 4**). This sequential addition most likely supports an increasing in the yield of the methacrylation reaction since less methacrylate compound is in excess each time during the process, reducing the amount of hydrolyzed compound unable to react with the alginate.

4.2. Molecular imprinting protocol optimization

Subsequently to the preparation of ALMA 5 and ALMA 7, production of alginate discs was studied and optimized regarding the molecular imprinting process. For instance, parameters such as pre-polymerization solution, time of UV exposure, thickness of the produced discs, pH

and salt conditions of incubation solutions could potentially affect the success of the molecular imprinting process.

Regarding the pre-polymerization solution, parameters used, particularly pH (4.2) and BSA concentration (1 % w/v), were set based on work developed by Bayer *et al.* [79] and Herrero *et al.* [80], some of the few existent literature reports on protein molecular imprinting systems solely based in alginate. While using BSA as the template, a pre-polymerization solution pH 4.2 promotes ionic interactions between the protein and the alginate [79, 80]. As BSA isoelectric point (pI) is around 4.7, at a pH value of 4.2 BSA will be positively charged while alginate is negatively charged, promoting non-covalent ionic interactions between the protein and the polymer chains. Despite being known that different BSA concentrations in the initial solution can affect imprinting features of produced MIPs [72], this parameter was kept constant.

The following results comprise a set of studies performed in order to restrict variables of the system. Studies regarding disc production (without template) were performed to set basic parameters such as UV exposure time and disc thickness. Differences in swelling behavior were evaluated for discs exposed to different UV exposure times and solution compositions. To homogenize the studies, the volume of polymer solution was kept constant (20μL). Minding this, disc thickness variation by the use of different spacers was evaluated. While surface imprinting usually presents better results than bulk imprinting, minimizing thickness was a goal, but an appropriate ratio between thickness and diameter was also required to enable good handling.

Concomitantly, these parameters were adjusted in a molecular imprinting perspective and aiming at optimizing a template removal protocol (type of solution to be used, number and duration of incubation cycles) and select the most suitable protein quantification methodologies.

4.2.1. Effect of different solutions in alginate discs

In order to further characterize and compare ALMA 5 or ALMA 7 materials, the effect of UV exposure time (60 or 70s) and the effect of potential incubation solutions for template removal [DI water, Tris HCl (pH 7.4), Tris HCl with 1% $CaCl_2$ (pH 7.4) or Tris HCl with 1% $MgCl_2$ (pH 7.4)] in

alginate discs with no template (non-imprinted polymer, NIP) were studied and results are presented in **Fig. 15**.

After a 3 hour-incubation period in a specific solution, discs were incubated in DI water until the end of the experiment. This incubation in DI water is used in some template removal protocols not only to promote swelling of the material to help removing the template by expanding the mesh, but also to remove any salts or ions left from the initial solutions [80].

As it can be perceived, while UV exposure time had little effect on the swelling ratio throughout time, the type of solution used in the first 3h of experiment and the type of alginate used had clear influence on the swelling behavior of discs.

For the same incubation solution and UV exposure time, ALMA 5 discs presented lower diameter variations than ALMA 7 discs. These data is in agreement with the differences observed in ALMA 5 and ALMA 7 discs during methacrylation optimization. As pH decreases, carboxylate groups in the alginate backbone become protonated and form hydrogen bonds, thus promoting a stiffening of the mesh upon polymerization which can justify this difference between ALMA 5 and ALMA 7 discs [70]. Contrarily to the accentuated differences caused by different pH values, increasing UV exposure time from 60s to 70s did not lead to major differences in swelling behavior, even though slightly smaller swelling ratio values occurred for discs produced under 70s UV light exposure.

Different primary incubation solutions led to different swelling profiles of discs produced under the same conditions. In fact, for the same incubation solution used, all four types of discs presented a similar swelling tendency. Discs incubated in DI water (pH ~5.6) rapidly increased diameter and were the first achieving the swelling equilibrium at t=3h. Incubating discs in a Tris HCl (pH 7.4) solution retarded this effect, with a lower diameter variation in the first 3h comparing to discs incubated in DI water and reaching a swelling equilibrium around 48h after the start of the experiment. Such retardation in water uptake can be explained by the existence of Tris salt in the solution since the presence of salts is known to affect the swelling behavior of hydrogels, being usually associated with decreased water uptake when compared with DI water [112, 116, 117].

Discs incubated for 3h in Tris HCl, 1% $MgCl_2$ (pH 7.4) caused a small constriction in ALMA 5 but barely no effect in ALMA 7 discs. Nevertheless, this constriction was recovered when incubating discs in DI water for the rest of the protocol. The same did not occur for discs

incubated in Tris HCl, 1% $CaCl_2$ (pH 7.4), which suffered an irreversible constriction. In fact, Tris HCl, 1% $CaCl_2$ (pH 7.4) is a widely used combination for template removal solution in BSA-molecular imprinting systems based on alginate [49, 72-75, 78-80].

At pH 7.4, BSA is negatively charged and interactions between BSA and the negatively charged alginate backbone are broken. In order to promote the exit of BSA from the polymer, some authors use $CaCl_2$ during template removal to attract BSA out by electrostatic interactions, which may occur between different functional groups of BSA and the divalent cation Ca^{2+} [49, 72-75, 78-80, 118]. A synergistic effect occurs by the existence of diffusion forces coupled with the interaction between the protein and the divalent cation. Oppositely, BSA can be removed by its binding sites by competition with Ca^{2+} for alginate negatively charged binding sites. However, all these systems are based in ionic crosslinking with $CaCl_2$, where the divalent cation Ca^{2+} works as the crosslinking agent, binding polymeric chains by electrostatic interactions [49, 72-75, 78-80]. Even so, when Herrero *et al.* [80] produced alginate microcapsules by ionic crosslinking with $CaCl_2$, a thickening of the capsule membrane was reported after a template removal process with cycles containing $CaCl_2$.

In the particular case of this project, since the crosslinking method used was photocrosslinking, spaces within the polymer mesh where Ca^{2+} would be able to interact as a crosslinking agent were still available when the incubation was performed. Therefore, when discs were incubated in the Tris HCl, 1% $CaCl_2$ solution it was expected that a secondary ionic crosslinking process would occur. Even 15 days after incubation in DI water this effect was not reversed.

The use of Tris HCl, 1% $MgCl_2$ solution was seen as a potential alternative as Mg^{2+} could be able to replace calcium's role as a template removal agent, while avoiding its associated ionic crosslinking events. However, this solution did cause a small constriction in ALMA 5 discs during incubation. Actually, Mg^{2+} cations were reported to have indeed a gelling effect in alginate, which is strongly dependent on M/G ratio and only reached after longer periods of time [119]. As G content increases, interactions between alginate and Mg^{2+} also increases, just like for Ca^{2+}. However, while Ca^{2+} ions are strongly site-bounded, crosslinking derived from Mg^{2+} occurs as these ions are diffusively bound [120]. This explains why ALMA 5 discs suffered a constriction when incubated in Tris HCl, 1% $MgCl_2$, even though in a much lower and reversible way than with Ca^{2+}.

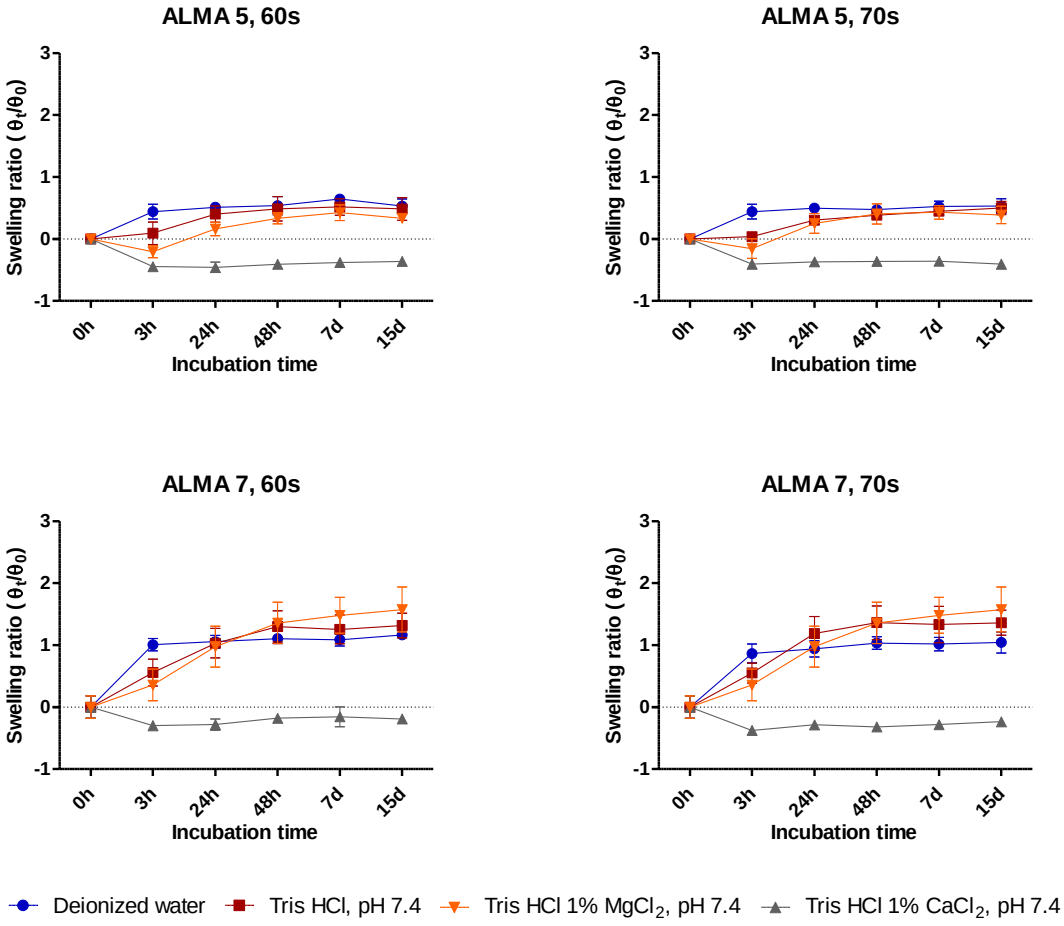

Figure 15. Effect of different solutions and incubation time in the swelling ratio of ALMA 5 and ALMA 7 discs exposed to 60s and 70s of UV light. Discs were incubated for 3h (3 cycles of 1h) in each specific solution, after which solutions were changed to DI water until the end of the experiment. Data shown represents the mean values of four diameter measurements and error bars represent ± SD (n=1 disc per condition).

Besides analyzing the swelling behavior of gels, it was necessary to know if absorbance reading at 280 nm was a viable method to perform protein quantification throughout the following steps of this project, namely during the template removal and the rebinding assays. This method is widely used as a protein quantification method, including in molecular imprinting literature, based on intrinsic fluorescence (excitation at λ=279nm and emission at λ=348nm) of proteins predominantly originated by tryptophan residues [104, 121]. However, driven by the knowledge that Irgacure 2959 absorbs preferentially at wavelengths of near 279nm [103], this could lead to quantification problems as small amounts of photoinitiator not able to react during

the photopolymerization could be released from discs to the supernatant and be accounted as protein.

Therefore, a spectrum reading from 200 up to 400nm was performed for supernatants after 1h incubation (**Fig. 16**). Results show higher peaks at wavelengths around 279nm which could be indeed caused by release of photoinitiator to the solution. Following these results, absorbance reading at 280nm as the protein quantification method was not considered a safe option for the following stages of development. Instead, a colorimetric assay (DC protein assay kit) was chosen to perform measurements by absorbance readings at 750nm [122].

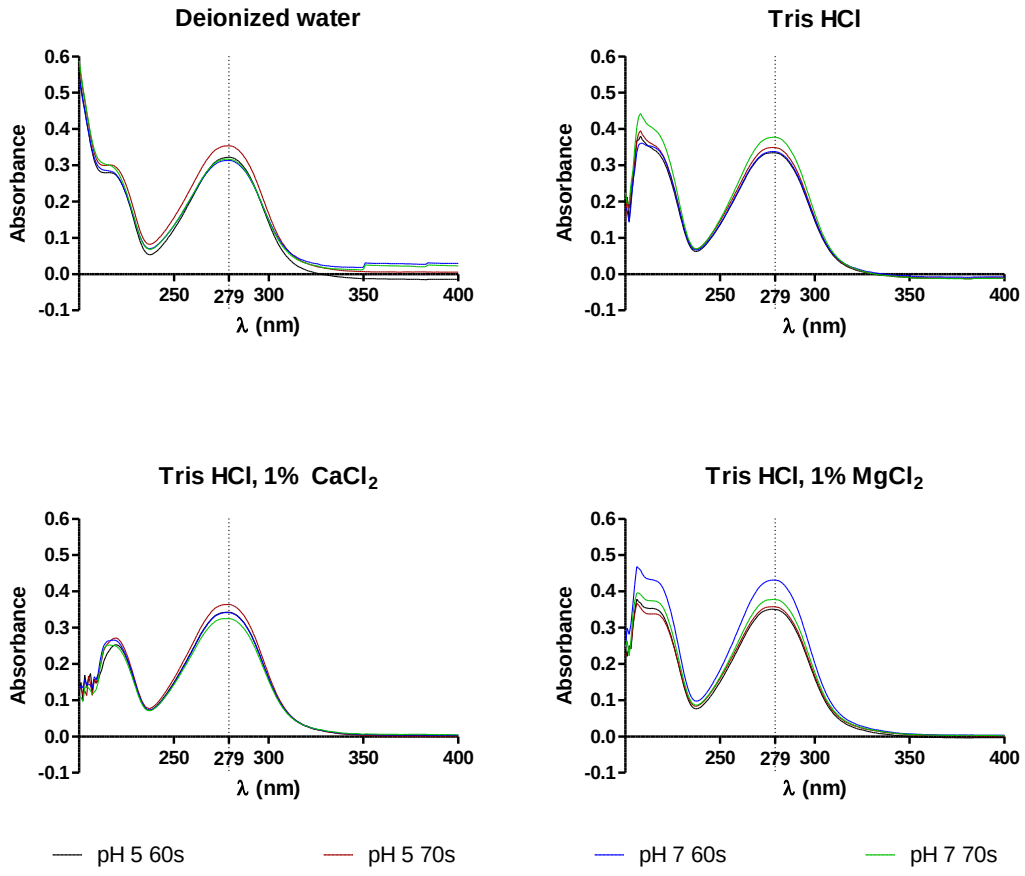

Figure 16. Absorbance spectra of incubation solutions after 1h incubation time.

4.2.2. Disc production and template removal protocol optimization

Throughout this project, different studies regarding protocols of template removal (**Tab. 5**) were performed with discs produced containing the template molecule (molecularly imprinted polymer, MIP). In a first attempt, only DI water was used as the template removal. Maintaining the same protocol as previously, 3 cycles of 1h incubation were performed at RT without agitation, after which discs were kept at 4°C for 24h. At the end of each cycle, the supernatant was collected and stored for testing with a protein quantification kit. Solutions containing Tris and divalent cations were not chosen for these studies to avoid further interferences with the material.

Table 5. Studies performed to optimize the template removal protocol and corresponding specifications.

Protocol	Initial solution	Cycles no.	T (°C)	Agitation	Volume/well (mL)	Disc thickness (µm)	Protein Detection
A	DI water	3 cycles 1h 1 cycle 24h	RT 4	No	1	750	No
B	DI water or Tris HCl (pH 7.4)	1 cycle total 96h	RT 4	Yes (3h) No (up to 96h)	0.25, 0.40, 0.60 and 0.80	750	Yes
C	Tris HCl (pH 7.4) and DI Water	1 cycle 3h 1 cycle 24h	RT 4	Yes (3h) No (up to 24h)	0.25	250 and 500	Yes
D	Tris HCl (pH 7.4) and DI Water	2 cycles 1.5h 2 cycles 24h	RT	Yes	0.25	500	Yes

On the first study (**protocol A**, **Tab. 5**), no conclusion regarding the amount of protein removed was possible to obtain since nothing was detected on the supernatant. This could be not only a consequence of the volume necessary to fully cover the discs on a 24-well plate, leading to protein concentrations in a range not appropriate to the quantification method used, but also due to the low capacity of DI water to promote protein exchange from the bulk to the solution.

Therefore, a second study (**protocol B, Tab. 5**) was developed to test different variables of the system and achieve protein detection. Firstly, both DI water and Tris HCl were tested as template removal agents. As referred above, to avoid any undesirable effect of divalent cations in the template removal process caused by secondary ionic crosslinking, solutions containing Ca^{2+} and Mg^{2+} were not used. The time of incubation was adjusted to 96 h (3h at RT with agitation

and the rest with no agitation at 4 °C). This was done to ensure the solution had reached its equilibrium of protein saturation when analyzed. At the end of 3h incubation, 20µL of supernatant were sampled and stored for further analysis and comparison with samples from 96h. Also, the volume of incubation solution was changed from 1 mL/well for 0.25, 0.4, 0.6 or 0.8 mL/well by using a 48-well plate which ensured the full covering of discs by the template removal solution. Applying these adjustments enabled protein quantification and results are presented on **Fig. 17**.

The results obtained show that ALMA 7 MIP discs allow higher levels of template removal than ALMA 5 discs and that this difference is more prominent when incubation is performed solely in DI water. The difference observed between both materials was expected since the lower swelling observed for ALMA 5 in the previously performed studies lead to higher protein entrapment within the bulk of the material. On the other hand, the greater capacity of ALMA 7 discs to swell, thus relaxing and expanding the polymer mesh, enabled higher protein diffusion.

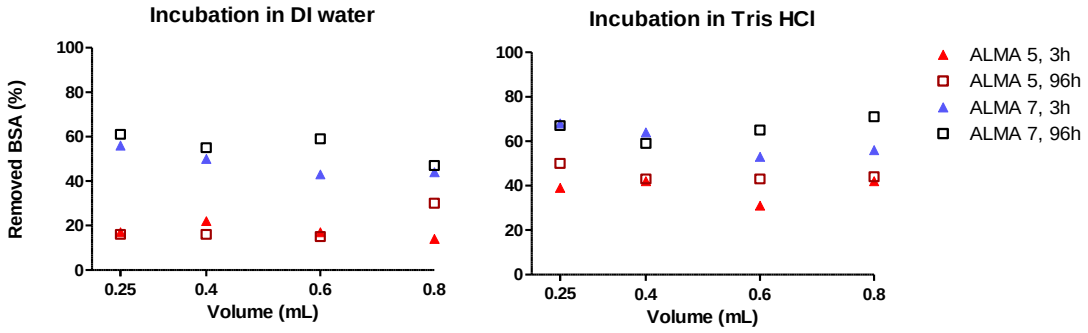

Figure 17. Effect of solution, volume and time of incubation in the amount of removed BSA from ALMA 5 and ALMA 7 alginate discs. Results obtained for n=1 disc per condition.

The best results for BSA removal were achieved in Tris HCl solution, being around 50 % and 70 % for ALMA 5 and ALMA 7 at 96 h, respectively, against 30 % and 61 % in DI water for the same samples. The higher protein removal observed in Tris HCl incubated discs is most likely caused by pH. While DI water has a pH value of around 5.5-5.6, Tris HCl solution was adjusted

to pH 7.4. This increase in pH value may stimulate protein removal as more BSA molecules become negatively charged and thus are repulsed from the negatively charged net of alginate [70, 79, 80].

Regarding the incubation solution volume, no conclusions can be made regarding its effect on amount of protein removed because saturation events occurred. In fact, at the end of 3h some of the solutions had the same or near amount of protein than at 96h, either caused by saturation of the solution or by incapacity to remove more protein from the disc. Nevertheless, these results were important for two main aspects: first, to understand the range of volumes that could be used that would still allow protein detection as fast as 3h after starting incubation; and secondly to determine how fast saturation could occur in order to further adjust incubation cycles in terms of number and duration.

Minding these results Tris HCl (pH 7.4) was selected as initial incubation solution to proceed to further tests, along with a 0.25mL solution which would allow obtaining more concentrated samples, thus enabling an easier detection of protein amounts and protein variations.

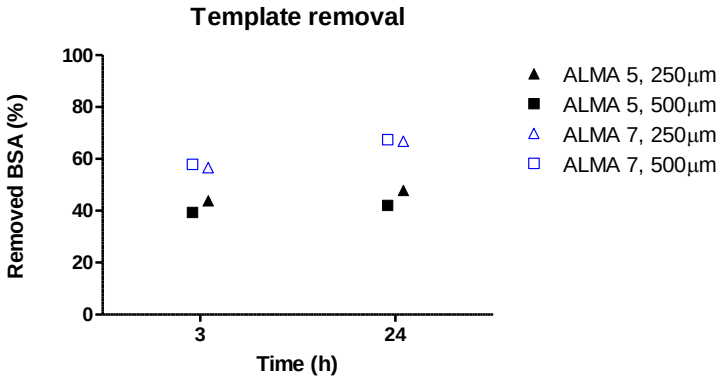

Figure 18. Effect of thickness in the amount of protein removed. Results obtained for n=1 disc per condition.

To further improve protein diffusion within discs and increase the area of available surface, a third study (**protocol C, Tab. 5**) was performed where disc thickness was reduced to either 250

or 500μm, in opposition to the initial 750μm. Results are presented on **Fig. 18**. This template removal protocol included a 3h cycle in Tris HCl and one cycle of 24 h in DI water. Once again, higher template removal occurred for ALMA 7 than ALMA 5. ALMA 7 discs had a protein release at the end of 24h of about 66% and 67%, for discs of 250 and 500μm, respectively, whereas ALMA 5 discs reached 48% and 42%, respectively for the same conditions.

No major differences in template removal were noticed for discs with different thickness, even when comparing with 750μm. Nevertheless, the selected spacer size to proceed to further experiments was 500 μm since these discs were easier to manipulate comparing to 250 μm. Comparing to discs produced with 750μm, 500 μm discs increase the area of exposed surface, reducing thickness by approximately 33 % while having an approximately 1.5 fold increase in diameter (3.7 ± 0.58 mm versus 5.6 ± 0.27 mm, respectively). This characteristic is important for protein diffusion within the disc, either in or out, as less material occupies the bulk region and becomes more superficial [123]. This height reduction may also improve crosslinking efficiency and homogeneity as less penetration of UV rays is required to achieve the bottom region of the disc and broader regions of polymer absorb the same UV light intensity.

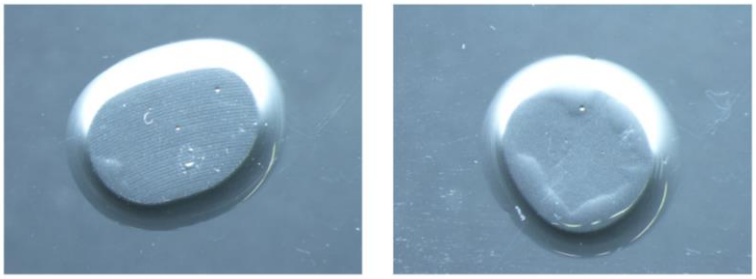

Figure 19. ALMA 5 (left) and ALMA 7 (right) discs as produced.

Non-imprinted polymer (NIP) and molecularly imprinted polymer (MIP) discs produced from ALMA 5 and ALMA 7 using 500μm spacers (**Fig. 19**) measured approximately 0.54±0.05 mm of height, 5.6±0.27mm of diameter (as mentioned above) and weighted approximately 16.7±1.48mg upon production (**S 3**). Additional analysis of ALMA 5 and ALMA 7 NIP and MIP discs was also performed by Cryo-SEM. No major differences were observed between ALMA 5

and ALMA 7 alginate discs nor between NIP and MIP discs. **Fig. 20** shows representative images obtained by Cryo-SEM. It was possible to observe the existence of macro-pores (**Fig.20A**) that were sometimes concomitant with the presence of a dense net of micro-pores (**Fig.20B**). For some preparations, a transition zone was also observed (**Fig.20C**). No major conclusions can be formulated regarding these data since the required Cryo-SEM processing of samples for the assay (freezing, fracturing, sublimation and coating).

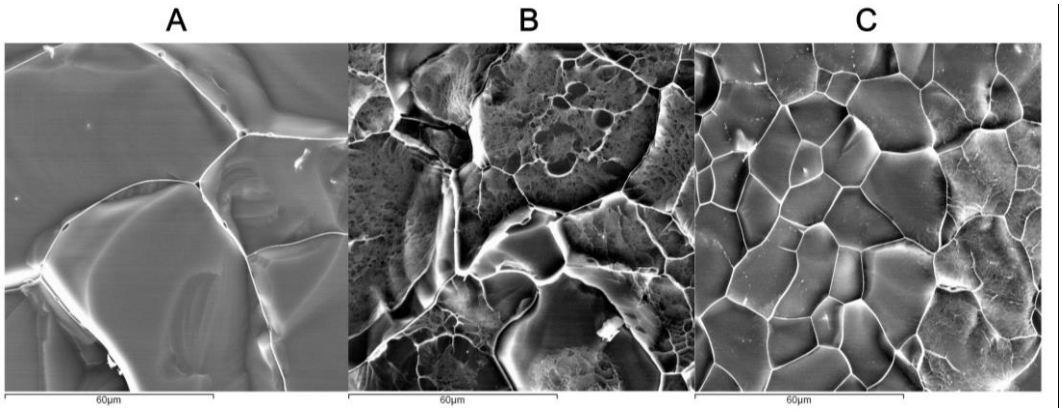

Figure 20. Representative Cryo-SEM images of ALMA 5 and ALMA 7 discs. For all four materials (ALMA 5 and 7, NIP and MIP discs), it was possible to observe the existence of either macro-pores (A), macro-pores with dense nets of micro-pores (B) and also transition zones (C). Scale bars represent 60µm.

Considering all data collected up until this point, a final template removal protocol (**protocol D, Tab. 5**) was defined: two cycles of 1h 30min each in Tris HCl (pH 7.4), instead of one cycle of 3h, to avoid protein saturation in the solution and promote higher protein diffusion at a stage where swelling events are pronounced; followed by 2 cycles of 24h incubation in DI water, instead of only 1 cycle of 24h, to further remove any remaining protein and Tris residues. Additionally, the whole protocol was performed in continuous agitation (150rpm, RT) to promote the diffusion of protein and solution throughout the discs.

This template removal protocol was further evaluated by different methodologies and results are presented and discussed in the following section.

4.3. Template removal analysis and characterization

4.3.1. Template removal quantification by analysis of supernatant

Fig. 21 and **Tab. 6** present results from template removal for ALMA 5 and ALMA 7 MIP discs by protein quantification in the incubation solution (supernatant), being therefore an indirect method of quantification.

As it can be observed on **Fig. 21** and **Tab. 6**, both ALMA 5 and ALMA 7 discs presented a significant protein removal in the first 1.5h of incubation, with more than 50% of protein removed during this period of time for both materials. At 3h of incubation, these values increased to 61.4% and 83.5%, with significant differences starting to be noticed between ALMA 5 and ALMA 7 discs. The same tendency was observed on the following 24 and 48h as these values increase to a maximum of 65.8% (24 h) for ALMA 5 and 94.2% (48 h) for ALMA 7.

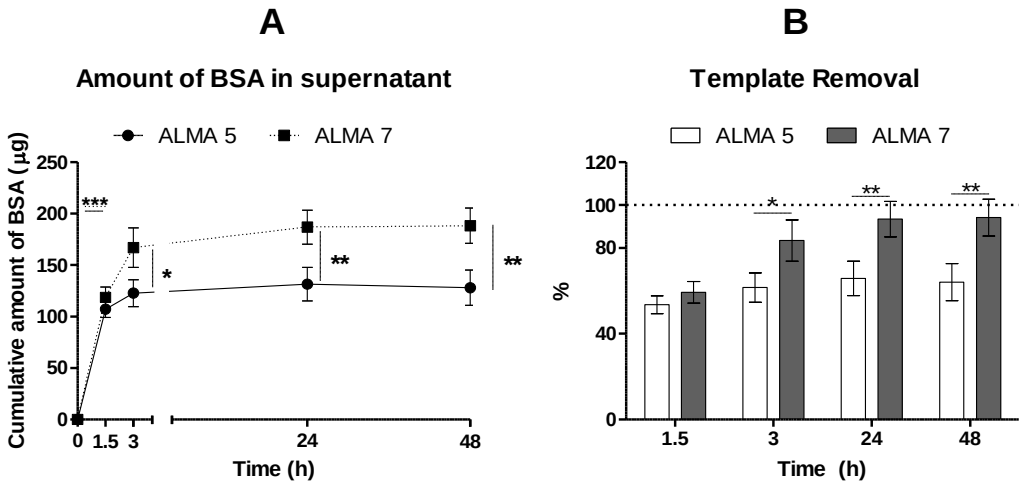

Figure 21. Amount of BSA removed in ALMA 5 and ALMA 7 discs (A) and percentage of template removal (B) by protein quantification in the supernatant (incubation solution). Points and bars represent mean values of n=4 discs ± SD; horizontal and vertical asterisks represent statistical differences (* $p < 0.05$, ** $p < 0.01$, *** $p < 0.001$) between different timepoints and different materials, respectively.

Table 6. Amount of BSA removed in ALMA 5 and ALMA 7 discs and percentage of template removal determined by protein quantification in supernatant (incubation solution). Data represent mean values of n=4 discs ± SD. Data corresponds to data shown in **Fig. 21**.

	Time (h)	1.5	3	24	48
ALMA 5	Cumulative m_{BSA} in supernatant (µg)	107.2±6.82	122.9±11.39	131.6±14.00	128.1±14.84
	Removed template (%)	53.61±3.41	61.4±5.69	65.8±7.00	64.0±7.42
ALMA 7	Cumulative m_{BSA} in supernatant (µg)	118.7±8.74	166.9±16.63	186.9±14.33	188.3±14.88
	Removed template (%)	59.3±4.37	83.5±8.32	93.5±7.17	94.2±7.44

Between 24h and 48h, the amount of protein removed from discs is barely altered. This may be indeed because the rest of protein remaining inside discs is deeply entrapped within the bulk, due to lower diffusional forces which are not enough to promote protein exit from the disc, or because the amount of protein present in the solution in comparison with its volume starts reaching the limit of the detection range of the protein assay kit used to perform these quantifications.

4.3.2. Template removal quantification by analysis of digested discs

Another approach used for quantifying the amount of protein being removed from the disc was by quantification of protein present in digested discs (direct method). Since this approach is destructive, only timepoints of 0, 3 and 48h were tested. Results are presented in **Fig. 22** and **Tab. 7**. Results obtained by this method were in concordance with previously shown data by supernatant analysis and tend to present lower standard deviations than the previous method.

It was possible to verify a significant amount of protein release occurring in the first 3h of incubation, at the end of which 56.7% and 89.9% of protein was removed from ALMA 5 and ALMA 7 MIP discs, respectively. At the end of the template removal protocol this values reached 69.8% and 98.5%, respectively, representing an additional 10% increase, approximately. Again, significant differences between ALMA 5 and ALMA 7 alginate were observed starting at 3h and

these differences were even more pronounced once the template removal protocol was completed.

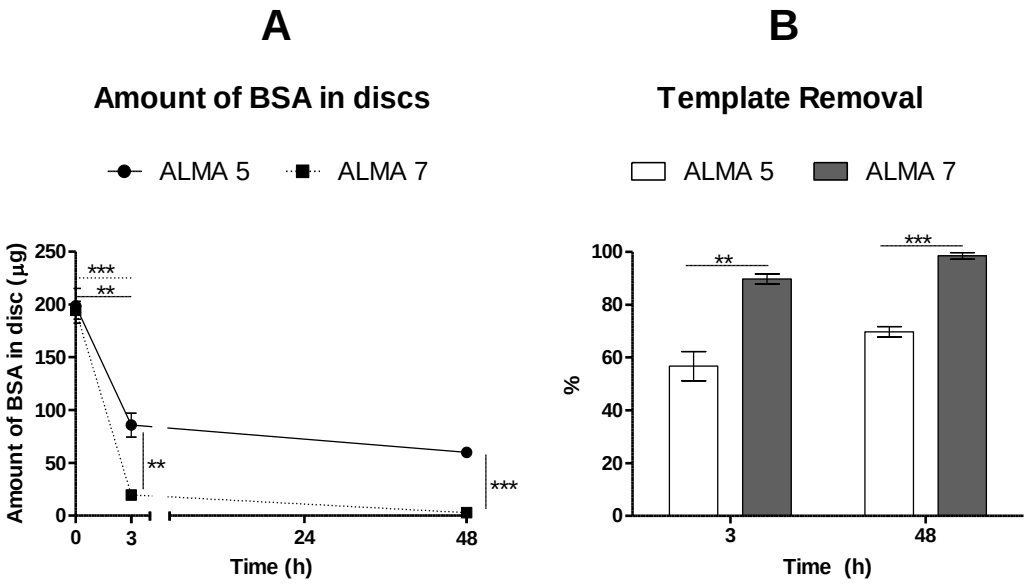

Figure 22 Amount of BSA removed in ALMA 5 and ALMA 7 discs (A) and percentage of template removal (B) by protein quantification in digested discs. Points and bars represent mean values of n=4 discs ± SD; horizontal and vertical asterisks represent statistical differences (** $p < 0.01$, *** $p < 0.001$) between different timepoints and different materials, respectively.

Table 7. Amount of BSA removed in ALMA 5 and ALMA 7 discs and percentage of template removal determined by protein quantification in digested discs. Points and bars represent mean values of n=4 discs ± SD. Values corresponding to **Fig. 22**.

	Time (h)	0	3	48
ALMA 5	m_{BSA} in disc (µg)	198.8±14.23	85.9±9.84	59.9±3.09
	Removed template (%)	-	56.7±4.81	69.8±1.84
ALMA 7	m_{BSA} in disc (µg)	194.6±7.35	19.8±3.11	2.9±1.53
	Removed template (%)	-	89.9±1.52	98.5±0.84

Overall, these data indicated that the first 3h of incubation were crucial for template removal, with more than half of the protein being removed at this stage. This was concomitant with the significant increase of swelling ratio occurring at this phase, caused by rapid entrance of solution into the discs (**Fig. 23**). This event not only helped protein removal by promoting polymer expansion, leading to more free space in the polymer mesh, allowing better protein mobility within the disc, but also by creating diffusional forces to support BSA exit out of the disc and into the solution.

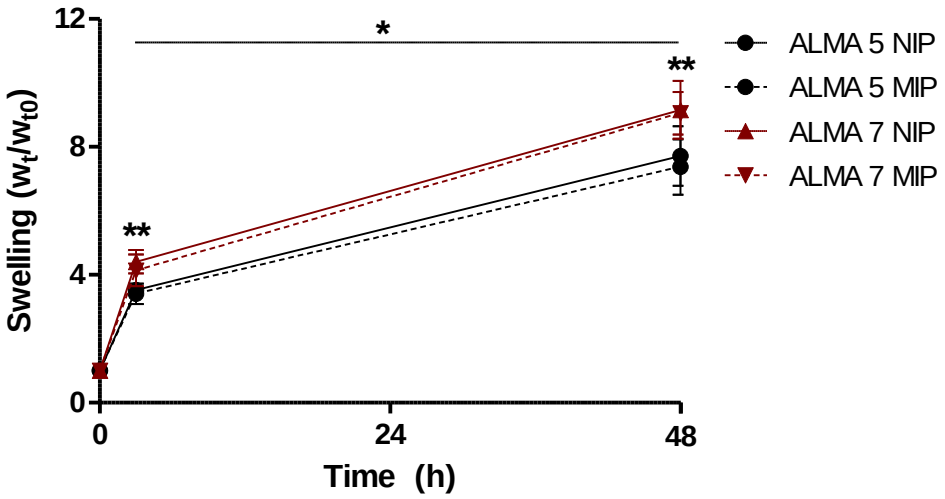

Figure 23. Swelling profile of ALMA 5 and ALMA 7 NIP and MIP discs during template removal protocol. Maximum swelling ratio of approximately 7 for ALMA 5 and 9 for ALMA 7 discs at 48h. Data represent mean values of n=4 discs ± SD. Statistical analysis performed in comparison with t=0 h by unpaired t test with Welch's correction. Asterisks represent statistical differences between timepoints, * < 0.05, ** p < 0.01.

Nevertheless, it was in the following 48h that major differences occurred between both materials. For ALMA 5 MIP discs, despite the amount of protein still present in the disc (approximately 40% at 3h) and the continuous increase in swelling ratio, template removal did not seem to follow the same tendency. This was namely true when analyzing results from quantifications in the supernatant, since by quantification of digested discs it was possible to

still detect more 13% of removed protein between 3 and 48h of protocol. Being an indirect method of quantification, determination of template removal by analysis of supernatant was more prone to fail detection of variations in protein content, and this was particularly true on the final washing steps. The small amount of protein being removed to the solution causes low protein variations that were most likely out of the detection range of the kit used during this last phase of template removal.

Differences between ALMA 5 and ALMA 7 discs may be caused by the different protonation state of these materials, already explained above, which also influences the swelling behavior. Even though no significant differences were obtained for ALMA 5 and ALMA 7 swelling ratios at 48 h (7 and 9, respectively, **Fig. 23**), a closer look at these values shows that they represent a difference of 200 % in swelling ratio. By other words, for the same condition and same timepoint, ALMA 7 discs suffered an additional doubling on weight (regarding its initial value) while comparing to the ALMA 5 discs. When working at a µg quantification range such differences become quite significant.

Results obtained by both detection methods were highly comparable, pointing to a total of protein removal of approximate 70% for ALMA 5 and over 94% for ALMA 7 at the end of the template removal process. The fact that no more protein was removed from ALMA 5 discs may be caused by a combination of lower diffusional forces and entrapment of the remaining protein deeply within the mesh of the alginate disc - thus being impossible to remove despite the number and duration of template removal cycles – and the lower swelling ratio. In the study reported by Bayer and colleagues [79], who developed a molecularly imprinted ionically-crosslinked alginate film system, only around 67% of the template was removed during the washing steps at the end of approximately 160h, indicating that the results obtained with the present template removal protocol are promising. These differences may be caused by different swelling ratios since in Bayer *et al.* [79] this parameter reached a maximum of approximately only 2.5 at the end of the sixth day. This is, of course, highly dependent on the type of alginate and the type of crosslinking used. Template removal protocols vary in the literature of alginate MIP systems and strongly depend on the type of MIP produced. Duration of these protocols also varies widely, from several hours to several days [44, 49, 72, 80, 81]. Herrerto *et al.* [80] optimized a template removal protocol for BSA-MIP alginate microcapsules (ionic crosslinking) using Tris HCl with 1% $CaCl_2$ (pH 7.4) and achieved almost 90 % of template removal at the end of 5 h [80]. In this project, at the end of 3h almost 60% for ALMA 5 and 90% for ALMA 7 of

template removal was already achieved. Comparing results obtained by Herrero *et al.* [80], this results are quite promising, especially because they refer to a nearly bulk system where template removal is harder to achieve.

4.3.2. Template removal quantification by GTA method

Throughout this project, in order to overcome obstacles regarding protein detection, an alternative GTA-based method was developed based on work presented by Ma *et al*. [104]. In their work, Ma and coworkers [104] created a green fluorescence protein hydrogel composed of BSA crosslinked with GTA, which was able to exhibit green and red fluorescence when excited at λ =470nm and 595nm, respectively [124]. Despite having an intrinsic fluorescence derived from two tryptophan residues (excitation at λ=279nm and emission at λ=348nm), this BSA profile is affected by reaction with GTA. In 1968, Habeeb *et al.* [125] studied the reactivity of functional groups of amino acid residues present in proteins with GTA. The authors described the reaction between GTA and proteins like BSA or ovalbumin as occurring predominantly with the ϵ-amino groups of lysine to form mainly intermolecular crosslinkages [125]. These interactions can explain the formation of new classes of compounds formed by BSA-GTA crosslinkage which are able to absorb and emit at different ranges of wavelengths.

As so, in preliminary studies, ALMA 5 NIP and MIP discs were incubated in GTA solution for 30mins at RT and observed in a wide-field microscope at different timepoints of processing: as produced (t=0h) and throughout template removal protocol (t=3, 24 and 48h) (**Fig. 24**). It is possible to see clear differences between t=0h NIP (**Fig. 24A**) and MIP discs (**Fig. 24B**). While MIP discs still containing protein presented high fluorescence for all channels in the disc region, the same was not observed for NIP discs which do not contain protein in their solution.

Throughout the template removal protocol, MIP discs presented continuously lower fluorescence, indicating progressively lower protein contents. Once again, a great difference was

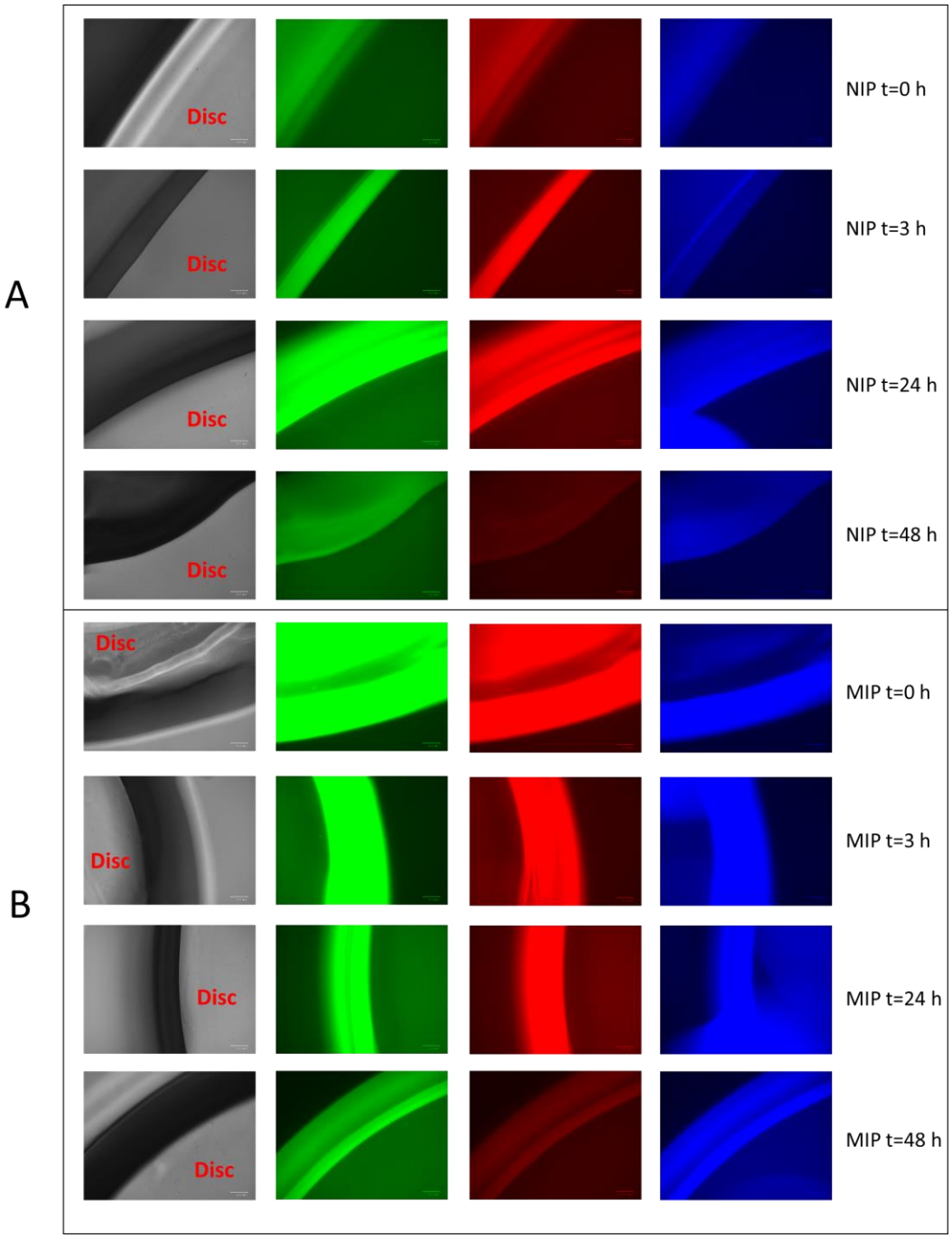

Figure 24. Images obtained by Zoe Fluorescent Cell imager for ALMA 5 NIP (A) and MIP (B) discs at different timepoints of production. Images of brightfield and green (G), red (R) and blue (B) channels can be observed, respectively.

observed between t=0h and t=3h, while from this timepoint on variations became narrower despite being perceptible.

It should be mentioned that for the three channels (G, R and B), in all discs, borders could be observed as a green, red or blue lines, respectively. This was not caused by any major fluorescence event occurring in the sample itself, but most likely due to light reflection occurring in the thick border of discs or coming from reflections on the walls of each well (samples were incubated in 24-well plates), due to the wide region of incidence of the LED lights and non-existent removal of out-of-focus light. Additionally, this border light varied in thickness due to low focus capacity caused by the thickness of the discs.

Overall, this method presented consistency between samples and returned expected results regarding the variations of protein content during the whole processing and the observed variations in fluorescence. Using a qualitative analysis, it could be concluded that the information obtained by this method was in agreement with data from the previously studied techniques.

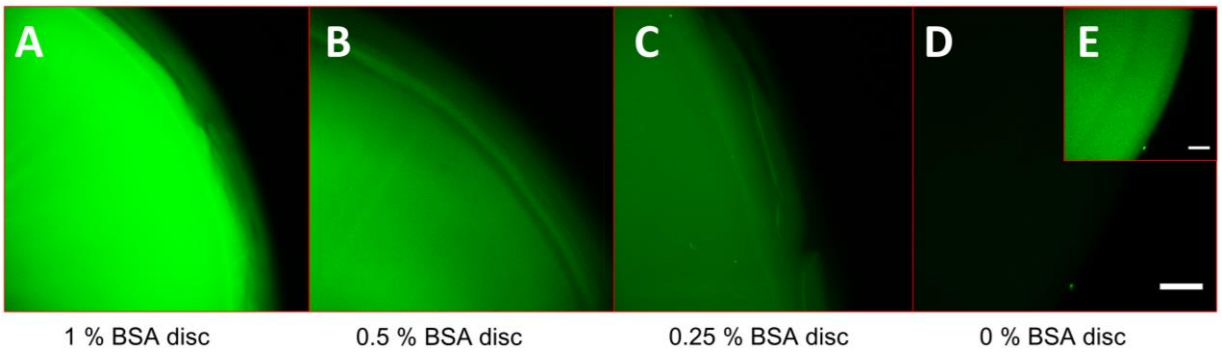

Figure 25. Representative images of standard samples obtained by inverted confocal microscopy. Images are the result of a z-projection (4 stacks per image) containing 1% (A), 0.5% (B), 0.25% (C) and 0% BSA (D) after incubation overnight in 25% glutaraldehyde solution (4°C). Section (E) is the result of contrast adjustment of section D. 0% and 1% BSA discs correspond to the same composition as NIP and MIP discs, respectively. Scale bar represents 200µm, λex= 488nm.

In order to provide quantitative analysis of the template removal protocol using this method, it was necessary to develop a strategy for protein quantification by correlation with BSA autofluorescence. To do so, inverted confocal microscopy was used to improve lateral and axial resolution (comparing to the previously used wide-field fluorescence microscopy), by eliminating out-of-focus light, an inherent characteristic of inverted confocal microscopy [126].

As a proof of concept, in an attempt to demonstrate that it was possible to correlate autofluorescence with protein content, a methodology was developed in which standard samples of ALMA 5 discs containing from 0 up to 1% BSA in their composition were analyzed under the microscope after incubation with GTA and at a λex = 488nm. Images obtained are shown in **Fig. 25**. As expected, a decrease in green fluorescence was observed, which was concomitant with a decrease in protein content with 1% BSA discs (**Fig. 25A**) presenting higher green fluorescence. For 0 % BSA discs (**Fig. 25D**) it was not possible to observe any fluorescence unless contrast and brightness are adjusted (**Fig. 25E**).

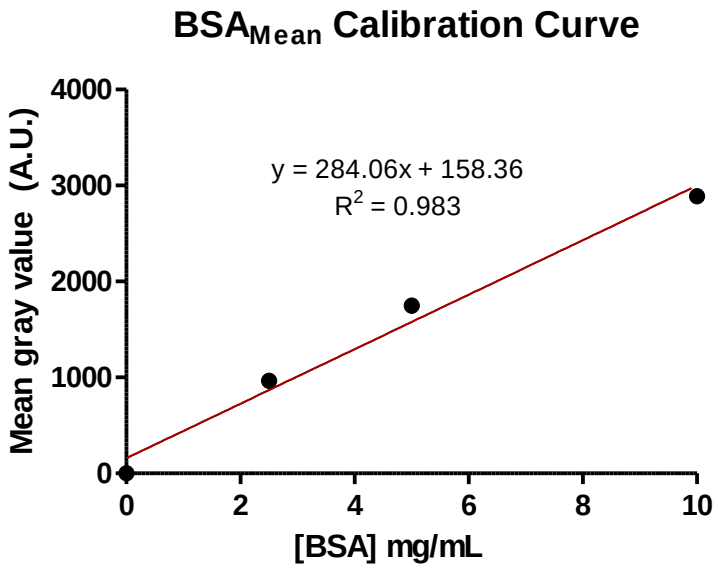

Figure 26. Calibration curve obtained by analysis of inverted confocal microscopy images to correlate the Mean Gray Value (A.U.) with the amount of BSA (mg/mL) present in discs. Results obtained from 3 measurements per disc, n=3 discs.

In order to check if the observed correlation between green fluorescence and protein concentration followed a linear correlation, the Mean gray value, or solely Mean (arbitrary units, A.U.) was used as a measure for quantifying fluorescence.

Following this approach, it was indeed possible to linearly correlate green fluorescence with the amount of protein present in discs (**Fig. 26**).

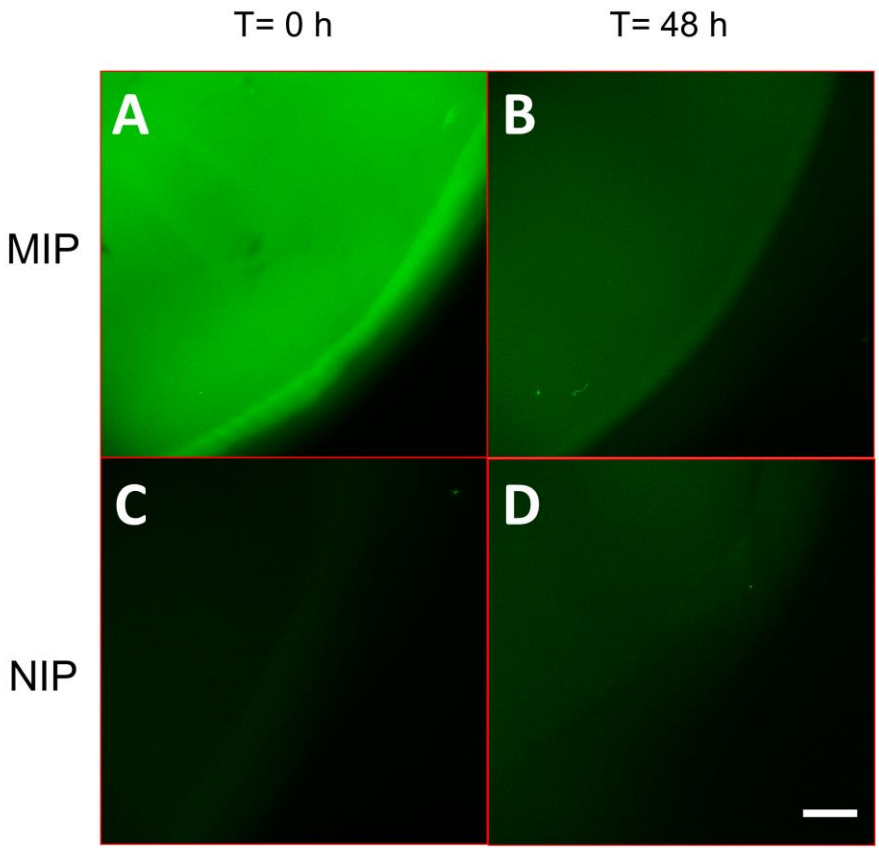

Figure 27. Representative images of samples before (A and C) and after (B and D) template removal protocol obtained by inverted confocal microscopy. Images are the result a z-projection (4 stacks per image) of t=0h and t=48h samples after incubation overnight in 25% GTA solution (4°C). Scale bar represents 200µm, λex= 488nm.

Even though using the Mean as measure of fluorescence was the selected approach, also Integrated Density (IntDen, A.U.) could have been used. However, since IntDen is obtained by

multiplying the Mean by the area of measurement and, in the case of this project, all measurements performed had exactly the same dimensions (area = 39921.913, **S 4**), results would be proportional. Examples of measurements performed and a calibration curve obtained by correlation of IntDen and protein concentration are shown in Supplementary Data (**S 4** and **S 5**).

Afterwards, ALMA 5 samples which undergone template removal protocol were analyzed following the same protocol and results are shown in **Fig. 27** and **Fig. 28**.

Differences in fluorescence were visible between ALMA 5 MIP discs as produced (**Fig. 27A**) and after template removal (**Fig. 27B**) and these differences correlated with significant differences in Mean values and amount of protein detected in discs (**Fig. 28A-B**). Oppositely, no major differences in NIP discs could be observed (**Fig. 27C-D** and **Fig. 28A**).

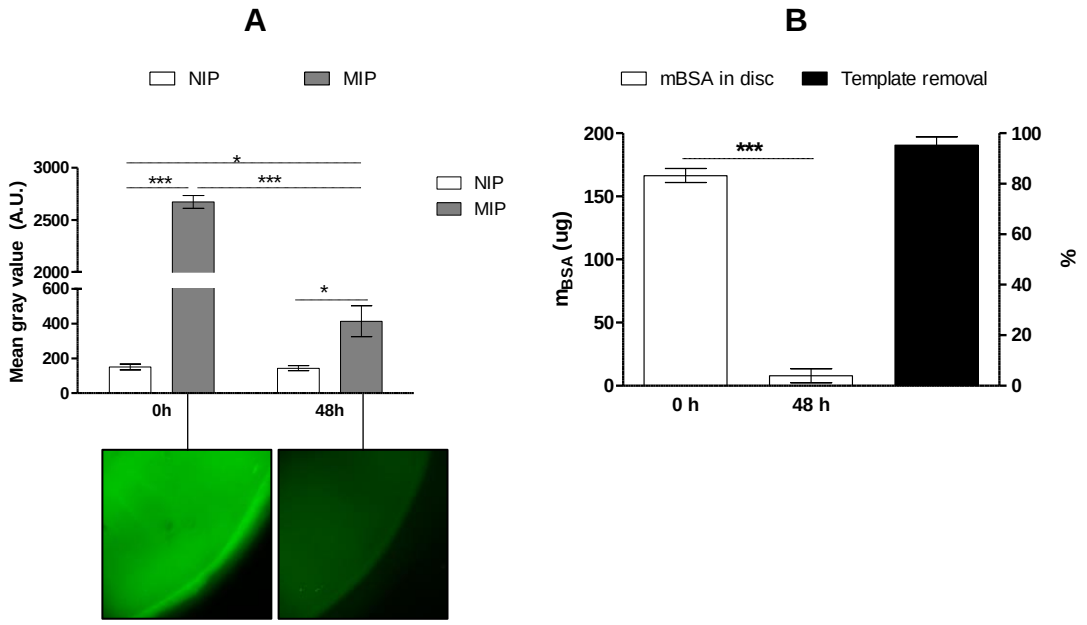

Figure 28. Representation of mean gray value of NIP and MIP discs (A) and amount of protein present in MIP discs and corresponding template removal (B) before (0h) and after template removal protocol (48h) determined by GTA method. Mean gray values represent absolute values measured. Bars represent mean values ± SD, n=3 discs (3 measurements per disc). Statistical analysis performed by unpaired t test with Welch's correction, * $p < 0.05$, *** $p < 0.001$.

Even though qualitative results were as expected, quantitative analysis of data showed a template removal of around 95%, much higher than the approximately 70% obtained for ALMA

5 by the two previously described methods. These differences may be a result of several factors. Besides not being a fully optimized protocol for protein quantification, this method seemed to be more dependent on sample structural quality than the previous methods. After GTA incubation, shrinking caused by GTA-crosslinking led to higher shrinking of discs with higher protein content than discs with residual protein. These differences in shrinking, also observed for standard samples with different percentages of BSA but were indirectly accounted when the calibration curve was determined. However, they may influence quantifications in samples subjected to long processing steps that inevitable lead to polymer loss with time. This loss of polymer from the discs may lead to differences in quantifications by two hypothetically ways: in one hand, slightly higher shrinking levels of discs may occur due to lower structural stability, thus increasing mean values measured; on the other hand this can lead to higher protein release when discs are incubated in the GTA solution and before crosslinking occurs.

4.4. Rebinding assays

Rebinding assays were performed to characterize the capacity of NIP and MIP discs to adsorb/absorb the template molecule, thus evaluating two main molecular imprinting parameters: the rebinding capacity (Q, μg/mg, Eq.1) and the imprinting factor (IF, Eq.2). Since the amount of protein present in the rebinding solution influences the recognition features [49], two experiments were performed where discs were incubated in 0.1% or 1% BSA in 0.9% NaCl solution (pH 4.2) for 72h at RT. For this particular analysis, the quantification method selected was by quantification of protein in the digested discs, since it presented lower standard deviations. A parallel comparison with the GTA method was performed for the experiment with 1% BSA solution solely in ALMA 5 discs. Analysis of the supernatant was also tested (**S 6**), but results retrieved had high standard deviations.

In this part of the work, the effective amount of protein contained in discs and the effective amount of protein sorption (adsorption and absorption) by discs during the rebinding assay were defined as separate concepts since template removal was not fully achieved (recalling, ALMA 5 MIPs had still a protein retention of around 30% at the end of the template removal protocol). The amount of protein contained in discs gives a m_{BSA}/m_{disc} (μg/mg) value which includes not

only the amount of protein adsorbed/absorbed but also protein remaining after template removal (only in the case of MIP discs).

Oppositely, the amount of protein adsorbed/absorbed during the rebinding assay was determined by excluding the influence of any protein remaining inside the discs after template removal. This second concept corresponds, therefore, to the rebinding capacity. Based on these values, an IF value was also determined. For NIP discs, both concepts (amount of protein contained in discs and adsorbed/absorbed by discs) correspond to the same value as these discs were never in contact with any protein content up until this stage.

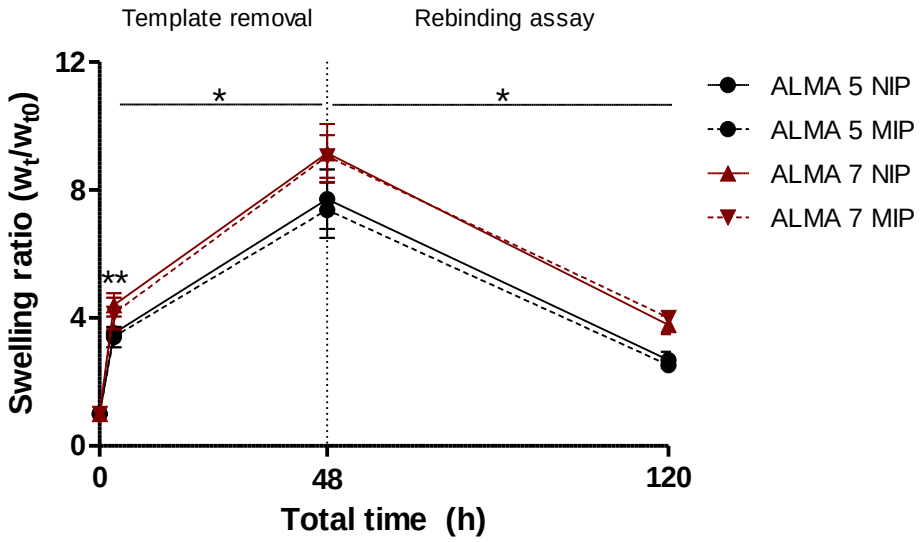

Figure 29. Swelling profile of ALMA 5 and ALMA 7 NIP and MIP discs during template removal (3h and 48h) and rebinding protocol (72h of rebinding assay, total 120h). Maximum swelling ratio of approximately 7 for ALMA 5 and 9 for ALMA 7 discs at 48h. Data represent mean values of n=4 discs ± SD. Statistical analysis performed in comparison with t=0h by unpaired t test with Welch's correction. Asterisks represent statistical differences between different timepoints, * < 0.05, ** p < 0.01.

Before proceeding to protein quantifications, it was possible to observe a clear alteration on swelling profile of ALMA discs. Contrarily to the high increase in swelling ratio occurring during the template removal process, during the rebinding assay both ALMA 5 and ALMA 7 discs suffered a shrinking process (**Fig. 29**). This deswelling event was so pronounced that led to

swelling ratios near or below the ones observed at t=3h of template removal (2.6 and 3.9 for ALMA 5 and 7 discs, respectively). In fact, this could be an explanation why protein quantification by analysis of the supernatant was affected during this assay: as water content in discs was released to the incubation solution, variations in incubation volume led to higher measuring errors.

This deswelling event was most likely caused by a combination of lower pH values (4.2 against 5.5 from DI water) and salt presence (0.9% NaCl) in the rebinding solution. On one hand, lowering the pH means a higher presence of H^+ in the solution, which strongly interact with the negatively charged alginate, namely the carboxylate (COO^-) groups. As pH decreases alginate COO- groups become carboxylic acid groups (COOH) with neutral electric charge, leading to a reduction on electrostatic repulsions and consequent contraction of the polymeric chains, lowering water absorbency [116] and decreasing hydrogel swelling.

On the other hand, decrease in swelling capacity of anionic gels is frequently affected by salts present in solution due to a "charge screening effect" [117]. This effect leads to electrostatic repulsion between anions and is caused by the presence of additional cations. The charge screening effect has been described for alginate and other anionic hydrogels [116, 117] and is strictly dependent on the type of salt and concentration in solution. For instance, in the case of divalent ions, an additional decrease in swelling due to ionic crosslinking events must be accounted [116]. Additionally, this effect can even depend on cation radius, as previously reported by other authors [116], since it affects electrostatic interactions with anionic groups, including carboxylate [127].

pH and salts can affect both the molecular imprinting process and consequent recognition features of produced MIPs [75]. As a consequence, for this part of the project rebinding studies were carried out maintaining the same pH (4.2) and salts (0.9% NaCl) as in the initial BSA solution. In fact, Zhao *et al.* [75] reported maximum Q and IF values at pH values of approximately 4.2 in calcium phosphate/polyacrylate/alginate hybrid polymer BSA-MIP microspheres [75].

4.4.1. Rebinding analysis by protein quantification in digested discs

Regarding the amount of protein present in discs at the end of the 72h (**Fig. 30**, **Tab. 8**), for both experiments, ALMA 5 had higher values of protein present in MIP discs than NIPs (3.3 and 2 times higher, respectively). For ALMA 7 discs, when incubated in 0.1% BSA solution, MIP presented a value for BSA content 1.3 times higher than NIP discs but such difference was not observed when increasing the amount of protein present in solution to 1%, with ALMA 7 MIP and NIP discs presenting similar amounts of protein content in this case.

Since ALMA 5 MIPs presented higher protein content at the end of protein removal protocol than ALMA 7 MIPs, protein remains could be affecting these results.

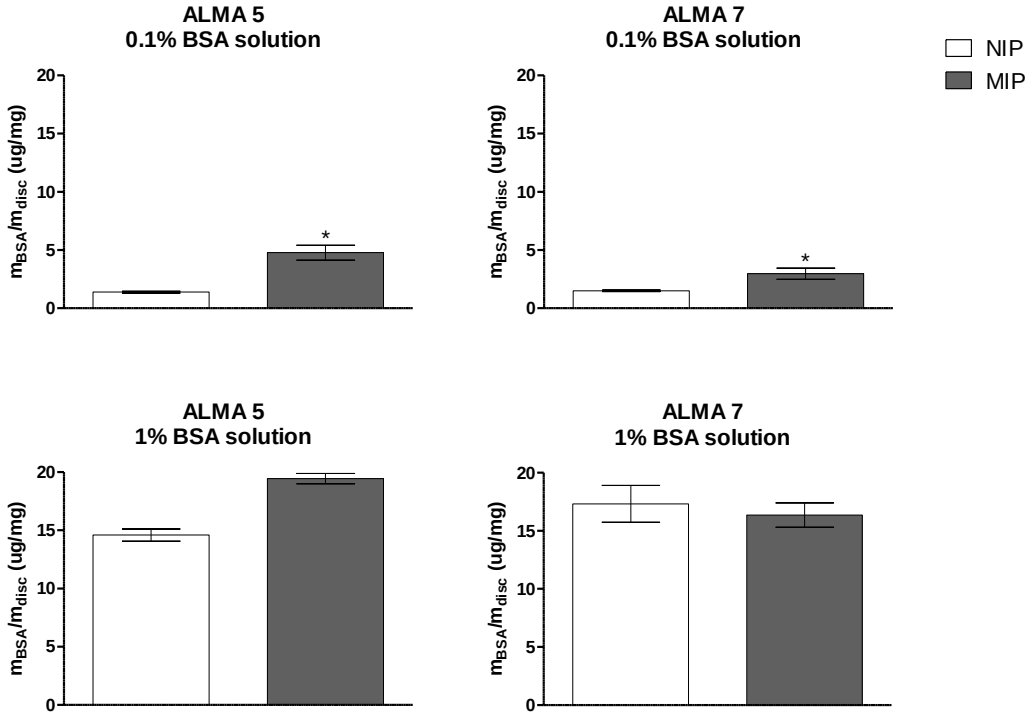

Figure 30. Amount of BSA present in ALMA 5 and ALMA 7 NIP and MIP discs after 72h incubation in 0.1% and 1% BSA solution in 0.9% NaCl (pH 4.2). Data obtained by protein quantification in digested discs, bars represent mean values of n=3 discs ± SD. Statistical analysis by unpaired t test with Welch's correction, * $p < 0.05$,.

Table 8. Amount of BSA present in ALMA 5 and ALMA 7 NIP and MIP discs after 72 h incubation in 0.1 % and 1 % BSA solution in 0.9 % NaCl (pH 4.2). Data represent mean values of n=3 discs ± SD and values correspond to data shown in **Fig. 30**.

		0.1% BSA	1% BSA
		mBSA/mdisc (µg/mg)	mBSA/mdisc (µg/mg)
ALMA 5	NIP	1.4 ± 0.07	14.6 ± 0.42
	MIP	4.7 ± 0.52	19.4 ± 0.36
ALMA 7	NIP	1.5 ± 0.05	17.3 ± 1.30
	MIP	3.0 ± 0.40	16.3 ± 0.85

In order to understand if this was the reason, the amount of protein adsorbed/absorbed to discs during the rebinding assays was determined. This was performed by simply changing the type of internal control used to do the calculations (item 3.10.2, **Fig. 9**). Briefly, while for determining the amount of protein present in discs, a NIP disc that went through all the processing steps but was incubated in a 0.9% NaCl solution during the rebinding process was used as control, to determine the amount of protein adsorbed/absorbed during rebinding the control used for MIP discs was a MIP that went through all the processing steps but was incubated in a 0.9% NaCl solution containing no protein (**Fig. 9**).

Regarding the amount of protein adsorbed/absorbed during the rebinding assay, existent differences between MIP or NIP discs were reduced (**Fig. 31**, **Tab. 9**). This reduction was mostly noticeable in ALMA 5 discs when incubated in 0.1% BSA solution. Values for ALMA 7 were affected at a lesser extent, which could be explained by the higher rates of protein removal registered for this material.

In fact, when the amount of protein was quantified in MIP discs incubated solely in 0.9% NaCl solution during the rebinding assay, approximately 34.2µg and 3.7µg were still detected in ALMA 5 and ALMA 7 discs, respectively. These values corresponded to 17.2% and 1.9% of the initial protein amount present in discs (approximately 200µg per disc). These data were in agreement with results obtained for template removal and further support the hypothesis that these protein remains were influencing the registered differences in **Fig. 30**. Despite this, the best recognition features occurred for ALMA 7 MIP discs when incubated in 0.1% BSA solution, with an imprinting factor of 1.4, even though these differences are not significant.

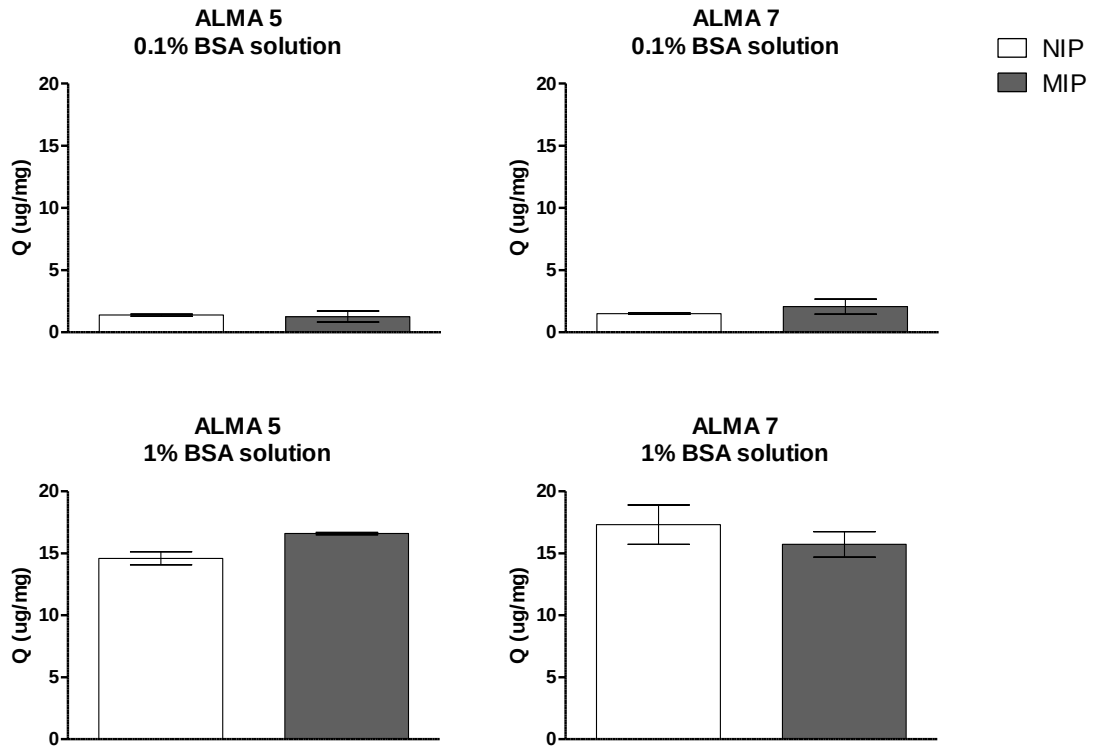

Figure 31. Rebinding capacity (amount of BSA adsorbed/absorbed during rebinding assay) of ALMA 5 and ALMA 7 NIP and MIP discs after 72h incubation in 0.1% and 1% BSA solution in 0.9% NaCl (pH 4.2). Data represent mean values of n=3 discs ± SD. Statistical analysis by unpaired t test with Welch's correction ($p < 0.05$).

Table 9. Rebinding capacity (amount of BSA adsorbed/absorbed during rebinding assay) of ALMA 5 and ALMA 7 NIP and MIP discs after 72h incubation in 0.1% and 1% BSA solution in 0.9% NaCl (pH 4.2). Data represent mean values of n=3 discs ± SD and values correspond to data shown in **Fig. 31**.

		0.1% BSA		1% BSA	
		Q (µg/mg)	IF	Q (µg/mg)	IF
ALMA 5	NIP	1.4 ± 0.07	0.9 ± 0.28	14.6 ± 0.42	1.1 ± 0.03
	MIP	1.3 ± 0.36		16.6 ± 0.07	
ALMA 7	NIP	1.5 ± 0.05	1.4 ± 0.30	17.3 ± 1.30	0.9 ± 0.10
	MIP	2.1 ± 0.48		15.7 ± 0.83	

The decrease in IF observed concomitantly to the increase of protein concentration in incubation solution was expected and most likely caused by increased diffusional forces due to

higher amount of protein present outside the disc, forcing its entrance and unspecific protein absorption into both NIP and MIP discs, and also by the possible increase in the amount of protein adsorbed unto the surface of the discs.

4.4.2. Rebinding analysis by GTA method

In order to further correlate the herein developed GTA method, a rebinding assay was performed on ALMA 5 NIP and MIP discs by incubation in a 1% BSA solution. Standard samples were again prepared for visualization under the confocal microscope on the same day ALMA 5 samples were visualized. A new calibration curve was determined and is presented on **Fig. 32**.

Comparing **Fig. 32** with the previous calibration curve (**Fig. 26**), it was possible to verify consistency between both equations and high coefficients of determination (R^2 ~0.98) even though these calibration curves were resultant of samples from different preparations. Once again, a calibration curve was obtained by correlation with the correspondent IntDen values and is presented in Supplementary Data (**S 7**).

Fig. 33 shows representative images of ALMA 5 NIP and MIP discs over the whole molecular imprinting process **(Fig.33A-D)** and rebinding assay (**Fig.33E-H**). In a qualitative analysis, it was possible to observe differences between NIP and MIP samples and between different timepoints. MIP discs presented slightly higher green fluorescence than NIP discs when incubated in 1% BSA solution (**Fig.33E-F**). Once again, this may have been caused by a cumulative effect of protein still remaining in MIP discs after template removal protocol. This hypothesis is supported by **Fig.33G** which represents a MIP disc after 72h in solution without BSA with still considerable green fluorescence. On the other hand, NIP discs exposed to the same conditions presented lower green fluorescence.

Green fluorescence was correlated with Mean values (**Fig.34A**), amount of protein present in discs and amount of protein sorption during rebinding assay (**Fig.34B**). No significant differences were found between NIP and MIP Mean values and the same tendency was verified for the amount of protein present in and adsorbed/absorbed into discs.

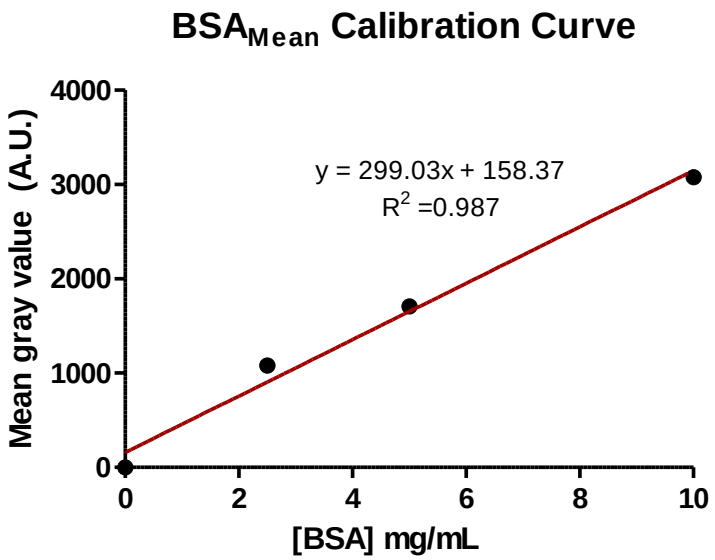

Figure 32. Calibration curve obtained by analysis of inverted confocal microscopy images to correlate the Mean Gray Value (A.U.) with the amount of BSA (mg/mL) present in discs. Results obtained from 3 measurements per disc, n=3 discs.

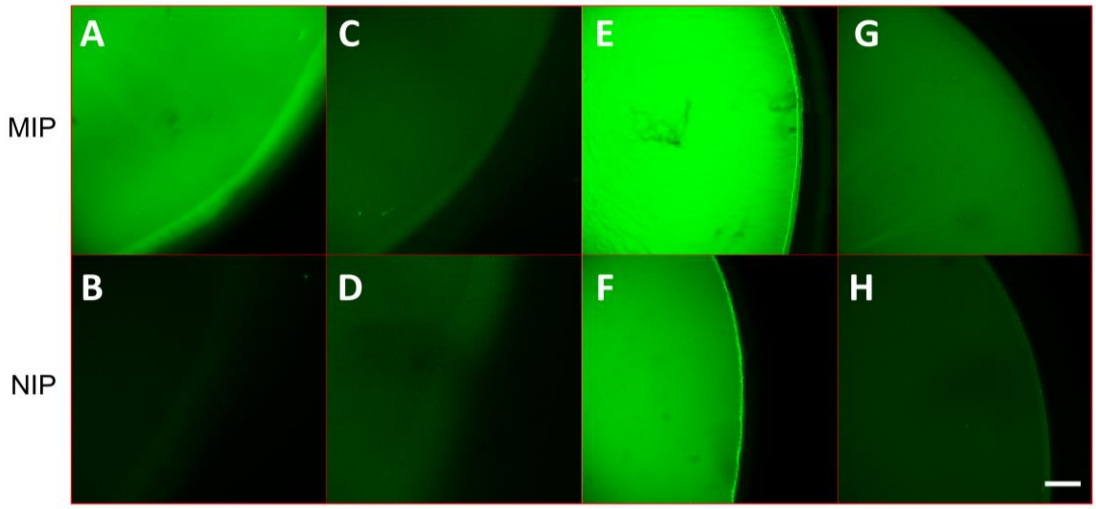

Figure 33. Representative images of ALMA 5 MIP and NP samples before (A and B) and after (C and D) template removal protocol, and after 72h incubation in 1% BSA in a 0.9% NaCl solution (E and F) or solely in 0.9% in NaCl solution (G and H), obtained by inverted confocal microscopy. Images are the result a z-projection (4 stacks per image) samples after incubation overnight in 25% GTA solution (4ºC). Scale bar represents 200µm.

Contrarily to what was expected, MIP discs incubated in 0.9% NaCl solution presented higher Mean values and corresponding amount of protein (~781A.U. and 31μg) after these 72h of incubation than after template removal (~413A.U. and 8μg). Such differences were not noticed for NIP discs which presented approximated Mean values for both assays (~150 versus ~161, respectively).

The increase in Mean values for MIP control discs was not expected since no protein was added after template removal to these internal controls and may have affected protein quantification results. This event supports the hypothesis that, as it is currently designed, this method is highly dependent on the structural quality of samples due to the shrinking effect caused by glutaraldehyde crosslinking.

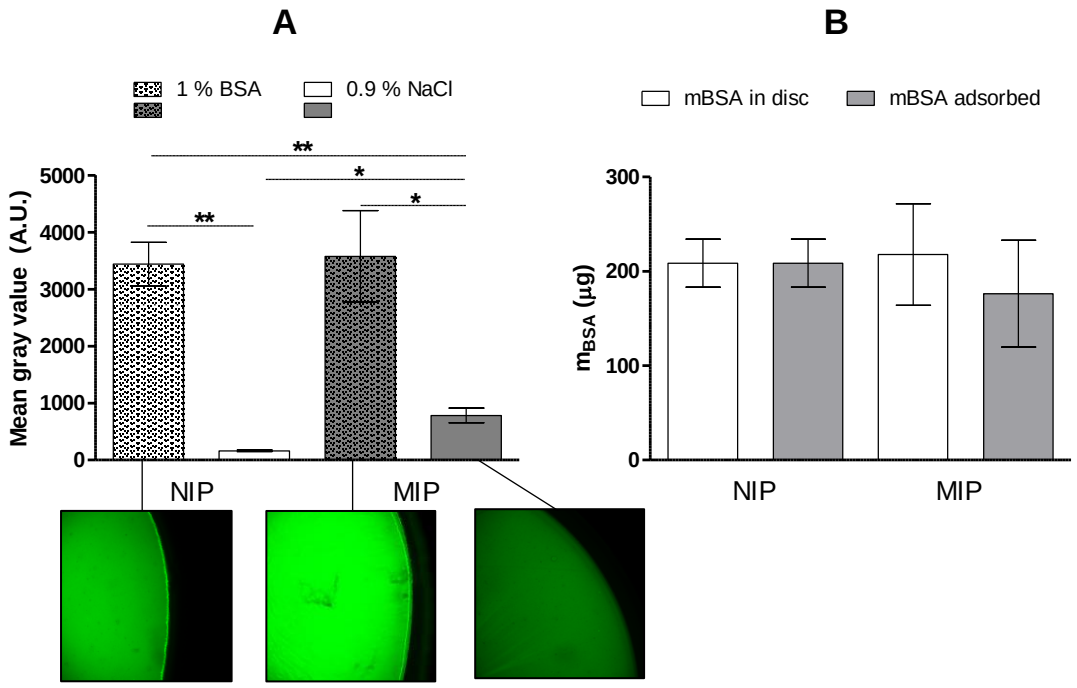

Figure 34. Representation of Mean gray value of NIP and MIP discs during rebinding assay (A) and amount of protein present in and adsorbed/absorbed into NIPs and MIPs (B) after incubation in 1% BSA solution or 0.9% NaCl (internal controls) for 72h determined by GTA method. Mean gray values represent absolute values measured. Bars represent mean values ± SD, n= 3 discs (3 measurements per disc). Statistical analysis by unpaired t test with Welch's correction, * $p < 0.05$, ** $p < 0.01$).

On the other hand, considering the initial amount of protein present in MIP discs at t=0h (~166μg) determined previously by GTA method (**Fig. 28B**), the amount of protein detected for this MIP control is in fact equivalent to 18% of this value. This was the approximate same relative amount of protein content also detected for the same samples when analyzed as digested discs (17.2%). If this is the case, then the quantification problem by GTA method occurred during quantifications of template removal, instead of during rebinding quantifications.

In fact, if quantifications obtained by analysis of digested NIP and MIP discs are converted from mBSA/mdisc (μg/mg) solely to total amount of protein (μg) per each disc after rebinding, results obtained were also similar: 267±15.7μg and 271±6.8μg for NIP and MIP, respectively, by analysis of digested discs, against 176±46.2μg and 218±43.9μg by the GTA method. It is noticeable that standard deviations generated by GTA method are considerable, but they are acceptable since this is hardly an optimized quantification method.

Independently of which theory is correct, both support the idea of a tight dependence of this method with structural features of the sample and its susceptibility to different processing parameters such as the type of incubation solution used. For instance, the fact that, at the end of the template removal protocol discs reached their maximum swelling ratio and presented higher water content than at the end of the rebinding assay, may have affected the results.

The effects of shrinking driven by GTA crosslinking, and how they are affected by the water content of discs upon incubation, were also not accounted. For example, samples from 48h with higher water content may lead to variations in the total concentration of GTA incubation solution enough to cause differences in crosslinking and thus the shrinking profile, affecting the observed green fluorescence and the resulting quantification. This may be the reason why internal control discs used for rebinding had results similar to the ones determined by analysis of digested discs, oppositely to the same discs when they were incubated in DI water.

Up until now, no literature exists exploring this BSA-autofluorescence event induced by GTA as a method for neither qualitative nor quantitative analysis of protein content. Minding the embrionary state of this methodology, the few experiments developed presenting congruent results, and the potential adjustments to be made to inherent characteristics of the quantification system (*e.g.* mathematical normalization of shrinking effects), results obtained herein are promising. These quantification method can be applied to BSA protein and also other proteins to which GTA may cause similar effects (*e.g.* ovalbumin). Additionally, even when not

optimized for quantitative analysis by confocal microscopy, this method was a facile and rapid way of follow through of the molecular imprinting process by qualitative analysis of fluorescence levels in an equipment requiring low technical requirements and expenses.

4.5. General overview of the MIP-ALMA system

In this topic, an evaluation of the MIP-ALMA system will be presented regarding the system as a whole. The success of any MIP system is the result of a combination between template removal and recognition capabilities which are dependent on the type of material and protocols followed.

In general, template removal was successfully achieved by following the herein optimized protocol with a template release of approximately 70% for ALMA 5 MIPs and an average value of 96% for ALMA 7 discs, for a total protocol duration of 48h. These data were quantitatively confirmed by two different methods of quantification and are quite positive when comparing to values achieved in the literature [44, 49, 72, 80, 81] [79]. As referred above (item 4.3.1), in a similar system based solely in alginate developed by Bayer *et al.* [79] only approximately 67% of the template was removed at the end of 160h. The protocol herein developed not only shortens the duration of washing steps, but also increases the amount of protein released from MIPs. Results obtained herein can even be further compared to the ones obtained by Herrero *et al.* [80] for alginate microcapsules where almost 90% of template removal was obtained at the end of 5h, against the 60% (ALMA 5) and 90% (AMA 7) obtained at 3h of the protocol described in this project. Minding that the MIP-ALMA discs are closer to a bulk imprinting approach, where template removal is usually harder to achieve, results were promising. Even though quantification by GTA method was not quantitatively comparable with both supernatant and digested disc analysis, qualitative results were as expected.

Rebinding evaluation is the ultimate test that a MIP system must go through in order to prove itself as viable. IF is the most direct parameter to evaluate how efficient a MIP system is comparing to non-modified systems, since rebinding capacity, *Q*, is usually presented in different units and dimensions which best fit each system design. Results obtained for rebinding by analysis of digested discs were in agreement with the GTA method also developed in this work.

In the case of this project, the best IF values obtained, 1.1. for ALMA 5 and 1.4 for ALMA 7 are far from ideal but already fit the range of reported IF for BSA MIP systems solely based on alginate (1.1 up to 4.9) [44, 49, 72, 79, 80]. It is noticeable, however, that direct comparisons can be hardly made because no BSA-MIP system based on photocrosslinking of any modified or methacrylated alginate is reported and imprinting parameters strongly depend on the type of molecular imprinting approach used. Thus, these results are a good starting point for further optimizations.

Altogether, results obtained by analysis of digested discs and GTA method indicate that this MIP system is still in its embryonary state, since no significant differences in template recognition are detected between NIP and MIP discs. The small differences observed between NIPs and MIPs in rebinding capacity may have distinct causes and shall be further scrutinized.

Firstly, the absence of recognition features indicate that most protein sorption occurring may be non-selective, either because no effective imprinting cavities are being produced upon ALMA polymerization or that, if existent, they cannot resist to the whole molecular imprinting process, including the template removal steps. This can be promoted by insufficient polymer content in comparison to the amount of protein present in the system or by insufficient crosslinking that, not only, but also, leads to the high swelling variations observed throughout the whole processing.

The swelling itself may be a reason for the weak recognition features observed: while being desirable during the template removal stage to improve protein exit as the polymer mesh expands, it may be undesirable as imprinted binding sites are distorted and lose their specificity. The swelling behavior is not only defined by the crosslinking degree or yield, but also by the type of material. As it was discussed earlier, alginate functional groups are highly sensitive to pH variations and this sensitivity was easily noticed at earlier stages of development of this project, with ALMA 5 and ALMA 7 presenting different behaviors right after disc production. This feature can be quite interesting if the possibilities of modulating the recognition capacity of MIPs accordingly to external pH are considered. However, as it is currently designed, alginate sensitivity to pH may be playing a prejudicial role in the rebinding capacity of MIPs comparing to NIPs since most of the protein retained in the discs after the rebinding assay may be caused by entrapment due to the constriction of the polymer mesh. This constriction can provoke such significant retention that selective protein binding becomes residual by comparison.

On the other hand, for ALMA 5 discs, it cannot be assured that the small differences in rebinding capacity between NIPs and MIPs was only due to the absence of molecular recognition, since they could also be a result of the presence of a considerable amount of protein, which led to lower diffusional forces and, consequently, less propensity of protein to be absorbed to the MIP discs.

Even though the disc system presented herein is closer to a bulk or surface imprinting approach, which is usually associated with obstacles in protein diffusion (in or out), it was an ideal approach to easily evaluate and understand how this newly fabricated material responded to different parameters and stimuli. This enabled an easier adjustment of the protocol in decisive stages of development without the need for time consuming and expensive methodologies, always good to avoid when so many variables are involved.

- *This page was intentionally left in blank* -

Chapter 5
Conclusions and Perspectives

In the present work a molecular imprinting system based on photosensitive methacrylated alginate (ALMA) was developed and evaluated. Molecularly imprinted polymers (MIP) discs were produced using bovine serum albumin (BSA) as a template molecule, to serve as an optimization platform of the system for future translation into proteins with greater interest for Tissue Engineering applications.

Regarding the first objective of this work, an alginate methacrylation protocol was successfully optimized and enabled the production of methacrylated alginate which then had their pH adjusted to 5 (ALMA 5) or 7 (ALMA 7). Both materials were able to form gels upon 60s of UV exposure.

During different optimization stages, it was possible to find that pH affected ALMA 5 and ALMA 7 swelling behavior, as well as the presence of salts in the incubation solutions. Even though both materials followed the same tendency when under the same conditions, swelling effects were more pronounced in ALMA 7 than ALMA 5 discs.

Regarding the molecularly imprinted methacrylated alginate (MIP-ALMA) system, studies were performed on template removal and rebinding capacity. A promising template removal protocol was developed and optimized, retrieving approximately 70% and 96% of template removal for ALMA 5 and ALMA 7 discs, respectively. The obtained results were confirmed by two different protein quantification methodologies (analysis of supernatant and digested discs) and qualitatively by GTA method developed herein.

Rebinding capacity of NIP and MIP discs was also evaluated but no significant differences were observed between both materials. Several factors may have contributed to this, namely

the swelling profile of both ALMA 5 and ALMA 7 discs during the molecular imprinting protocol and rebinding assay.

Indeed, the swelling/deswelling profile observed during variations in pH and salts conditions seems to be a pivotal factor affecting protein diffusion events and, consequently, protein absorption and entrapment. A simple way to test this hypothesis can be, for instance, by performing rebinding assays in solutions with variable pH values and salts present with parallel comparison of their effect in the swelling behavior of the material.

If proven right, *i.e.*, that swelling and deswelling events are indeed interfering with the efficiency of the system to recognize the template, then efforts to improve mechanical properties of ALMA discs must be optimized in such a way that negative effects on the template removal are reduced. One possibility can be testing different ALMA concentrations in the initial polymer solution to generate stiffer discs. Another possibility relies in exploring the advantageous features of ALMA of enabling the combination of photo and ionic crosslinking with potential for mechanical properties improvement [113], which allow a whole wide range of possible combinations.

The same way, combination of two different polymers to produce heteropolymeric systems can help on producing better imprinting features by the existence of different functional groups capable of interacting with different domains of the macromolecules [111].

Finally, future miniaturization of the system from discs into a particle imprinting approach should also be considered.

References

[1] Byrne ME, Park K, Peppas NA. Molecular imprinting within hydrogels. Advanced Drug Delivery Reviews. 2002;54:149-61.
[2] Schirhagl R. Bioapplications for Molecularly Imprinted Polymers. Analytical Chemistry. 2014;86:250-61.
[3] Kryscio DR, Peppas NA. Critical review and perspective of macromolecularly imprinted polymers. Acta biomaterialia. 2012;8:461-73.
[4] Culver H, Daily A, Khademhosseini A, Peppas N. Intelligent recognitive systems in nanomedicine. Current opinion in chemical engineering. 2014;4:105-13.
[5] Byrne ME, Salian V. Molecular imprinting within hydrogels II: Progress and analysis of the field. International Journal of Pharmaceutics. 2008;364:188-212.
[6] Li S, Cao S, Whitcombe MJ, Piletsky SA. Size matters: Challenges in imprinting macromolecules. Progress in Polymer Science. 2014;39:145-63.
[7] Kryscio DR, Shi Y, Ren P, Peppas NA. Molecular docking simulations for macromolecularly imprinted polymers. Industrial & engineering chemistry research. 2011;50:13877-84.
[8] Mathur A, Blais S, Goparaju CM, Neubert T, Pass H, Levon K. Development of a biosensor for detection of pleural mesothelioma cancer biomarker using surface imprinting. PLoS One. 2013;8:e57681.
[9] Zhao K, Chen T, Lin B, Cui W, Kan B, Yang N, et al. Adsorption and recognition of protein molecular imprinted calcium alginate/polyacrylamide hydrogel film with good regeneration performance and high toughness. Reactive and Functional Polymers. 2015;87:7-14.
[10] Pang X, Cheng G, Li R, Lu S, Zhang Y. Bovine serum albumin-imprinted polyacrylamide gel beads prepared via inverse-phase seed suspension polymerization. Analytica Chimica Acta. 2005;550:13-7.
[11] Ding Z, Annie Bligh SW, Tao L, Quan J, Nie H, Zhu L, et al. Molecularly imprinted polymer based on MWCNT-QDs as fluorescent biomimetic sensor for specific recognition of target protein. Materials Science and Engineering: C. 2015;48:469-79.
[12] Guo TY, Xia YQ, Hao GJ, Song MD, Zhang BH. Adsorptive separation of hemoglobin by molecularly imprinted chitosan beads. Biomaterials. 2004;25:5905-12.
[13] Guo T, Xia Y, Hao G, Zhang B, Fu G, Yuan Z, et al. Chemically modified chitosan beads as matrices for adsorptive separation of proteins by molecularly imprinted polymer. Carbohydrate Polymers. 2005;62:214-21.
[14] Guo TY, Xia YQ, Wang J, Song MD, Zhang BH. Chitosan beads as molecularly imprinted polymer matrix for selective separation of proteins. Biomaterials. 2005;26:5737-45.

[15] Gao R, Zhao S, Hao Y, Zhang L, Cui X, Liu D, et al. Facile and green synthesis of polysaccharide-based magnetic molecularly imprinted nanoparticles for protein recognition. RSC Adv. 2015;5:88436-44.
[16] Oryan A, Alidadi S, Moshiri A, Maffulli N. Bone regenerative medicine: classic options, novel strategies, and future directions. J Orthop Surg Res. 2014;9:18.
[17] Nichol JW, Khademhosseini A. Modular Tissue Engineering: Engineering Biological Tissues from the Bottom Up. Soft Matter. 2009;5:1312-9.
[18] Eming SA, Krieg T, Davidson JM. Inflammation in Wound Repair: Molecular and Cellular Mechanisms. J Invest Dermatol. 2007;127:514-25.
[19] Fernandez-Yague MA, Abbah SA, McNamara L, Zeugolis DI, Pandit A, Biggs MJ. Biomimetic approaches in bone tissue engineering: Integrating biological and physicomechanical strategies. Advanced Drug Delivery Reviews. 2015;84:1-29.
[20] Tonnesen MG, Feng X, Clark RA. Angiogenesis in wound healing. The journal of investigative dermatology Symposium proceedings / the Society for Investigative Dermatology, Inc [and] European Society for Dermatological Research. 2000;5:40-6.
[21] Harty M, Neff AW, King MW, Mescher AL. Regeneration or scarring: an immunologic perspective. Developmental dynamics : an official publication of the American Association of Anatomists. 2003;226:268-79.
[22] Ferguson MW, O'Kane S. Scar-free healing: from embryonic mechanisms to adult therapeutic intervention. Philos Trans R Soc Lond B Biol Sci. 2004;359:839-50.
[23] Leal-Filho MB. Spinal cord injury: From inflammation to glial scar. Surg Neurol Int. 2011;2:112.
[24] Koh TJ, DiPietro LA. Inflammation and wound healing: The role of the macrophage. Expert reviews in molecular medicine. 2011;13:e23-e.
[25] Chan BP, Leong KW. Scaffolding in tissue engineering: general approaches and tissue-specific considerations. European Spine Journal. 2008;17:467-79.
[26] Cox TR, Erler JT. Remodeling and homeostasis of the extracellular matrix: implications for fibrotic diseases and cancer. Disease Models & Mechanisms. 2011;4:165-78.
[27] Muschler GF, Nakamoto C, Griffith LG. Engineering Principles of Clinical Cell-Based Tissue Engineering. The Journal of Bone & Joint Surgery. 2004;86:1541-58.
[28] Oliveira SM, Ringshia RA, Legeros RZ, Clark E, Yost MJ, Terracio L, et al. An improved collagen scaffold for skeletal regeneration. J Biomed Mater Res A. 2010;94:371-9.
[29] Guerreiro SG, Oliveira MJ, Barbosa MA, Soares R, Granja PL. Neonatal human dermal fibroblasts immobilized in RGD-alginate induce angiogenesis. Cell Transplant. 2014;23:945-57.
[30] Fonseca KB, Gomes DB, Lee K, Santos SG, Sousa A, Silva EA, et al. Injectable MMP-Sensitive Alginate Hydrogels as hMSC Delivery Systems. Biomacromolecules. 2014;15:380-90.
[31] Amaral IF, Unger RE, Fuchs S, Mendonca AM, Sousa SR, Barbosa MA, et al. Fibronectin-mediated endothelialisation of chitosan porous matrices. Biomaterials. 2009;30:5465-75.
[32] Wang Y, Kim H-J, Vunjak-Novakovic G, Kaplan DL. Stem cell-based tissue engineering with silk biomaterials. Biomaterials. 2006;27:6064-82.
[33] O'Brien FJ. Biomaterials and scaffolds for tissue engineering. Materials Today. 2011;14:88-95.
[34] Teixeira S, Rodriguez MA, Pena P, De Aza AH, De Aza S, Ferraz MP, et al. Physical characterization of hydroxyapatite porous scaffolds for tissue engineering. Materials Science and Engineering: C. 2009;29:1510-4.
[35] Teixeira S, Oliveira S, Ferraz M, Monteiro F. Three dimensional macroporous calcium phosphate scaffolds for bone tissue engineering2008.

[36] Marty J, Mauzac M. Molecular Imprinting: State of the Art and Perspectives. Microlithography · Molecular Imprinting: Springer Berlin Heidelberg; 2005. p. 1-35.
[37] Taguchi H, Sunayama H, Takano E, Kitayama Y, Takeuchi T. Preparation of molecularly imprinted polymers for the recognition of proteins via the generation of peptide-fragment binding sites by semi-covalent imprinting and enzymatic digestion. Analyst. 2015;140:1448-52.
[38] Verheyen E, Schillemans JP, van Wijk M, Demeniex MA, Hennink WE, van Nostrum CF. Challenges for the effective molecular imprinting of proteins. Biomaterials. 2011;32:3008-20.
[39] Xia Y-q, Guo T-y, Song M-d, Zhang B-h, Zhang B-l. Hemoglobin Recognition by Imprinting in Semi-Interpenetrating Polymer Network Hydrogel Based on Polyacrylamide and Chitosan. Biomacromolecules. 2005;6:2601-6.
[40] Chou P-C, Rick J, Chou T-C. C-reactive protein thin-film molecularly imprinted polymers formed using a micro-contact approach. Analytica Chimica Acta. 2005;542:20-5.
[41] Ou SH, Wu MC, Chou TC, Liu CC. Polyacrylamide gels with electrostatic functional groups for the molecular imprinting of lysozyme. Analytica Chimica Acta. 2004;504:163-6.
[42] Kryscio DR, Fleming MQ, Peppas NA. Protein conformational studies for macromolecularly imprinted polymers. Macromol Biosci. 2012;12:1137-44.
[43] Cormack PAG, Elorza AZ. Molecularly imprinted polymers: synthesis and characterisation. Journal of Chromatography B. 2004;804:173-82.
[44] Zhao K, Huang J, Ying X, Cheng G. Macromolecularly imprinted calcium phosphate/alginate hybrid polymer microspheres with the surface imprinting of bovine serum albumin in inverse-phase suspension. Journal of Applied Polymer Science. 2008;109:2687-93.
[45] Lulinski P. Molecularly imprinted polymers as the future drug delivery devices. Acta poloniae pharmaceutica. 2013;70:601-9.
[46] Bergmann NM, Lauten EH, Peppas NA. Intelligent biomaterials for drug delivery: combining molecular recognition with drug delivery. DRUG DELIVERY SYSTEMS AND SCIENCES. 2005;5:35.
[47] Hawkins DM, Stevenson D, Reddy SM. Investigation of protein imprinting in hydrogel-based molecularly imprinted polymers (HydroMIPs). Analytica Chimica Acta. 2005;542:61-5.
[48] Pérez-Moral N, Mayes AG. Comparative study of imprinted polymer particles prepared by different polymerisation methods. Analytica Chimica Acta. 2004;504:15-21.
[49] Ying X, Cheng G, Liu G, Qu R, Wang Y, Zhang L. Specific rebinding property of protein macromolecularly imprinted polymer microspheres based on calcium alginate hydrogel via gas jetting-dropping method. Journal of Applied Polymer Science. 2010;117:2331-9.
[50] Hoshino Y, Koide H, Urakami T, Kanazawa H, Kodama T, Oku N, et al. Recognition, neutralization, and clearance of target peptides in the bloodstream of living mice by molecularly imprinted polymer nanoparticles: a plastic antibody. J Am Chem Soc. 2010;132:6644-5.
[51] Valenick LV, Hsia HC, Schwarzbauer JE. Fibronectin fragmentation promotes α4β1 integrin-mediated contraction of a fibrin–fibronectin provisional matrix. Experimental Cell Research. 2005;309:48-55.
[52] Bergmann NM, Peppas NA. Molecularly imprinted polymers with specific recognition for macromolecules and proteins. Progress in Polymer Science. 2008;33:271-88.
[53] Lv Y, Tan T, Svec F. Molecular imprinting of proteins in polymers attached to the surface of nanomaterials for selective recognition of biomacromolecules. Biotechnology Advances. 2013;31:1172-86.
[54] Guo H, Yuan D, Fu G. Enhanced surface imprinting of lysozyme over a new kind of magnetic chitosan submicrospheres. J Colloid Interface Sci. 2015;440:53-9.
[55] Zhao X-L, Li D-Y, He X-W, Li W-Y, Zhang Y-K. An epitope imprinting method on the surface of magnetic nanoparticles for specific recognition of bovine serum album. Journal of Materials Chemistry B. 2014;2:7575-82.

[56] Papaioannou E, Koutsas C, Liakopoulou-Kyriakides M. Molecularly imprinted polymers for RGD selective recognition and separation. Amino Acids. 2009;36:563-9.
[57] Gribova V, Gauthier-Rouviere C, Albiges-Rizo C, Auzely-Velty R, Picart C. Effect of RGD functionalization and stiffness modulation of polyelectrolyte multilayer films on muscle cell differentiation. Acta biomaterialia. 2013;9:6468-80.
[58] Fonseca KB, Bidarra SJ, Oliveira MJ, Granja PL, Barrias CC. Molecularly designed alginate hydrogels susceptible to local proteolysis as three-dimensional cellular microenvironments. Acta biomaterialia. 2011;7:1674-82.
[59] Wang C, Howell M, Raulji P, Davis Y, Mohapatra S. Preparation and Characterization of Molecularly Imprinted Polymeric Nanoparticles for Atrial Natriuretic Peptide (ANP). Advanced functional materials. 2011;21:4423-9.
[60] Asliyuce S, Uzun L, Say R, Denizli A. Immunoglobulin G recognition with Fab fragments imprinted monolithic cryogels: Evaluation of the effects of metal-ion assisted-coordination of template molecule. Reactive and Functional Polymers. 2013;73:813-20.
[61] Xu L, Hu Y, Shen F, Li Q, Ren X. Specific recognition of tyrosine-phosphorylated peptides by epitope imprinting of phenylphosphonic acid. J Chromatogr A. 2013;1293:85-91.
[62] Corman ME, Armutcu C, Uzun L, Say R, Denizli A. Self-oriented nanoparticles for site-selective immunoglobulin G recognition via epitope imprinting approach. Colloids Surf B Biointerfaces. 2014;123:831-7.
[63] Jacobsen J, Kiselyov V, Bock E, Berezin V. A peptide motif from the second fibronectin module of the neural cell adhesion molecule, NCAM, NLIKQDDGGSPIRHY, is a binding site for the FGF receptor. Neurochem Res. 2008;33:2532-9.
[64] Wang J, Zheng J, Zheng Q, Wu Y, Wu B, Huang S, et al. FGL-functionalized self-assembling nanofiber hydrogel as a scaffold for spinal cord-derived neural stem cells. Materials Science and Engineering: C. 2015;46:140-7.
[65] Ansari S, Freire M, Choi MG, Tavari A, Almohaimeed M, Moshaverinia A, et al. Effects of the orientation of anti-BMP2 monoclonal antibody immobilized on scaffold in antibody-mediated osseous regeneration. Journal of biomaterials applications. 2015;30:558-67.
[66] Sunayama H, Ooya T, Takeuchi T. Fluorescent protein-imprinted polymers capable of signal transduction of specific binding events prepared by a site-directed two-step post-imprinting modification. Chemical Communications. 2014;50:1347-9.
[67] Takeuchi T, Sunayama H, Takano E, Kitayama Y. Post-imprinting and In-Cavity Functionalization. In: Mattiasson B, Ye L, editors. Molecularly Imprinted Polymers in Biotechnology: Springer International Publishing; 2015. p. 95-106.
[68] Hoffman AS. Hydrogels for biomedical applications. Advanced Drug Delivery Reviews. 2002;54:3-12.
[69] Herrero E, Valle E, Galan M. Development of a new technology for the production of microcapsules based in atomization processes. Chemical Engineering Journal. 2006;117:137-42.
[70] Lee KY, Mooney DJ. Alginate: properties and biomedical applications. Prog Polym Sci. 2012;37:106-26.
[71] Miao T, Rao KS, Spees JL, Oldinski RA. Osteogenic differentiation of human mesenchymal stem cells through alginate-graft-poly(ethylene glycol) microsphere-mediated intracellular growth factor delivery. Journal of Controlled Release. 2014;192:57-66.
[72] Zhao K, Cheng G, Huang J, Ying X. Rebinding and recognition properties of protein-macromolecularly imprinted calcium phosphate/alginate hybrid polymer microspheres. Reactive and Functional Polymers. 2008;68:732-41.

[73] Zhao K, Wei J, Cheng G, Yang C, Chen L. Preparation of bovine serum albumin-imprinted calcium polyacrylate/alginate hybrid microspheres via Ca2+crosslinking. Journal of Applied Polymer Science. 2009;113:1133-40.
[74] Zhao KY, Kan BH, Wei J-f, Cheng GX, Chen L. Bovine serum albumin imprinted calcium phosphate/polyacrylate/alginate multi-hybrid polymer microspheres in inverse-phase suspension. E-Polymers. 2008;8:1150.
[75] Zhao KY, Wei JF, Zhou JY, Zhao YP, Cheng GX. The Rebinding Properties of Bovine Serum Albumin Imprinted Calcium Phosphate/Polyacrylate/Alginate Hybrid Polymer Microspheres. Advanced Materials Research. 2010;152-153:1636-40.
[76] Zhao K, Lin B, Cui W, Feng L, Chen T, Wei J. Preparation and adsorption of bovine serum albumin-imprinted polyacrylamide hydrogel membrane grafted on non-woven polypropylene. Talanta. 2014;121:256-62.
[77] Xia YQ, Guo TY, Zhao HL, Song MD, Zhang BH, Zhang BL. Protein recognition onto silica particles using chitosan as intermedium substrate. J Biomed Mater Res A. 2009;90:326-32.
[78] Li L, Ying X, Liu J, Li X, Zhang W. Protein-imprinted polyurethane-grafted calcium alginate hydrogel microspheres. Journal of Applied Polymer Science. 2015;132:n/a-n/a.
[79] Bayer CL, Herrero EP, Peppas NA. Alginate films as macromolecular imprinted matrices. J Biomater Sci Polym Ed. 2011;22:1523-34.
[80] Herrero EP, Martín Del Valle EM, Peppas NA. Protein Imprinting by Means of Alginate-Based Polymer Microcapsules. Industrial & Engineering Chemistry Research. 2010;49:9811-4.
[81] Zhang F, Cheng G, Ying X. Emulsion and macromolecules templated alginate based polymer microspheres. Reactive and Functional Polymers. 2006;66:712-9.
[82] Zhu D-W, Chen Z, Zhao K-Y, Kan B-H, Liu L-X, Dong X, et al. Polypropylene non-woven supported fibronectin molecular imprinted calcium alginate/polyacrylamide hydrogel film for cell adhesion. Chinese Chemical Letters. 2015;26:807-10.
[83] Qian L, Hu X, Guan P, Gao B, Li J, Wang C, et al. Preparation of bovine serum albumin imprinting sensitive hydrogels using ionic liquid as co-monomer and stabilizer. Talanta. 2014;121:56-64.
[84] Liu Y, Gu Y, Li M, Wei Y. Protein imprinting over magnetic nanospheres via a surface grafted polymer for specific capture of hemoglobin. New J Chem. 2014;38:6064-72.
[85] Pang X, Cheng G, Zhang Y, Lu S. Soft-wet polyacrylamide gel beads with the imprinting of bovine serum albumin. Reactive and Functional Polymers. 2006;66:1182-8.
[86] Jaklenec A, Wan E, Murray ME, Mathiowitz E. Novel scaffolds fabricated from protein-loaded microspheres for tissue engineering. Biomaterials. 2008;29:185-92.
[87] Guo P, Yuan Y, Chi F. Biomimetic alginate/polyacrylamide porous scaffold supports human mesenchymal stem cell proliferation and chondrogenesis. Mater Sci Eng C Mater Biol Appl. 2014;42:622-8.
[88] Fukazawa K, Ishihara K. Fabrication of a cell-adhesive protein imprinting surface with an artificial cell membrane structure for cell capturing. Biosensors and Bioelectronics. 2009;25:609-14.
[89] Goubko CA, Cao X. Patterning multiple cell types in co-cultures: A review. Materials Science and Engineering: C. 2009;29:1855-68.
[90] Dan R, Wang Y, Du L, Du S, Huang M, Yang S, et al. The synthesis of molecular imprinted chitosan-gels copolymerized with multiform functional monomers at three different temperatures and the recognition for the template ovalbumin. Analyst. 2013;138:3433-43.
[91] Zheng X-F, Lian Q, Wu H, Liu H, Song S. Molecularly imprinted polymer for L-tyrosine recognition and controlled release. Russian Journal of Applied Chemistry. 2015;88:160-8.

[92] Singh LK, Singh M, Singh M. Biopolymeric receptor for peptide recognition by molecular imprinting approach--synthesis, characterization and application. Mater Sci Eng C Mater Biol Appl. 2014;45:383-94.
[93] Nishad PA, Bhaskarapillai A, Velmurugan S, Narasimhan SV. Cobalt (II) imprinted chitosan for selective removal of cobalt during nuclear reactor decontamination. Carbohydrate Polymers. 2012;87:2690-6.
[94] Monier M, El-Sokkary AM. Preparation of molecularly imprinted cross-linked chitosan/glutaraldehyde resin for enantioselective separation of L-glutamic acid. International journal of biological macromolecules. 2010;47:207-13.
[95] Kyzas GZ, Lazaridis NK, Bikiaris DN. Optimization of chitosan and β-cyclodextrin molecularly imprinted polymer synthesis for dye adsorption. Carbohydrate Polymers. 2013;91:198-208.
[96] Xia Y-q, Guo T-y, Song M-d, Zhang B-h, Zhang B-l. Selective separation of quercetin by molecular imprinting using chitosan beads as functional matrix. Reactive and Functional Polymers. 2006;66:1734-40.
[97] Fu GQ, Yu H, Zhu J. Imprinting effect of protein-imprinted polymers composed of chitosan and polyacrylamide: a re-examination. Biomaterials. 2008;29:2138-42.
[98] DePorter SM, Lui I, McNaughton BR. Programmed cell adhesion and growth on cell-imprinted polyacrylamide hydrogels. Soft Matter. 2012;8:10403-8.
[99] Jeon H, Kim G. Effects of a cell-imprinted poly(dimethylsiloxane) surface on the cellular activities of MG63 osteoblast-like cells: preparation of a patterned surface, surface characterization, and bone mineralization. Langmuir. 2012;28:13423-30.
[100] Peppas NA, Clegg JR. The challenge to improve the response of biomaterials to the physiological environment. Regenerative biomaterials. 2016;3:67-71.
[101] Sigma-Aldrich. Methacrylic anhydride. 2016.
[102] Williams CG, Malik AN, Kim TK, Manson PN, Elisseeff JH. Variable cytocompatibility of six cell lines with photoinitiators used for polymerizing hydrogels and cell encapsulation. Biomaterials. 2005;26:1211-8.
[103] Sigma-Aldrich. 2-Hydroxy-4′-(2-hydroxyethoxy)-2-methylpropiophenone. 2016.
[104] Ma X, Sun X, Hargrove D, Chen J, Song D, Dong Q, et al. A Biocompatible and Biodegradable Protein Hydrogel with Green and Red Autofluorescence: Preparation, Characterization and In Vivo Biodegradation Tracking and Modeling. Sci Rep. 2016;6:19370.
[105] Laboratories B-R. Zoe TM Fluorescent Cell Imager Instructon Manual, Catalog # 145-0031. 2015.
[106] Jeon O, Bouhadir KH, Mansour JM, Alsberg E. Photocrosslinked alginate hydrogels with tunable biodegradation rates and mechanical properties. Biomaterials. 2009;30:2724-34.
[107] Chou AI, Akintoye SO, Nicoll SB. Photo-crosslinked alginate hydrogels support enhanced matrix accumulation by nucleus pulposus cells in vivo. Osteoarthritis Cartilage. 2009;17:1377-84.
[108] Rouillard AD, Berglund CM, Lee JY, Polacheck WJ, Tsui Y, Bonassar LJ, et al. Methods for photocrosslinking alginate hydrogel scaffolds with high cell viability. Tissue Eng Part C Methods. 2011;17:173-9.
[109] Smeds KA, Pfister-Serres A, Miki D, Dastgheib K, Inoue M, Hatchell DL, et al. Photocrosslinkable polysaccharides for in situ hydrogel formation. Journal of biomedical materials research. 2001;54:115-21.
[110] Wang X, Hao T, Qu J, Wang C, Chen H. Synthesis of Thermal Polymerizable Alginate-GMA Hydrogel for Cell Encapsulation. Journal of Nanomaterials. 2015;2015:1-8.

[111] Neves MI, Wechsler ME, Gomes ME, Reis RL, Granja PL, Peppas NA. Molecularly Imprinted Intelligent Scaffolds for Tissue Engineering Applications. Tissue engineering Part B, Reviews. 2016.
[112] Trakhtenberg S, Kumar R, Bianchini J, Thor S, Martino DM, Warner JC. Influence of pH and Salt on the Photocrosslinking in Polyelectrolyte Thymine - Containing Films. Journal of Macromolecular Science, Part A. 2007;44:1311-5.
[113] Samorezov JE, Morlock CM, Alsberg E. Dual Ionic and Photo-Crosslinked Alginate Hydrogels for Micropatterned Spatial Control of Material Properties and Cell Behavior. Bioconjug Chem. 2015;26:1339-47.
[114] Kadokawa J-i, Saitou S, Shoda S-i. Preparation of alginate-polymethacrylate hybrid material by radical polymerization of cationic methacrylate monomer in the presence of sodium alginate. Carbohydrate Polymers. 2005;60:253-8.
[115] Burdick JA, Chung C, Jia X, Randolph MA, Langer R. Controlled Degradation and Mechanical Behavior of Photopolymerized Hyaluronic Acid Networks. Biomacromolecules. 2005;6:386-91.
[116] Pourjavadi A, Kurdtabar M, Ghasemzadeh H. Salt- and pH-Resisting Collagen-based Highly Porous Hydrogel. Polymer Journal. 2007;40:94-103.
[117] Mirdarikvande S, Sadeghi H, Godarzi A, Alahyari M, Shasavari H, Khani F. Effect of pH, and Salinity onto Swelling Properties of Hydrogels Based on H-alginate-g-poly(AMPS). Biosciences Biotechnology Research Asia. 2014;11:205-9.
[118] Liu Y, Hunziker EB, Randall NX, de Groot K, Layrolle P. Proteins incorporated into biomimetically prepared calcium phosphate coatings modulate their mechanical strength and dissolution rate. Biomaterials. 2003;24:65-70.
[119] Topuz F, Henke A, Richtering W, Groll J. Magnesium ions and alginate do form hydrogels: a rheological study. Soft Matter. 2012;8:4877.
[120] Donati I, Asaro F, Paoletti S. Experimental Evidence of Counterion Affinity in Alginates: The Case of Nongelling Ion Mg2+. The Journal of Physical Chemistry B. 2009;113:12877-86.
[121] Ghisaidoobe AB, Chung SJ. Intrinsic tryptophan fluorescence in the detection and analysis of proteins: a focus on Forster resonance energy transfer techniques. Int J Mol Sci. 2014;15:22518-38.
[122] Bio-Rad. DC Protein Assay Instruction Manual. 2016.
[123] !!! INVALID CITATION !!! .
[124] Ma X, Sun X, Hargrove D, Chen J, Song D, Dong Q, et al. A Biocompatible and Biodegradable Protein Hydrogel with Green and Red Autofluorescence: Preparation, Characterization and In Vivo Biodegradation Tracking and Modeling. Scientific Reports. 2016;6:19370.
[125] Habeeb AFSA, Hiramoto R. Reaction of proteins with glutaraldehyde. Archives of Biochemistry and Biophysics. 1968;126:16-26.
[126] Paddock SW. Principles and practices of laser scanning confocal microscopy. Molecular Biotechnology. 2000;16:127-49.
[127] Pass G, Phillips GO, Wedlock DJ. Interaction of Univalent and Divalent Cations with Carrageenans in Aqueous Solution. Macromolecules. 1977;10:197-201.

- *This page was intentionally left in blank* -

Supplementary data

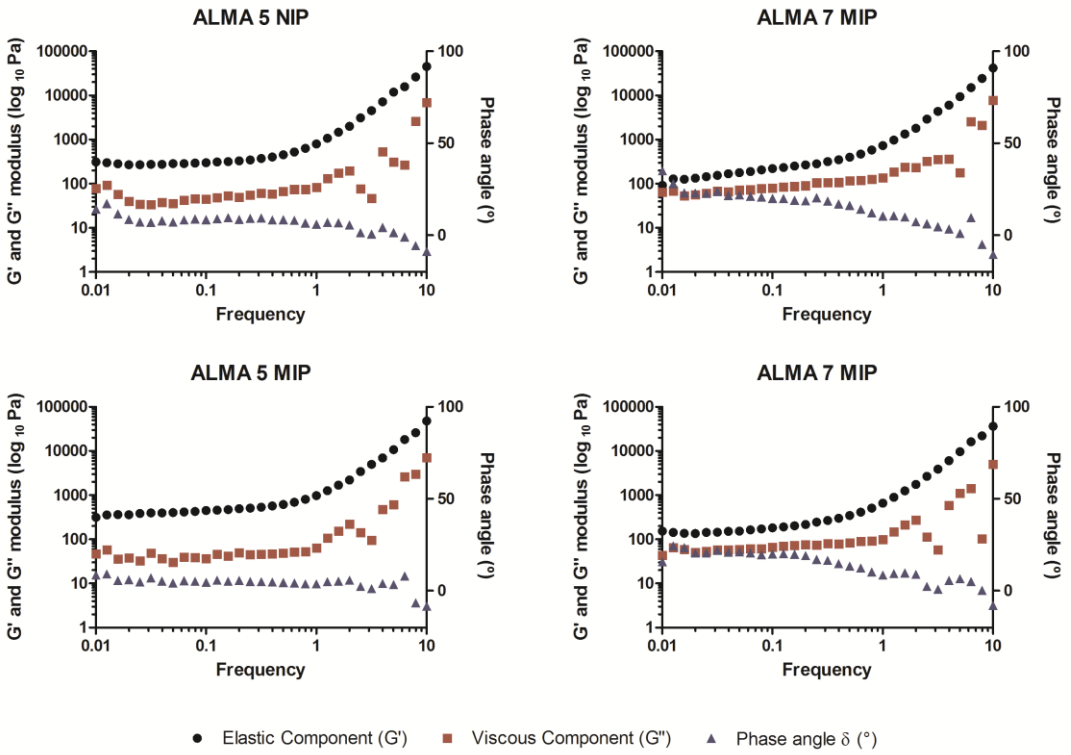

S 1. Preliminary rheological analysis of ALMA 5 and ALMA 7 NIP and MIP discs right after production.

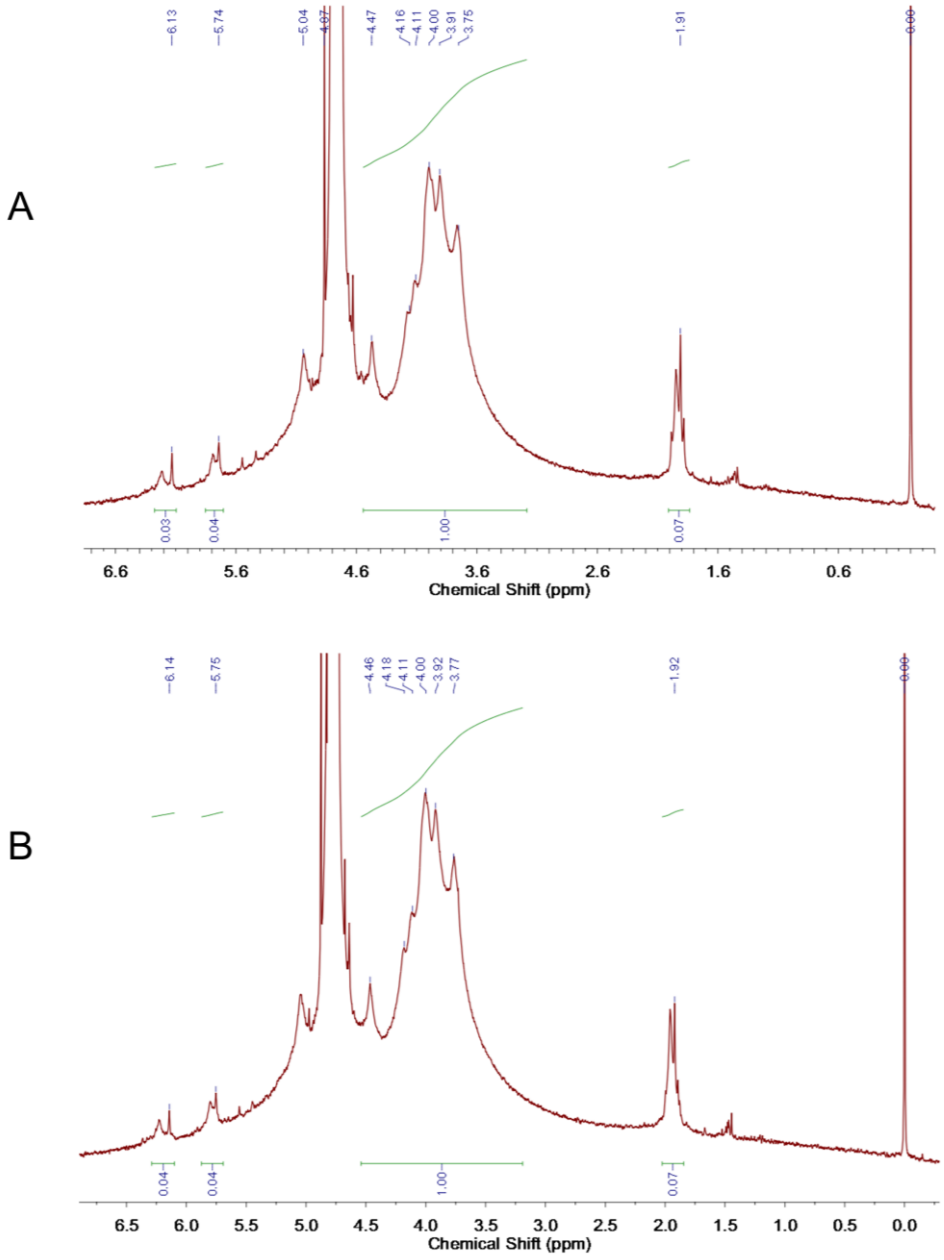

S 2. ^{1}H NMR spectra integration of modified alginate ALMA 5 (A) and ALMA 7 (B).

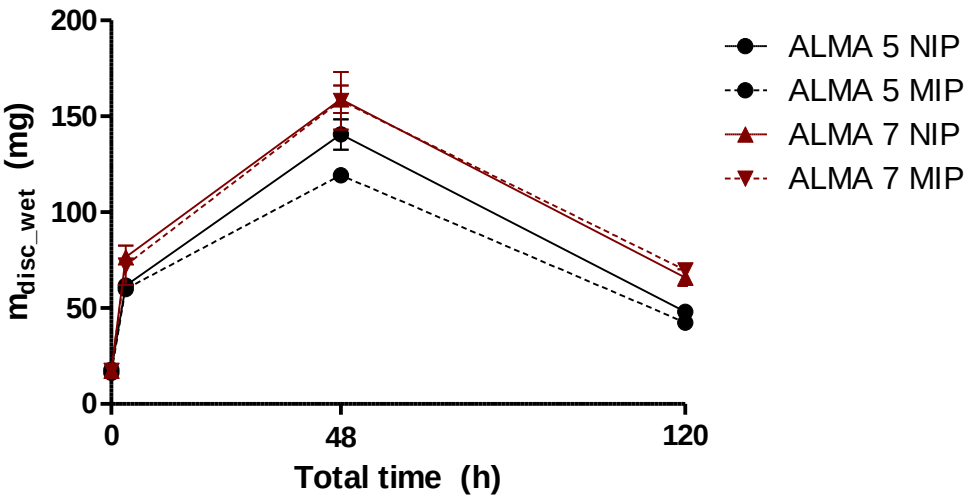

S 3. Weight of ALMA 5 and ALMA 7 NIP and MIP discs during template removal (48h) and rebinding protocol (72h of rebinding, total 120h). Data represent mean values of n=4 discs ± SD.

Sample	Location	Area	Mean	IntDen
1 % BSA, rep. 1	disc	39921.913	3400.799	5.926E+07
1 % BSA, rep. 1	disc	39921.913	2598.305	4.527E+07
1 % BSA, rep. 1	disc	39921.913	2978.800	5.190E+07
1 % BSA, rep. 1	background	39921.913	43.604	7.598E+05
1 % BSA, rep. 1	background	39921.913	41.730	7.271E+05
1 % BSA, rep. 1	background	39921.913	44.714	7.791E+05
1 % BSA, rep. 2	disc	39921.913	2634.927	4.591E+07
1 % BSA, rep. 2	disc	39921.913	2809.812	4.896E+07
1 % BSA, rep. 2	disc	39921.913	3514.557	6.124E+07
1 % BSA, rep. 2	background	39921.913	40.782	7.106E+05
1 % BSA, rep. 2	background	39921.913	41.062	7.155E+05
1 % BSA, rep. 2	background	39921.913	42.482	7.402E+05
1 % BSA, rep. 3	disc	39921.913	3926.779	6.842E+07
1 % BSA, rep. 3	disc	39921.913	3897.720	6.791E+07
1 % BSA, rep. 3	disc	39921.913	3992.776	6.957E+07
1 % BSA, rep. 3	background	39921.913	41.050	7.153E+05
1 % BSA, rep. 3	background	39921.913	42.058	7.328E+05
1 % BSA, rep. 3	background	39921.913	46.032	8.021E+05
1 % BSA, rep. 4	disc	39921.913	3675.638	6.404E+07
1 % BSA, rep. 4	disc	39921.913	3820.373	6.657E+07
1 % BSA, rep. 4	disc	39921.913	3075.635	5.359E+07
1 % BSA, rep. 4	background	39921.913	41.036	7.150E+05
1 % BSA, rep. 4	background	39921.913	40.740	7.099E+05
1 % BSA, rep. 4	background	39921.913	54.821	9.552E+05

Sample	Location	Area	Mean	IntDen
0.5 % BSA, rep. 1	disc	39921.913	1480.334	2.579E+07
0.5 % BSA, rep. 1	disc	39921.913	1661.755	2.895E+07
0.5 % BSA, rep. 1	disc	39921.913	1935.950	3.373E+07
0.5 % BSA, rep. 1	background	39921.913	41.131	7.167E+05
0.5 % BSA, rep. 1	background	39921.913	40.771	7.104E+05
0.5 % BSA, rep. 1	background	39921.913	41.026	7.148E+05
0.5 % BSA, rep. 2	disc	39921.913	2498.121	4.353E+07
0.5 % BSA, rep. 2	disc	39921.913	2582.198	4.499E+07
0.5 % BSA, rep. 2	disc	39921.913	2424.452	4.224E+07
0.5 % BSA, rep. 2	background	39921.913	41.835	7.289E+05
0.5 % BSA, rep. 2	background	39921.913	48.827	8.508E+05
0.5 % BSA, rep. 2	background	39921.913	61.965	1.080E+06
0.5 % BSA, rep. 3	disc	39921.913	1907.661	3.324E+07
0.5 % BSA, rep. 3	disc	39921.913	1993.599	3.474E+07
0.5 % BSA, rep. 3	disc	39921.913	1858.118	3.238E+07
0.5 % BSA, rep. 3	background	39921.913	41.253	7.188E+05
0.5 % BSA, rep. 3	background	39921.913	40.650	7.083E+05
0.5 % BSA, rep. 3	background	39921.913	45.685	7.960E+05
0.5 % BSA, rep. 4	disc	39921.913	1661.725	2.895E+07
0.5 % BSA, rep. 4	disc	39921.913	1967.314	3.428E+07
0.5 % BSA, rep. 4	disc	39921.913	1948.002	3.394E+07
0.5 % BSA, rep. 4	background	39921.913	50.225	8.751E+05
0.5 % BSA, rep. 4	background	39921.913	42.034	7.324E+05
0.5 % BSA, rep. 4	background	39921.913	42.900	7.475E+05

Sample	Location	Area	Mean	IntDen
0.25 % BSA, rep. 1	disc	39921.913	832.782	1.451E+07
0.25 % BSA, rep. 1	disc	39921.913	1094.702	1.907E+07
0.25 % BSA, rep. 1	disc	39921.913	1240.171	2.161E+07
0.25 % BSA, rep. 1	background	39921.913	41.907	7.302E+05
0.25 % BSA, rep. 1	background	39921.913	41.898	7.300E+05
0.25 % BSA, rep. 1	background	39921.913	41.974	7.313E+05
0.25 % BSA, rep. 2	disc	39921.913	1360.058	2.370E+07
0.25 % BSA, rep. 2	disc	39921.913	1530.868	2.667E+07
0.25 % BSA, rep. 2	disc	39921.913	1413.108	2.462E+07
0.25 % BSA, rep. 2	background	39921.913	42.380	7.384E+05
0.25 % BSA, rep. 2	background	39921.913	45.415	7.913E+05
0.25 % BSA, rep. 2	background	39921.913	61.724	1.075E+06
0.25 % BSA, rep. 3	disc	39921.913	1040.884	1.814E+07
0.25 % BSA, rep. 3	disc	39921.913	1371.466	2.390E+07
0.25 % BSA, rep. 3	disc	39921.913	1629.345	2.839E+07
0.25 % BSA, rep. 3	background	39921.913	40.593	7.073E+05
0.25 % BSA, rep. 3	background	39921.913	40.735	7.098E+05
0.25 % BSA, rep. 3	background	39921.913	40.966	7.138E+05
0.25 % BSA, rep. 4	disc	39921.913	1498.084	2.610E+07
0.25 % BSA, rep. 4	disc	39921.913	1680.033	2.927E+07
0.25 % BSA, rep. 4	disc	39921.913	1672.723	2.915E+07
0.25 % BSA, rep. 4	background	39921.913	40.858	7.119E+05
0.25 % BSA, rep. 4	background	39921.913	41.908	7.302E+05
0.25 % BSA, rep. 4	background	39921.913	44.011	7.668E+05

Sample	Location	Area	Mean	IntDen
0% BSA, rep. 1	disc	39921.913	243.066	4.235E+06
0% BSA, rep. 1	disc	39921.913	273.711	4.769E+06
0% BSA, rep. 1	disc	39921.913	245.335	4.275E+06
0% BSA, rep. 1	background	39921.913	40.574	7.070E+05
0% BSA, rep. 1	background	39921.913	40.710	7.093E+05
0% BSA, rep. 1	background	39921.913	41.932	7.306E+05
0% BSA, rep. 2	disc	39921.913	237.935	4.146E+06
0% BSA, rep. 2	disc	39921.913	287.448	5.008E+06
0% BSA, rep. 2	disc	39921.913	292.597	5.098E+06
0% BSA, rep. 2	background	39921.913	40.992	7.143E+05
0% BSA, rep. 2	background	39921.913	40.643	7.082E+05
0% BSA, rep. 2	background	39921.913	40.924	7.131E+05
0% BSA, rep. 3	disc	39921.913	247.321	4.309E+06
0% BSA, rep. 3	disc	39921.913	266.296	4.640E+06
0% BSA, rep. 3	disc	39921.913	319.919	5.574E+06
0% BSA, rep. 3	background	39921.913	40.895	7.125E+05
0% BSA, rep. 3	background	39921.913	40.896	7.126E+05
0% BSA, rep. 3	background	39921.913	44.770	7.801E+05
0% BSA, rep. 4	disc	39921.913	325.525	5.672E+06
0% BSA, rep. 4	disc	39921.913	300.337	5.233E+06
0% BSA, rep. 4	disc	39921.913	332.780	5.798E+06
0% BSA, rep. 4	background	39921.913	40.547	7.065E+05
0% BSA, rep. 4	background	39921.913	40.924	7.131E+05
0% BSA, rep. 4	background	39921.913	42.239	7.360E+05

S 4. Panel showing measurements performed to obtain calibration curves for the GTA method.

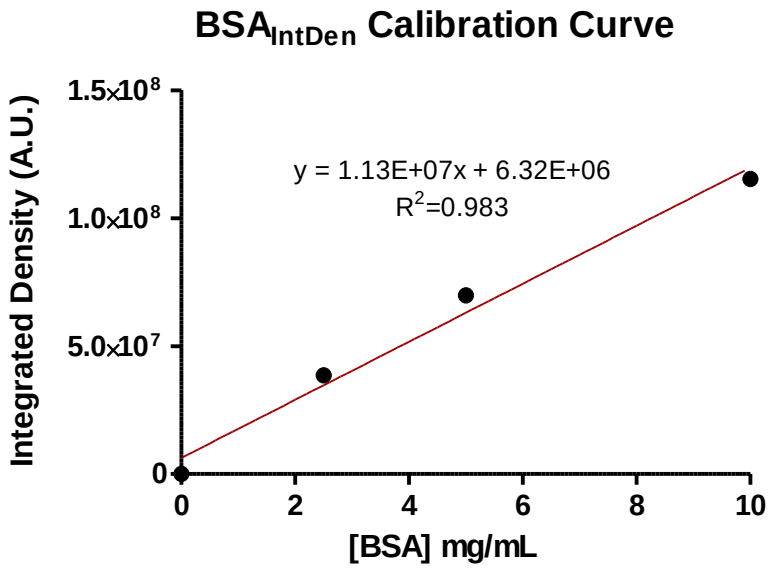

S 5. Calibration curve obtained by analysis of inverted confocal microscopy images to correlate the Integrated Density (A.U.) with the amount of BSA (mg/mL) present in discs (template removal). Results obtained from 3 measurements per disc, n=3 discs.

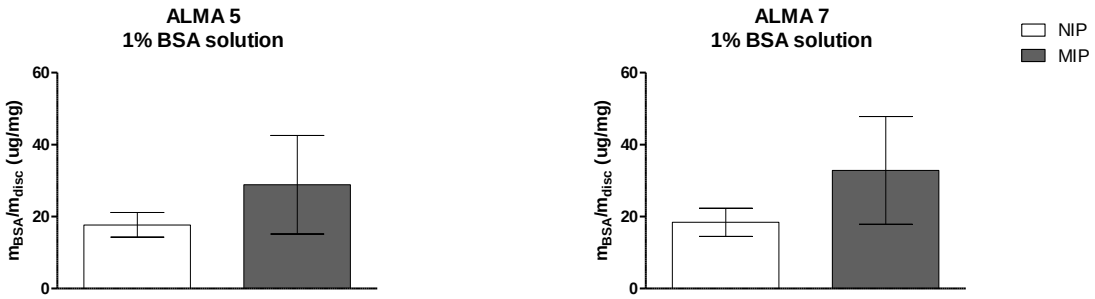

S 6. Amount of BSA present in ALMA5 and ALMA 7 NIP and MIP discs after 72h incubation in 1% BSA solution in 0.9% NaCl (pH 4.2). Data obtained by protein quantification in supernatant, bars represent mean values of n=3 discs ± SD.

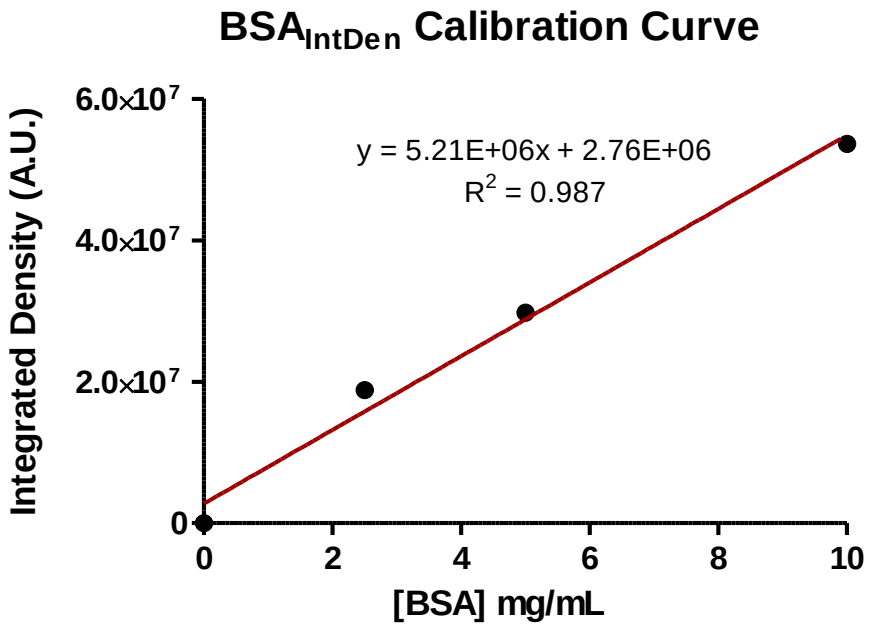

S 7. Calibration curve obtained by analysis of inverted confocal microscopy images to correlate the Integrated Density (A.U.) with the amount of BSA (mg/mL) present in discs (rebind assay). Results obtained from 3 measurements per disc, n=3 discs.